Title

Modeling and Observations of Human Constructed Dunes in Wave and Tidally Dominated Coastal Environments

Author

Winters, Maria

Publication Date

2023

Peer reviewed|Thesis/dissertation

UNIVERSITY OF CALIFORNIA

Los Angeles

Modeling and Observations of Human Constructed Dunes in Wave and Tidally Dominated Coastal Environments

A dissertation submitted in partial satisfaction
of the requirements for the degree
Doctor of Philosophy in Civil Engineering

by

Maria Alexandra Winters

2023

ABSTRACT OF THE DISSERTATION

Modeling and Observations of Human Constructed Dunes
in Wave and Tidally Dominated Coastal Environments

by

Maria Alexandra Winters
Doctor of Philosophy in Civil Engineering
University of California, Los Angeles, 2023
Professor Timu Gallien, Chair

Sea-level rise will increase the frequency and severity of coastal flooding events. Even minor water level increases will propagate wave energy landward, promote coastal erosion and, in turn, jeopardize backshore infrastructure. Critical infrastructure requires evolving coastal management and advanced engineering designs to facilitate long-term urban coastal realignment compatible with rising seas. Traditional coastal engineering uses hard infrastructure such as sea walls and revetments to protect urbanized backshores. Infrastructure failure during extreme water levels leads to catastrophic human and economic consequences. Evolving, nature-inspired features such as living shorelines and artificial dunes present an attractive hardscape alternative. Although dune erosion modeling is prevalent in the literature, there is a paucity of information regarding the construction, design and efficacy of the hybrid dune counterparts, especially on energetic, wave-dominated coastlines (e.g., Pacific). The objective of this research is to advance nature-based coastal engineering through high-resolution spatiotemporal observations and numerical modeling.

The dissertation of Maria Alexandra Winters is approved.

Mackenzie Denali Day

Marcelo Chamecki

Steven Adam Margulis

Scott Brandenberg

Timu Gallien, Committee Chair

University of California, Los Angeles

2023

To all my friends and family. To John, who has always been by my side.

TABLE OF CONTENTS

1 Introduction **1**

1.1 Coastal Flooding 1

1.2 Coastal Flood Defenses 2

1.3 Hybrid Structures 5

1.4 Dune Modeling 6

1.4.1 Numerical Models 8

1.5 Beach-Dune System Resilience to Wave Runup and Overtopping 10

1.6 Scope of Doctoral Research 11

2 Cardiff State Beach Living Shoreline **13**

2.1 Study Site Description 13

2.1.1 Hybrid Dune Description 14

2.2 Observations and Monitoring 16

2.2.1 Topographic and Bathymetric Data 16

2.2.2 Dune and Beach Evolution 22

2.3 Vulnerability Assessment 24

2.3.1 Total Water Levels Estimation 24

2.3.2 Vulnerability to Extreme Total Water Levels and Sea-level Rise . . . 28

3 Cardiff Dune Modeling **31**

3.1 Multi-substrate Observations and Modeling 31

3.2 Cardiff Observations 34

3.3 Model Grid Generation 39
3.4 Cardiff Modeling 39
3.4.1 Analytical Dune Erosion Modeling: Larson et al. (2004) 39
3.4.2 XBeach Dune Modeling 41

4 Naval Amphibious Base Coronado 43

4.1 Site Description 43
4.2 Event Description 45
4.3 Observations 47
4.3.1 Topobathy 47
4.3.2 Beach and Dune Observed Morphology Changes 50
4.3.3 Swash and Overtopping Observations 51
4.4 Grid Generation 54
4.5 Numerical Model Descriptions and Setup 55
4.5.1 SBeach 55
4.5.2 CSHORE 56
4.5.3 XBeach 61
4.5.4 Model Scenarios and Evaluation 68
4.6 Results 70
4.6.1 Hydrodynamic Modeling 70
4.6.2 Modeled Overtopping 70
4.6.3 Morphological Modeling 72
4.7 Discussion 79
4.7.1 Morphological Modeling 79

4.7.2 Overtopping Modeling 83
4.7.3 Limitations 84
4.8 Conclusions 85

5 Conclusions and Future Work 86
5.1 Conclusions 86
5.2 Future Work 86

LIST OF FIGURES

2.1 (**a**) Study site outlined in black of the Cardiff Living Shoreline project in northern San Diego County, California, United States. (**b**) Study site with red outline indicating project footprint, section labels indicating each stage of project construction, and black numbered lines indicating each Coastal Data Information Program (CDIP) Monitoring and Prediction (MOP) beach profile that was analyzed in this study (See Section 2.3 for details). 14

2.2 Original construction cross-section drawing of the Cardiff Living Shoreline Project. The dune is backed by large rip-rap, fronted by a native, smaller grain size native cobble toe, and topped with native sand. All measurements are in feet and elevations are NAVD88. Courtesy of Moffatt and Nichol, 2015 (Moffatt & Nichol, 2015). 16

2.3 Pre-construction (**a**) and post-construction (**b**) digital elevation models derived from UAV photogrammetric surveys from 9 October 2018 and 28 August 2019, respectively. Section labels indicate each stage of project construction, and black numbered lines indicate each Monitoring and Prediction (MOP) beach profile that was analyzed in this study (See Section 2.3 for details). 21

2.4 (**a**) Three-dimensional representation of living shoreline derived from UAV orthoimagery collected 20 December 2019 viewing northward. Blue line indicates toe delineation. (**b**) View looking southward on heavily vegetated section 1 with pedestrian access ways. (**c**) View looking southward on sections 2 and 3 with sand fences visible. 22

2.5 Dune crest (solid red line) and toe (blue dashed line) elevations estimated from 28 August 2019 UAV survey. Low crest elevations at about 4.5 m NAVD88 indicate pedestrian access way locations. Each section of the dune and MOP transect locations are labeled. 22

2.6 (a) DEM differences (color bar) from 8/28/2019 to 12/20/2019. Significant foreshore erosion is observed. MOP profiles 677 (b), 675 (c), and 671 (d) are shown with an additional spring survey (4/30/2020) highlighting significant vegetation growth along MOP677 (magenta). 25

2.7 Annual maximum total water level (TWL) values from 1948 to 2008 for each MOP line without sea-level rise (blue markers). TWL time series superposed to 2020 to 2080 with projected sea-level rise for RCP 4.5 and 8.5 added (green and red markers, respectively). Black horizontal lines indicate values of mean beach crest pre-construction, dune crest and toe post-construction, and the 50 and 100-yr TWL values. 27

2.8 Average hours per year of dune toe interaction (collision hours) for MOP lines 671 (black curve) and 677 (blue curve) with added sea-level rise projected under RCP 4.5 and 8.5 at 2050 (circles) and 2070 (triangles). 29

3.1 Winter 2020-2022 Cardiff beach offshore significant wave heights and total water levels. Black line indicates approximate dune toe elevation. 35

3.2 Winter 2020-2022 Cardiff beach and dune evolution 35

3.3 Deep water wave conditions from the nearest CDIP buoy (101 Torrey Pines Outer) during the January 2023 storm event. 37

3.4 Selected photos of the overwash and erosion event on January 6, 2023. Photo credit: Maria Winters and Margit Maple. 37

3.5 Cross-shore transects from selected surveys at MOP cross-shore locations. 38

3.6 Fall and winter Cardiff beach and dune erosion from October 2022 to January 2023. 38

3.7 Cardiff beach from April to June 2023. Increase in sand elevation along the project includes sand placement along toe of dune in May 2023. 38

3.8 Selected cross-shore profile from the study site depicting pre- and post-storm dune topography measured by UAV surveys, as well as predicted dune toe retreat, $z_b(t)$, predicted by the Larson et al. (2004) model. 41

3.9 Selected cross-shore profile from the study site depicting pre- and post-storm dune topography measured by UAV surveys, as well as dune erosion predicted by XBeach. 42

4.1 (a) Study site of the Naval Amphibious Base Coronado persistent dune in San Diego County, California, United States. Sand dune structure of interest outlined in red. (b) Image of dune and beach overlapped on nearshore bathymetry. Location of CTD, PUV (wave gauge), and pressure sensors indicated by green star, green asterisk, and magenta polygon, respectively. Modeled cross-shore transects indicated and labeled. 44

4.2 Photos of Coronado berm failure during March 5-7th, 2016 resulting in backshore parking lot flooding and undermining. 45

4.3 (a) Tide, Stockdon et al. (2006) R_2%, total water level (TWL), and salinity signal from backshore CTD. Reader is referred to Section 4.2 for Stockdon et al. (2006) definitions. (b) offshore wave conditions from nearest deep water CDIP buoy (191 Point Loma) for duration of simulated storm from January 21-22, 2017. 46

4.4 Observed (a) hourly swash face slope, (b) Iribarren number, and (c) R^{IG}/R ratios at each modeled transect (1D) for duration of storm event. 49

4.5 (a) Observed dune pre-storm on 1/21/2017 (b) observed post-storm on 1/24/2017 and (c) elevation difference map between the two dates. Modeled cross-shore transects of interest are indicated with black lines and corresponding labels. (d) Observed elevations of the dune toe and crest pre- and post-storm. (e) Observed changes in dune toe and crest elevations. Green asterisk indicates alongshore location of the buried dune face pressure sensor, P1. 52

4.6 (a) Dune volume pre-storm and post storm from UAV observations. (b) Dune volume change along length of dune between pre and post storm. (c) Distance from dune toe and crest to mean sea level elevation pre-storm. Green asterisk indicates alongshore location of the buried dune face pressure sensor, P1. 53

4.7 (a) Pre-storm beach beach slope, β_{beach}, estimated from MLLW to the dune toe (b) Pre and post-storm dune slope, β_{dune}, estimated from the dune toe to dune crest and (c) the change in dune slope after the storm event, dβ_{dune}. 53

4.8 (a) Buried pressure sensor, P1, water level elevation measurements and (b) CTD water depth and salinity measurements in backshore ditch during peak of storm. 54

4.9 Observed and modeled significant wave height and power wave spectra at PUV location. 71

4.10 Cumulative overtopped volume in cubic meters predicted by different modes of XBeach (1D non-hydrostatic, 1D hydrostatic, and 2D hydrostatic) into backshore drainage ditch and observed cumulative overtopping. 72

4.11 SBeach and CSHORE modeling results 73

4.12 XBeach 1D and 2D modeling results 74

4.13 Regression plots of observed and modeled dune characteristics. 75

4.14 BSS values across all models and cross-shore locations. BSS only estimated from 2 m NAVD88 to the dune crest. 76

4.15 (a) Observed pre-storm elevation bed with modeled cross-shore transects of interest indicated by black lines. (b) Observed post-storm bed. (c) Observed beach elevation change from pre- to post-storm (d),(e) XBeach 2D modeled beach elevation change from pre- to post-storm. (f),(g) Brier Skill Score for every cross-shore location (each cross-shore grid row) for both 2D XBeach simulations. BSS only estimated from 2 m NAVD88 to the dune crest. 77

4.16 Observed and XBeach 2D modeled (a) dune crest and toe heights (b) crest and (c) toe changes from pre- to post-storm (d) dune volume change from pre- to post-storm (e) dune face slope change from pre- to post-storm. Green asterisk indicates alongshore location of the buried pressure sensor, P1. 78

LIST OF TABLES

2.1 Survey dates, hydrodynamic conditions and beach volumes. Tide (NOAA gauge 9410230), significant wave height, and peak period (CDIP buoy 100) at time of survey are listed. Beach volumes in cubic meters are listed above mean sea-level (MSL, 0.774 m NAVD88) and the upper beach (>2 m NAVD88). Hyphens indicate no data available. 19

4.1 Ranges of beach conditions during duration of storm at each cross-shore location. Deepwater wave height obtained by reverse shoaling wave parameters obtained from CDIP MOP program at 10 meter depth to deep water. 48

4.2 Priority of geospatial data for creation of digital terrain model (DTM) used for Coronado breach and dune erosion modeling. 49

4.3 Parameters, listed by model, considered in this study along with parameter descriptions. Boldface parameter values indicate model default values. 67

4.4 Simulations, listed by cross-shore location and model, considered in this study. A dash indicates the model was not run at the selected locations. 69

4.5 Observed and modeled wave interaction/collision hours at the buried pressure sensor 1 (P1). 71

ACKNOWLEDGMENTS

The list here is not completely comprehensive, and there are a large amount of people who I would like to thank who supported and contributed to my Ph.D. Below I would like to give special acknowledgement to the following people and organizations. I would like to thank Evyan Borgnis Sloane and California Coastal Conservancy for supporting the scientific monitoring and making the Cardiff Living Shoreline project happen. Kathy Weldon (former Coastal Manager for the City of Encinitas), Jayme Timberlake (former Coastal Manager for the City of Encinitas), Darren Smith (California State Parks), Brian Leslie (GHD), Connor Ofsthun (Moffatt & Nichol), Robert Patton, and West-Tech Construction were instrumental in site access and facilitating Cardiff surveys. Moffatt and Nichol and GHD (Brian Leslie) generously provided key dune design information and facilitated construction survey coordination. Adam Young (Scripps Institution of Oceanography) graciously provided geospatial data. Li Erikson (USGS) provided Cardiff State Beach wave hindcast data. Bradley Nussbaum (The Nature Collective) and Carolyn Lieberman (U.S. Fish and Wildlife Service) provided plant palette information. Burson Tang, Marie-Pierre Delisle, Joseph Lucey, Margit Maple, Michael Angelis, Nikos Kalligeris, Yeulwoo Kim, Brian Woodward, Kent Smith, Bill Boyd, Rob Grenzeback, Greg Boyd, Lucian Parry and CEE 129L students participated in field observations that made this dissertation possible. Critically, I would like to thank the funders that made this research possible. A special thank you goes to the California Coastal Commission for its long term monitoring support (17-005). Additionally, this work was supported by the California Department of Parks and Recreation Division of Boating and Waterways (C1670006), USACE Contract W912HZ-14-2-0025, UCLA Cota-Robles Fellowship, the Robert L. Wiegel Scholarship for Coastal Studies, the UCLA Center for Diverse Leadership in Science, Anchor QEA, and The Barbra Streisand Foundation. Thank you to Bob Guza, Michele Okihiro, and Kathleen Ritzman who secured funding to facilitate the valuable Coronado field observations. Finally, the greatest thank you to my advisor Timu Gallien, without whom none of this would have been possible. Thank you for

introducing me to coastal engineering and for all of your mentorship and endearing support throughout the course of my graduate education.

VITA

2016 Branson, Oscar, Elisa A. Bonnin, Daniel E. Perea, Howard J. Spero, Zihua Zhu, Maria Winters, Bärbel Hönisch, Ann D. Russell, Jennifer S. Fehrenbacher, and Alexander C. Gagnon. "Nanometer-Scale Chemistry of a Calcite Biomineralization Template: Implications for Skeletal Composition and Nucleation." Proceedings of the National Academy of Sciences 113.46 (2016): 12934-12939.

2017 B.S. (Environmental Engineering), University of California, San Diego, La Jolla, California.

2018 Gallien, Timu W., Nikos Kalligeris, Marie-Pierre C. Deslisle, Bo-Xiang Tang, Joseph T.D. Lucey, and Maria A. Winters. "Coastal flood modeling challenges in defended urban backshores." Geosciences 8.12 (2018): 450.

2020 M.S. (Civil Engineering), University of California, Los Angeles, Los Angeles, California.

2020 Brandenberg, Scott J., Jonathan P. Stewart, Pengfei Wang, Chukwuebuka C. Nweke, Kenneth Hudson, Christine A. Goulet, Xiaofeng Meng, Craig A. Davis, Sean K. Ahdi, Martin B. Hudson, Andrea Donnellan, Gregory Lyzenga, Marlon Pierce, Jun Wang, Maria A. Winters, Marie-Pierre Delisle, Joseph Lucey, Yeulwoo Kim, Timu W. Gallien, Andrew Lyda, J. Sean Yeung, Omar Issa, Tristan Buckreis, and Zhengxiang Yi. “Ground deformation data from GEER investigations of Ridgecrest earthquake sequence.” Seismological Research Letters 91.4 (2020): 2024-2034.

2020 Winters, Maria A., Brian Leslie, Evyan B. Sloane, Timu W. Gallien. "Observations and preliminary vulnerability assessment of a hybrid dune-based living shoreline." Journal of Marine Sciences and Engineering 8.11 (2020): 920.

2021 Goulet, Christine A., Yongfei Wang, Chukwuebuka C. Nweke, Bo-xiang Tang, Pengfei Wang, Kenneth S. Hudson, Sean K. Ahdi, Xiaofeng Meng, Martin B. Hudson, Andrea Donnellan, Gregory A. Lyzenga, Scott J. Brandenberg, Jonathan P. Stewart, Timu Gallien, Maria A. Winters. "Comparison of Near-Fault Displacement Interpretations from Field and Aerial Data for the M 6.5 and 7.1 Ridgecrest Earthquake Sequence Ruptures." Bulletin of the Seismological Society of America 111.5 (2021): 2317-2333.

2023 Winters, Maria A., Michael A. Angelis, and Timu W. Gallien. "Hydromorphodynamic 1D and 2D Modeling and Observations of a Dune Breaching Event." Coastal Engineering, in preparation.

CHAPTER 1

Introduction

1.1 Coastal Flooding

Urban coastal flooding is a global humanitarian and socioeconomic hazard. Over 20 million people reside below present day high tide levels, and 200 million are vulnerable to storm flooding (Nicholls, 2011). Global mean sea levels are expected to rise between 0.38 m and 0.77 m, (Fox-Kemper, 2021). Regional trends show significant variability (Carson et al., 2016) and relatively modest sea level rise (i.e., 0.50 m) will significantly increase flood frequencies Hunter (2012). Global sea-level rise will increase the frequency and severity of high water levels and flooding events (Wong et al., 2014). Over 30 days of annual flooding will be reached by 2050, and near daily flooding (under RCP 4.5) will occur by 2100 for many areas across the globe (Sweet and Park, 2014). Similarly, Taherkhani et al. (2020) suggest extreme flood frequency will double every 5 years, and by 2100 nearly 90 percent of the U.S. will experience near daily coastal flooding. This acceleration in coastal flooding will impact increasingly larger coastal populations (Nicholls et al., 2007; Crossett et al., 2013). Upgrading coastal defenses and nourishing beaches would reduce these impacts roughly by three orders of magnitude (Wong et al., 2014). Implementing coastal protection against increased flooding events far outweigh the costs of inaction, and without these protection measures, hundreds of millions of people will be displaced (Wong et al., 2014; Hinkel et al., 2018).

1.2 Coastal Flood Defenses

Traditional coastal engineering practice uses hard infrastructure such as sea walls, revetments, and rubble-mound dikes to armor vulnerable landward regions against extreme flooding, especially along highly energetic coastlines. Research on hard engineering structure design and critical runup and overtopping limits are found extensively in the literature (e.g., De Waal and Van der Meer, 1993; Pullen et al., 2007; van der Meer et al., 2016; Almarshed et al., 2020). Hard structures are effective at reducing wave impact and damage from extreme storm events; however, they may adversely impact the coast by limiting recreation opportunities, damaging coastal ecosystems and promoting passive, or long-term, erosion (Griggs, 2005; Pendleton et al., 2012; Temmerman et al., 2013). Additionally, they alter coastline accretion and erosion dynamics and are incapable of natural adaptation to evolving sea levels and energetic waves (Temmerman et al., 2013; Sutton-Grier et al., 2015).

Soft engineering structures (i.e., human-made dunes) are an alternative to these traditional designs. Artificial sand dunes, also referred to as beach berms, are sand structures that deflect high water or energetic wave events (Bruun, 1983; Edge et al., 2003; Gallien et al., 2015). These dune-like structures mitigate energetic wave forcing (Edge et al., 2003) and are widely deployed along the coasts of the United States, Europe, and Australia. In California, they are commonly used as seasonal coastal protection from winter wave storms (Edge et al., 2003; Gallien et al., 2014, 2015). They serve as a sediment reservoir for the lower beach and can be adapted to sea-level rise with additional sediment without requiring extensive redesign and expensive hard structure building (Almarshed et al., 2020). These structures may be particularly effective in highly urbanized, constrained coastal areas lacking space to accommodate other natural defense solutions (Temmerman et al., 2013; Gallien et al., 2015, 2018). Additionally, the capital and maintenance costs of soft or hybrid structures may be less than similarly sized hard structures (Basco, 1999; Rella and Miller, 2012; Glick et al., 2014; Almarshed et al., 2020). Soft dune structures present a number of potential manage-

ment challenges on highly energetic coastlines including emergency post-storm maintenance, nourishment and sand budget maintenance Notably, when energetic storm events coincide with high water inadequately designed dunes may fail in a single storm or tide cycle (Gallien et al., 2015).

Nature-based, or eco-engineering, living shoreline elements such as artificial reefs, marsh restoration, and native vegetated dune systems may be directly incorporated into hybrid designs (Temmerman et al., 2013; Sutton-Grier et al., 2015; Saleh and Weinstein, 2016; Morris et al., 2018). Living shorelines are a coastal engineering stabilization method to protect coastlines while at the same time restoring and providing natural habitats and coastal ecosystems (Temmerman et al., 2013). They utilize nature-based components, such as planting vegetation or restoring marshlands (Temmerman et al., 2013). Living shorelines represent an attractive sea-level rise adaptation strategy balancing coastal protection, available adaptation space, and ecological and recreational benefits. Dune restorations, a soft eco-engineering approach, are typically built for coastal defense and have the potential to follow and adapt with natural erosion and accretion patterns; they can be successful if properly maintained and nourished (Morris et al., 2018). Recently an eco-friendly dune stabilization pilot project utilizing mineral colloidal silica has shown potential promise for increasing dune resilience (D'Alessandro et al., 2020).

Vegetated sand dunes are successfully utilized in many countries to limit the effects of coastal erosion and flooding, from Europe (Dias et al., 2003; Matias et al., 2005; Nordstrom et al., 2009; Ceia et al., 2010; Garcia et al., 2010; Hanley et al., 2014; Karunarathna et al., 2018; Pagán et al., 2019) to the United States (Mendelssohn et al., 1991; Miller et al., 2001; Nordstrom et al., 2007; Sigren et al., 2014; Harris et al., 2020; Wernette et al., 2020). Vegetation has the ability to attenuate waves, absorb and reduce storm surge, and minimize backshore flooding (Temmerman et al., 2013; Sutton-Grier et al., 2015; Saleh and Weinstein, 2016; Morris et al., 2018), and several studies have been published on the benefits of vegetation in other living shoreline coastal protection projects, such as wetlands and mangroves

(Temmerman et al., 2012; Zhang et al., 2012; Temmerman et al., 2013; Morris et al., 2018). Additionally, it has been found that vegetation incorporated into beach dunes can dissipate wave energy and reduce dune erosion (Silva et al., 2016; Odériz et al., 2020). High-energy and urbanized coastlines, such as those in southern California, would benefit from hybrid dune-based living shoreline structures that provide the necessary coastal protection in the available footprint while simultaneously enhancing the ecological and recreational aspects of public beach spaces.

Larger grain sizes such as cobbles represent an intermediary on the continuum of soft (sand) to hard (e.g, revetment, sea wall) structures. Cobble ($\sim$ 70-300 mm) naturally occurs on west coast beaches, are resilient to large wave events (Everts et al., 2002) and have been considered as a superior backshore armoring method (Allan and Komar, 2004; McCall et al., 2014). Komar and Allan (2010) report on a large composite dune at Cape Lookout State Park that consisted of geotextile bags, cobble and sand and found that despite significant construction flaws (low cobble elevations along portions of berm), it has successfully protected the backshore at a lower cost than a traditional revetment. A cobble "mattress" (berm) was installed in September 2000 at Surfer's Point in Ventura, California as a part of a managed retreat program. Generally, the project has been considered a success and Phase 1 was completed in 2011 (Kochnower et al., 2015); however, no scientific literature has been published summarizing the findings of berm stability. Limited field observations fundamentally limit our understanding of cobble stability and transport (Dickson et al., 2011; Matsumoto et al., 2020). Recently, high resolution dynamic cobble berm revetment laboratory experiments have been conducted by Blenkinsopp et al. (2021) and Foss et al. (2023), and field experiments by Bayle et al. (2021) and Bayle et al. (2023).

1.3 Hybrid Structures

Hybrid coastal structures combine the strengths of both the soft and hard structures to better defend against coastal flooding (Boers, 2012). Typically, for hybrid dunes, these structures consist of a static, hard structure, such as a wall, rubble mound, dike, or revetment buried and covered with a dynamic sand dune. The 'soft' portion of the structure (vegetation, sand) provides protective benefits (i.e., reducing flow velocities, minimizing transport) and adapts to coastal forcing, while the hard structure provides traditional protective measures. The work on hybrid structures is highly limited. There are many types of hybrid coastal protection structures (Temmerman et al., 2013; Morris et al., 2018); this work focuses on the definition by Boers (2012) of a hybrid structure: a hybrid coastal approach is a combination of sand dunes with a hard structure that acts as a flood defense. The Cardiff Living Shoreline is defined as such given that it is a sand dune with an internal revetment.

There are few published case studies of hybrid dune structures in the literature, with only limited examples in North America and Europe (Almarshed et al., 2020). In Europe, hybrid coastal protection has been utilized across the North Sea coast of The Netherlands. Voorendt et al. (2015) examined two Dutch structures, Katwijk aan Zee and Noordwijk. The Katwijk structure is an engineered dune with an armored rubble-mound dike core, and additionally incorporates a parking garage in the lee of the structure (Voorendt et al., 2015). Noordwijk, is a a wide dune with a dike core to protect from coastal flooding (Stronkhorst et al., 2012; Voorendt et al., 2015). In the United States, examples of hybrid protective coastal structures have been implemented along the East Atlantic and Gulf Coasts. A buried seawall in a dune system protects coastal infrastructure in Dam Neck, Virginia (Basco, 1999). A rubble-mound core dune structure in Maui, Hawaii, USA protects a coastal wastewater reclamation plant (Boudreau et al., 2018).

A relic seawall buried by a sand dune in Bay Head, New Jersey has been the focus of numerous observational and modeling efforts. There have been several studies modeling

and investigating the hydrodynamics and morphodynamics of this particular buried seawall, and potential advantages over typical sand dunes in the area (Nederhoff et al., 2015; Walling et al., 2016; Smallegan et al., 2016). Overall, the hybrid structure was found to have resulted in less overwash and damage to the structures behind it compared to a similar sand-only dune which was breached in the neighboring community Mantoloking during Hurricane Sandy in 2012 (Irish et al., 2013; Walling et al., 2016; Nordstrom and Jackson, 2018). Of note, Walling et al. (2016) investigated the damage to the oceanfront residential structures of Bay Head, New Jersey, and its neighboring community Mantoloking which is protected by a sand dune. The study found that the structure distance from the waterline and the beach width and steepness influenced the amount of damage more than whether the protection was a dune or buried seawall.

In 2019, a novel hybrid dune-based living shoreline was constructed in Southern California which has substantially reduced the vulnerability of critical infrastructure (i.e., Pacific Coast Highway 101) to coastal flooding (Winters et al., 2020). Although beach morphology and erosion of sand-fronted hard structures have been addressed in the literature, the impact of hybrid structures on backshore vulnerability are critically lacking. The paucity of design guidance is identified as a fundamental coastal engineering challenge (Almarshed et al., 2020).

1.4 Dune Modeling

Dune erosion modeling is a classic coastal engineering problem and work spans over fifty years, from the work done by Edelman (1968) to present-day modeling utilizing modern numerical models (e.g., Schweiger et al. (2020); Cohn et al. (2021); Simmons and Splinter (2022); Hovenga et al. (2023)). Numerous empirical, analytical and numerical models have been developed to predict morphological dune response to elevated water levels and storms.

Two general dune erosion models exist: the equilibrium profile and the wave impact approach. The first type utilize the 'equilibrium profile' concept (Bruun, 1954a), where

beach profiles evolve to an equilibrium state. The application of the equilibrium profile to dune erosion during a storm event was applied by several models that followed (Edelman, 1968, 1972; van de Graaff, 1977; Vellinga, 1982; Kriebel and Dean, 1985; Kriebel, 1991). Later equilibrium analytical models expanded to include additional variable dependencies such as profile width and breaker depth (Hughes and Chiu, 1981; Kobayashi, 1987; Kriebel, 1991), but are time-independent and over-predict dune erosion (Larson et al., 2004). Equilibrium models that have a water level time dependency (i.e., the water level changes in time) include the model SBeach and others (e.g., Dette and Uliczka, 1987; Larson and Kraus, 1989). SBeach lacks process physics descriptions (van Rijn, 2009), and is limited to simple one-dimensional transects with normally incident waves (Kobayashi, 2009). Although these studies serve as a basis for modeling and understanding dune erosion, they and the Bruun rule are a "one-model-fits-all" with highly restrictive assumptions such as there must be no net longshore transport or accretion, that there is a depth of closure, that continental shelf slope does not affect shoreline retreat rate, and that beach profiles will maintain original shore-normal geometry and only translate upward with higher water levels (Cooper and Pilkey, 2004). These restrictions and simplistic assumptions make it inapplicable to a wide variety of complex coastal environments (Cooper and Pilkey, 2004).

The second model type, the wave impact approach, has been used to consider dune erosion (e.g., Fisher and Overton, 1985; Nishi and Kraus, 1997). The wave impact theory was initially validated by several wave-tank experiments (Fisher et al., 1987; Overton et al., 1988, 1990; Kraus and Smith, 1994; Overton et al., 1994). These previous studies are limited to a local, single beach transect; however, a wave-action model developed by Larson et al. (2004) partially addressed this by allowing both spatially and temporally large datasets. The model combines impact wave theory with sediment volume conservation. It has been used successfully in predicting long time-scale dune erosion (years to decades) because it is insensitive to numerical instabilities and calibration parameters, and does not require offshore bathymetry, unlike newer numerical models like XBeach (Splinter and Palmsten,

2012). However, it may not be adequate on coasts with alongshore variation (Roelvink et al., 2009).

1.4.1 Numerical Models

Various numerical models have been created to predict beach and dune erosion, and can include modeling of more complex hydromorphodynamic interactions. Numerical models have been used mostly to model extreme events on individual storm time scales (e.g., Roelvink et al., 2009; McCall et al., 2010; Harter and Figlus, 2017). CSHORE is a one-dimensional numerical coastal response model that is applied to cross-shore transects (Kobayashi, 2016). Its main components are a combined wave and current model based on a time- and depth-averaged continuity equation, wave-action (energy) and roller energy equations, and a time-averaged sediment transport model for both suspended and bed load (Kobayashi, 2016). CSHORE has been successfully utilized in wave flume experiments and on beaches on the East Coast and Europe (e.g., Kobayashi and Jung, 2012; Do et al., 2016; Quan and Kobayashi, 2015; Harter and Figlus, 2017; Kobayashi et al., 2018; Payo et al., 2020). More recently, CSHORE was applied to a wave dominated coast with limited success (Kalligeris et al., 2020).

XBeach is an open-source lagrangian based non-linear shallow water model that is utilized to simulate sandy coast hydrodynamic and morphodynamic processes within domains on the order of kilometers in size and at time scales on the order of individual storms (Deltares, 2018). XBeach has been applied and validated in numerous wave-flume laboratory experiments (Roelvink et al., 2009; Williams et al., 2012; Palmsten and Splinter, 2016; Berard et al., 2017; Elsayed and Oumeraci, 2017; Do et al., 2018; Roelvink et al., 2018; Masselink et al., 2019; Schweiger and Schuettrumpf, 2021). XBeach has also been used extensively to model dune erosion in Europe (de Winter et al., 2015; Harley and Ciavola, 2013; Karunarathna et al., 2018; Schweiger et al., 2020; Athanasiou et al., 2022) and the Eastern and Gulf coasts of the United States (McCall et al., 2010; Passeri et al., 2018; Roelvink et al.,

2018; Schambach et al., 2018; van Ormondt et al., 2020; Cohn et al., 2021; Hovenga et al., 2023). In these storm-surge dominated environments it has been proven to have fair success in accurately predicting dune erosion (e.g. Dissanayake et al., 2014; Gharagozlou et al., 2020; Schweiger et al., 2020). However, XBeach is less successful in high-energy, wave-dominated environments like the Pacific (Kalligeris et al., 2020). Work is needed applying and validating XBeach to wave-dominated coasts, especially in two-dimensions to resolve alongshore wave field variability (Kalligeris et al., 2020). A key benefit of utilizing a numerical model with 2D capabilities is that alongshore movement of sediment on the coastline can be resolved, a limitation of previous analytical models, which are only applied on 1D cross-shore transects.

XBeach and CSHORE have been extended to model beaches with hard substrate structures. CSHORE has the capability to handle sand-covered impermeable hard structures as well as rubble-mound structures (Johnson et al., 2012; Kobayashi et al., 2018; Almarshed et al., 2020). Recently, Payo et al. (2020) utilized CSHORE on a mixed gravel-sand beach to predict longshore sediment transport. XBeach has also been implemented to model storm impacts on impermeable hard structures covered by sand (e.g., Muller et al., 2017; Nederhoff et al., 2015). It has also been extended to XBeach-G to model the response of gravel beaches and barriers during a storm (McCall et al., 2014). XBeach-G includes wave-by-wave modeling of the surface elevation and depth-averaged flow, infiltration and exfiltration through permeable gravel beds with a groundwater model, and modeling of the bed load transport to predict bed level changes (morphology) (McCall et al., 2014, 2015).

Despite extensive dune erosion modeling efforts, only extremely limited information regarding the construction, design and efficacy of artificial dunes is presented in the literature. FEMA guidance, known as the 540 rule, suggests 540 ft^2 (50 m^2) of sand in the frontal half of a dune above the 100-year still water level (SWL) elevation is required to resist the 100-year storm, an order of magnitude greater than typical constructed west coast dunes (Gallien et al., 2015). This guidance was developed for storm surge (hurricane) dominated coasts where a sustained surge of $\sim$5 m is expected for hours and has little relevance to tide

and wave dominated erosion that occurs with minimal (∼10 cm) surge on the time scales of minutes to an hour. FEMA has advocated for a similar geometric method for the Pacific coast (Federal Emergency Management Agency (FEMA) of the United States, 2005), however, no guidance has been developed.

1.5 Beach-Dune System Resilience to Wave Runup and Overtopping

Protective coastal structures fail when coastal water overtops, or exceeds, the highest point (the crest) on a beach or structure, such as a dike or dune. Repeated overtopping can occur during large storm events and can flood urbanized backshores causing significant infrastructure damage. Sallenger (2000) developed a storm impact scale to assess dune vulnerability. The swash regime is characterized by the incident wave field interacting only with the beach foreshore, the collision regime occurs when waves runup onto the dune, the overwash regime begins when waves overtop the dune and finally, the inundation regime occurs when the backshore becomes flooded (Sallenger, 2000). During the collision regime, the incident wave field is directly interacting with the dune and may result in notching, avalanching, and ultimately dune crest lowering and failure.

Dune erosion is typically parameterized with marine forcing (i.e., water level, wave characteristics) and antecedent dune topography (e.g., Sallenger, 2000; Larson et al., 2004; Stockdon et al., 2007; Armaroli et al., 2012; Splinter et al., 2018). Critically, literature presents conflicting arguments on which design parameters affect resilience during large storm events. Sallenger (2000); Stockdon et al. (2009); U.S. Army Corps of Engineers (2008) suggest that high dune crest elevations limit overtopping and are associated with dune resilience. However, Hughes and Chiu (1981) suggest that dune height may be associated with increased erosion. Similarly, Judge et al. (2003) suggest that dune elevation is ineffective as a vulnerability predictor. The majority of studies have focused on storm surge dominated coasts

where high water levels interact with the dune over extended time periods (e.g., Judge et al., 2003; Stockdon et al., 2007; Plant and Stockdon, 2012). More recently Beuzen et al. (2019) considered dune erosion controls on wave dominated coasts and suggested the antecedent beach foreshore and berm are fundamental controls. A paucity of field data, particularly storm by storm observations limit model validation; high resolution beach foreshore data are critically needed in a variety of locations (Van Rijn, 2011; Kratzmann and Hapke, 2012). Collectively, this research highlights the critical importance of high resolution beach-dune observations and analysis on wave dominated coasts (Beuzen et al., 2019).

A simplistic method for considering potential flood risk in beach-dune protected communities involves adding maximum wave runup (e.g., Stockdon et al., 2006) to determine a total water level (TWL) and projecting this water level across backshore topography (e.g., Federal Emergency Management Agency (FEMA) of the United States, 2005; Heberger et al., 2009; Gallien et al., 2018). TWL methods rely upon static (bathtub) methods which project the maximum water level across the backshore and may significantly overpredict backshore vulnerability in dune defended urban backshores (e.g., Gallien et al., 2014). More recently, hydrodynamic modeling has been used to consider backshore vulnerability (Gallien, 2016; Elsayed and Oumeraci, 2016; Didier et al., 2019; Stokes et al., 2021). Although wave runup is generally well characterized, overtopping processes on dune defended coastal profiles have not been well validated (Stokes et al., 2021).

1.6 Scope of Doctoral Research

The need for tested and optimized coastal protective dunes specifically for wave-dominated coastlines (i.e., Pacific) stems from a fundamental knowledge gap regarding the current performance of these structures and their physical responses to various hydrodynamic and morphological conditions. The purpose of this research is to address several key gaps in the current state of knowledge including:

1. High resolution spatiotemporal observations of dune morphological evolution
2. Numerical modeling and validation of human-constructed dune erosion in wave-dominated environments
3. Quantitative backshore vulnerability assessment in wave-dominated, dune protected environments

This dissertation seeks to address the fundamental knowledge gaps through a mix of high-resolution observations and numerical modeling at two human constructed dunes sites, Cardiff State Beach and Naval Amphibious Base Coronado. This includes monitoring seasonal- and annual-term beach-dune evolution, as well as capturing extreme morphological change during highly energetic wave events. Two human constructed dune projects were observed and modeled: a dune based living shoreline at Cardiff State Beach, and the persistent sand dune at Naval Amphibious Base Coronado. Both sites have a historical record of coastal flooding and require permanent protection.

Monitoring, evaluating, and modeling these structures require a suite of topographic, bathymetric, and hydrodynamic data. Here, coastal hydrodynamic and dune morphological response during extreme storm events are modeled. This is performed using a mix of analytical (Larson et al., 2004) and numerical models (i.e., XBeach and CSHORE) and validated with field observations. The validated models are used to quantitatively characterize backshore vulnerability to current and future marine forcing and dune conditions.

Chapters 2 focuses on the construction monitoring and assessment of a novel hybrid structure. Chapter 3 focuses on the long-term/event based monitoring and modeling of the hybrid structure, while Chapter 4 details event based monitoring and modeling of a FEMA 540 like sand dune under failure conditions. Lastly, Chapter 5 provides a summary of all doctoral work and future research.

CHAPTER 2

Cardiff State Beach Living Shoreline

Construction of a novel hybrid dune-based living shoreline project at Cardiff State Beach in Encinitas, California began in November 2018 and was completed in May 2019. Current work focuses on observing and monitoring the evolution of this structure, as well as utilizing empirical and statistical models to evaluate the vulnerability of this site. Future research goals at this site includes modeling the hydromorphodynamics of this unique hybrid dune structure.

2.1 Study Site Description

Cardiff State Beach is a low-lying sand spit fronted by the Pacific Ocean and backed by San Elijo Lagoon located in northern San Diego County (Figure 2.1a). These low-lying lagoon systems are prevalent along the West Coast and are particularly vulnerable to sea level rise (Harvey et al., 2020). Highway 101 along Cardiff State Beach has been flooded and damaged numerous times from extreme wave events, coastal erosion, and high tides (Moffatt & Nichol, 2015). The highway serves as a critical coastal transportation artery and has been closed over 40 times during energetic wave events (Moffatt & Nichol, 2015). The California State Coastal Conservancy and Ocean Protection Council were the principal funders of a large living shoreline project intended to protect Highway 101 until 2050, serve as a sea-level rise adaptation strategy, provide native dune habitat, and increase public access to the coast. The central protective feature is a novel hybrid sand-cobble-rock dune design. The dune is planted with native vegetation to limit aeolian transport, stabilize sediment, and enhance

ecological productivity.

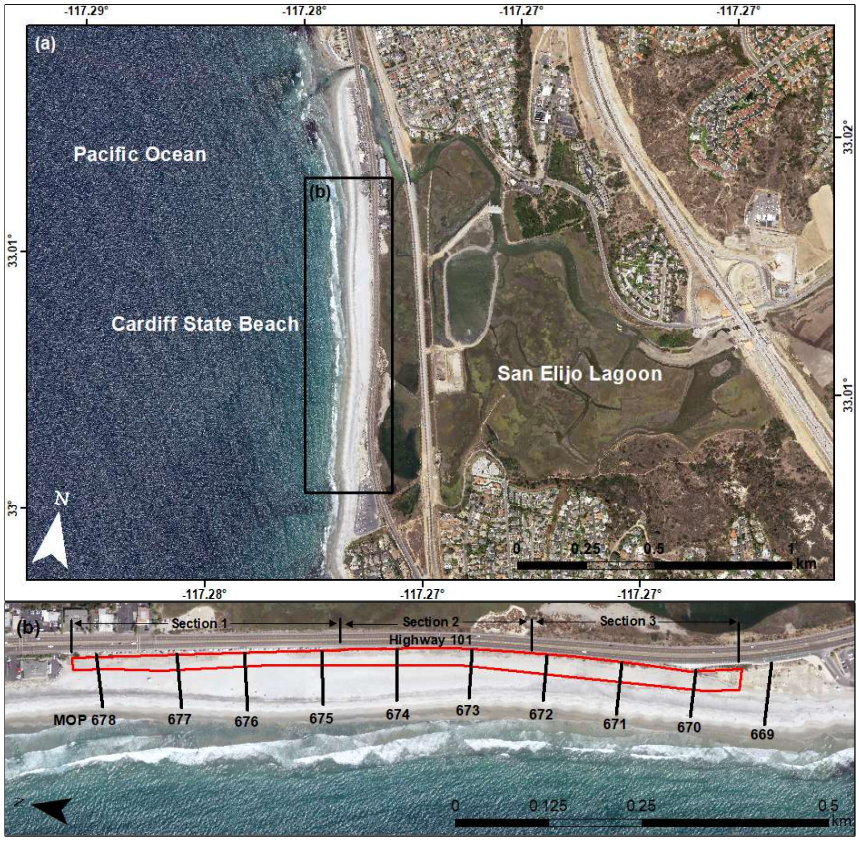

Figure 2.1: (**a**) Study site outlined in black of the Cardiff Living Shoreline project in northern San Diego County, California, United States. (**b**) Study site with red outline indicating project footprint, section labels indicating each stage of project construction, and black numbered lines indicating each Coastal Data Information Program (CDIP) Monitoring and Prediction (MOP) beach profile that was analyzed in this study (See Section 2.3 for details).

2.1.1 Hybrid Dune Description

The hybrid dune consists of buried rip-rap (remnant and imported) topped by a sand berm with a native cobble toe. It was constructed between November 2018 and June 2019 in a series of four phases: 1a, 1b, 2, and 3 (Figure 2.1b). Each construction phase began with a trench excavation and placement of geotextile lining to limit sediment settlement.

Buried rip-rap was placed on the landward slope of the trench into a revetment (Figure 2.2) and then filled with native dredged sand from the adjacent San Elijo Lagoon mouth. The rip-rap used for the revetment was a combination of existing rock (approximately 1.8 to 3.6 metric tons each), reuse of rock from a nearby source, and purchased quarry rock. Imported rock was sized to match the existing in-situ rock. The native sand grain size for San Elijo/Cardiff State Beach is approximately 0.16 mm (Ludka et al., 2019). The buried rubble-mound revetment was designed in accordance with the U.S. Army Corps of Engineers (2008) Coastal Engineering Manual and provides additional protection against undermining and flooding of Highway 101 should all top sand erode. A cobble berm was placed on top of this sand to serve as the toe of the dune (Figure 2.2). Similarly, the cobble toe behaves as additional fortification if the sand is removed during energetic events (Moffatt & Nichol, 2015). Finally, sand was placed atop revetment, sand fill, and cobble toe and contoured into mounds for planting native vegetation. In total, approximately 13,266 metric tons of rip-rap, 1682 m^3 of cobble, and 22,937 m^3 of native dredged sand was placed for the project.

Section 1 (Figure 2.1b), closest to parking at the northern entrance of the project, is characterized by a series of pedestrian access ways that run through the project, as well as native vegetation seeded from adjacent San Elijo Lagoon. The access ways are concentrated in the northern portion of the project to reduce foot traffic in the snowy plover nesting area further southward. Sections 2 and 3 (Figure 2.1b) were also seeded with native vegetation later after project completion. The goal of the planted vegetation is to prevent sand loss during overtopping events, promote aeolian accretion, and provide habitat. The entire project is backed by a sand fence adjacent to the highway to prevent wind-blown sand accumulation on the highway. Sand fences were also placed approximately every 15 m in section 1 and every 10 m in sections 2 and 3 in the southwest to northeast direction along the dune.

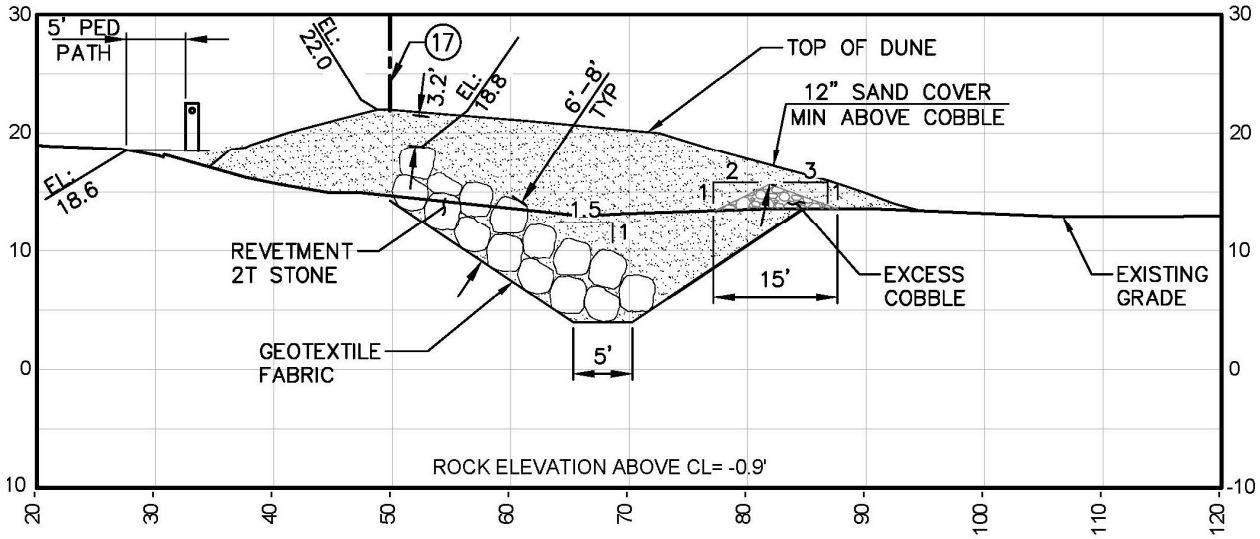

Figure 2.2: Original construction cross-section drawing of the Cardiff Living Shoreline Project. The dune is backed by large rip-rap, fronted by a native, smaller grain size native cobble toe, and topped with native sand. All measurements are in feet and elevations are NAVD88. Courtesy of Moffatt and Nichol, 2015 (Moffatt & Nichol, 2015).

2.2 Observations and Monitoring

2.2.1 Topographic and Bathymetric Data

Monitoring and modelling coastal dunes requires a suite of coastal topographic and bathymetric data. Beach topography data is required to determine beach and dune erosion and accretion at both long-term scales and shorter-time scales, such as before and after an erosive winter-storm event. Knowledge of nearshore bathymetry is essential in understanding sediment-transport dynamics, as well as determining potential wave-run up estimates, as it is foreshore slope dependent. Additionally, topobathy digital elevation models (DEMs) are required for numerical model grid creation.

Traditional beach and dune topographic surveying utilizes Global Navigation Satellite System (GNSS) surveys, and more recent techniques including real-time kinematic (RTK)

capabilities, to measure beach and dune elevation along transects on the order of every couple of hundred meters. However, these are labor and time-intensive, and do not resolve all detailed features of a beach-dune system, which are especially vital to flood modelling of these areas (Mitasova et al., 2005; Gallien et al., 2018). Light Detection and Ranging (LiDAR) surveying techniques are sufficient to resolve larger beach area topography and detailed features (Woolard and Colby, 2002); however, they are high-cost which limits the temporal coverage of the data (Andrews et al., 2002; Pagán et al., 2019). UAV surveying is low-cost, which allows higher temporal coverage, while providing similar high-resolution data quality as LiDAR, and is what is used to collect beach topography in this work. Required topography outside the UAV survey domains are obtained from United States Geological Survey LiDAR datasets available online (NOAA Office for Coastal Management, 2021). Nearshore bathymetry, from about 0 m to -8 m NAVD88, is collected via traditional RTK dolly and jetski transect surveying. Offshore bathymetry beyond -8 m NAVD88 depth is obtained from large-scale merged bathymetry data available from the National Oceanic and Atmospheric Administration.

Accurate coastal dune erosion modeling requires immediate pre- and post-storm beach topography data, and previous modeling work has been hampered by a lack of this data (Splinter et al., 2018). Modeling studies by Roelvink et al. (2009); McCall et al. (2010); Splinter and Palmsten (2012) utilized pre-storm data that preceded the event by months or years and required calibration (Splinter et al., 2018). All data utilized for modeling in this work have been collected hours to days before a storm event to ensure accurate modeling.

Finally, beach topography and nearshore and offshore bathymetry are merged to create a large DEM covering the domain of the dune or beach area of interest as well as an offshore depth that allows for correct wave shoaling based off storm-specific wave parameters and site bathymetry.

Beach and dune topographic data were derived from UAV photogrammetry to monitor project construction and seasonal sand volume changes. The surveys were conducted with

the goal of capturing the spatial placement and volumes of each substrate placement during construction and seasonal beach and dune evolution. Data collected spans from October 2018 to April 2020, capturing the entire construction phase and two winter erosion seasons (Table 2.1). Obtaining internal substrate dimensions (placement and grain size dimensions) is critical to future numerical modeling efforts. One pre-construction survey (10/9/2018), fourteen construction surveys, and six post-construction surveys were conducted and analyzed. Surveys post April 2019 captured the project's evolution and performance during its first winter erosion season. The monitoring project is ongoing, with quarterly surveys and pre/post storm event surveys planned through 2024.

A DJI (SZ DJI Technology Company, Shenzen, China) Phantom 4 Pro UAV with a 20 million pixel camera was used to capture aerial images. UAV flight missions were planned with the free DJI GS Pro application (SZ DJI Technology Company, Shenzen, China) for Apple iPad mini 4. The flight was planned as a 3D Map Area mission type, with latitudinal and longitudinal image overlap both set to 80%, flight altitude set to about 73 m above ground level, and image acquisition frequency of about 0.5 Hz for each survey. The altitude was chosen to obtain a final data resolution of about 2 cm/pixel.

A ProMark 700 GNSS receiver was used to geolocate ground control points (GCPs) using network Realtime Kinematic (RTK) position corrections from Scripps Orbit and Permanent Array Center (SOPAC) SIO5 base with a baseline of $\sim$18 km. GCP density is approximately 3 GCP/hectare, higher than the 0.5 GCP/ha recommendation for generating highly accurate digital elevation models (DEM) and orthomosaics (Coveney and Roberts, 2017). GCPs consist of 0.3 by 0.3 m wooden panels with a 2.54 by 2.54 cm center to easily identify and mark in images during photogrammetric processing.

Table 2.1: Survey dates, hydrodynamic conditions and beach volumes. Tide (NOAA gauge 9410230), significant wave height, and peak period (CDIP buoy 100) at time of survey are listed. Beach volumes in cubic meters are listed above mean sea-level (MSL, 0.774 m NAVD88) and the upper beach (>2 m NAVD88). Hyphens indicate no data available.

	Tide	$\mathbf{H_s}$	$\mathbf{T_p}$	**Section 1**		**Section 2**		**Section 3**	
Date	**(m)**	**(m)**	**(s)**	**MSL**	**Upper**	**MSL**	**Upper**	**MSL**	**Upper**
10/09/2018	0.39	1.46	12.5	87,665	48,601	60,390	34,984	53,330	27,269
11/28/2018	1.53	1.56	14.29	84,146	50,839	-	-	-	-
12/04/2018	0.02	0.44	12.50	68,396	41,976	-	-	-	-
12/11/2018	1.30	1.47	15.38	64,051	41,019	-	-	-	-
12/14/2018	1.08	1.34	14.29	66,375	40,723	40,615	23,216	-	-
12/17/2018	0.38	2.10	20.00	68,855	41,175	40,234	23,420	-	-
12/18/2018	0.23	1.87	16.67	68,062	41,156	39,391	22,607	-	-
12/19/2018	−0.44	1.57	15.38	65,945	39,826	37,479	21,795	-	-
01/10/2019	1.33	2.21	13.33	61,399	36,113	37,587	36,113	39,735	18,907
01/22/2019	0.187	1.37	10.53	50,563	28,792	28,586	15,645	32,681	16,094
02/01/2019	0.126	0.9	15.38	-	-	-	-	-	-
03/07/2019	1.06	1.26	11.11	-	-	31,455	17,401	-	-
03/22/2019	1.358	1.42	13.33	-	-	34,492	19,604	38,060	20,446
04/15/2019	−0.089	0.87	12.5	56,158	31,962	38,402	22,592	41,258	22,935
05/31/2019	0.385	1.36	14.29	63,932	34,103	45,477	25,669	50,803	28,400
08/28/2019	0.646	1.07	20.00	73,871	40,288	53,696	30,157	57,251	32,154
10/25/2019	0.173	0.72	9.09	73,375	39,967	52,130	30,087	54,743	32,046
12/12/2019	0.304	1.07	12.5	-	35,598	-	26,191	-	26,636
12/20/2019	0.365	0.93	11.76	61,451	34,223	40,831	24,320	44,845	26,254
04/30/2020	0.047	0.96	10.53	63,017	34,580	45,224	25,224	51,008	28,764

Structure-from-motion (SfM) software was utilized to generate topographical data products (e.g., DEMs) from UAV imagery data. Automatic photogrammetric image processing was conducted using Pix4Dmapper (version 4.4.12) software, from which georectified point clouds, orthomosaics, and digital elevation models were produced from the raw UAV images and ground control point x, y, z information (Figures 2.3 and 2.4). GNSS GCPs were used to

improve geolocalization accuracy and were imported into Pix4D, where the centers of each were manually identified in each UAV image they appeared. Pix4D utilizes binary descriptors to photo-match points (Küng et al., 2011). The matched points are then used, along with the image positions and orientations, to obtain the exact position (three-dimensional coordinates) and orientation of the UAV camera for every image. The three-dimensional points (point clouds) are interpolated to then form a triangulated irregular network (TIN), from which the digital elevation model and orthomosaic are obtained (Küng et al., 2011). The orthomosaic and DEM resolutions average about 2 cm^2 per pixel, with a projected coordinate system of WGS 1984 UTM Zone 11N, North American Vertical Datum of 1988 (NAVD88). All elevation values here, from both UAV-derived elevation products and water levels, are referenced to NAVD88 unless otherwise specified.

The dune crest was identified at the interface of the west and east flow directions. Delineation of dune geometries is required to assess vulnerability of the project to runup, overtopping, and high total water levels (TWLs), as well as to monitor erosion and movement of dune features. Autodesk (San Rafael, CA) AutoCAD 2020 was utilized to inspect and compare construction as-built data obtained as each portion of the dune was constructed (trench, revetment, cobble, sand).

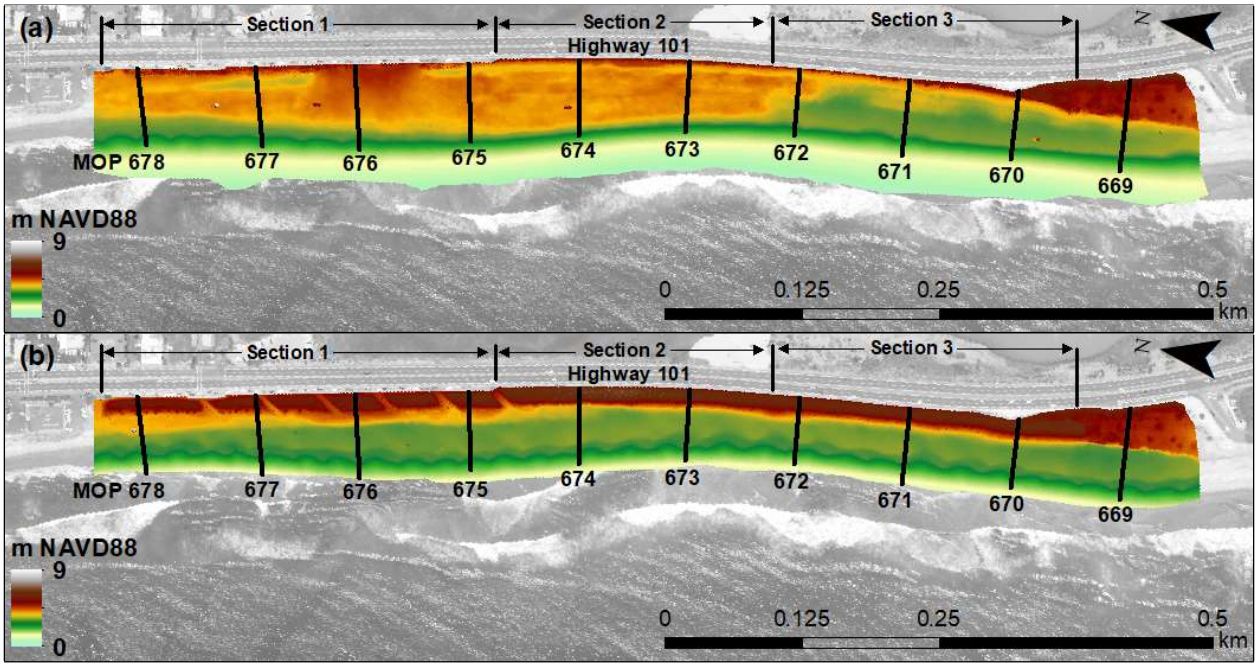

Figure 2.3: Pre-construction (**a**) and post-construction (**b**) digital elevation models derived from UAV photogrammetric surveys from 9 October 2018 and 28 August 2019, respectively. Section labels indicate each stage of project construction, and black numbered lines indicate each Monitoring and Prediction (MOP) beach profile that was analyzed in this study (See Section 2.3 for details).

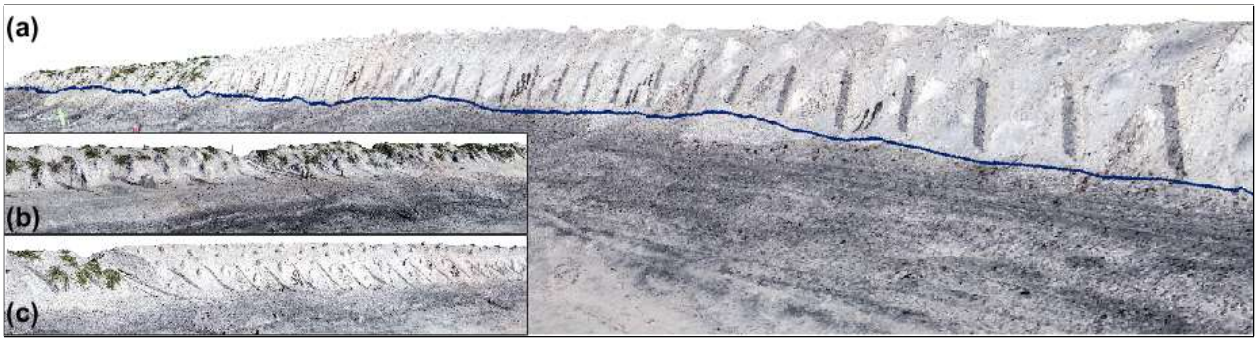

Figure 2.4: (**a**) Three-dimensional representation of living shoreline derived from UAV orthoimagery collected 20 December 2019 viewing northward. Blue line indicates toe delineation. (**b**) View looking southward on heavily vegetated section 1 with pedestrian access ways. (**c**) View looking southward on sections 2 and 3 with sand fences visible.

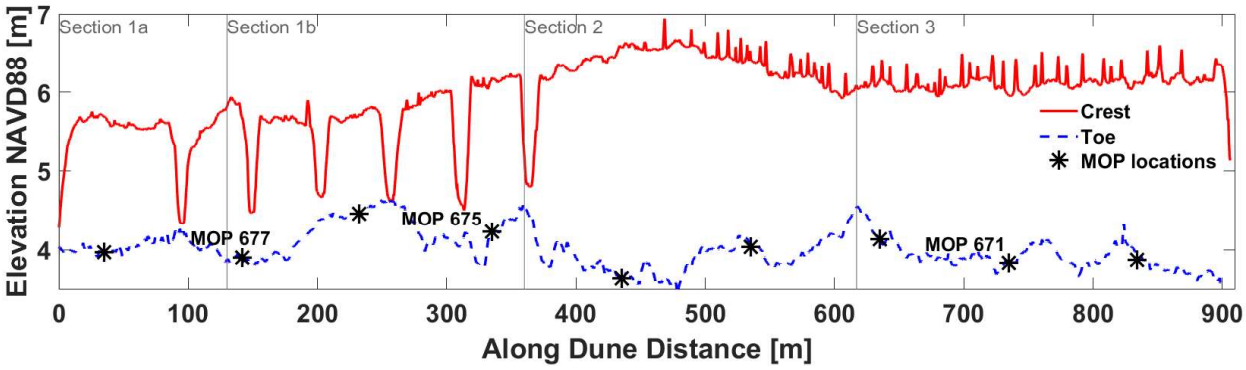

Figure 2.5: Dune crest (solid red line) and toe (blue dashed line) elevations estimated from 28 August 2019 UAV survey. Low crest elevations at about 4.5 m NAVD88 indicate pedestrian access way locations. Each section of the dune and MOP transect locations are labeled.

2.2.2 Dune and Beach Evolution

The final dune topography immediately post-construction is shown in Figures 2.3 and 2.4. It is approximately 900 m in length, with the crest varying from about 5.5 m in section 1 to 6.5 m in sections 2 and 3 (Figure 2.5). The dune toe elevation is about 4 m across

the length of the dune (Figure 2.5). Six full-beach photogrammetric UAV surveys were conducted post-construction to monitor topographic changes. From August 2019 to April 2020, the dune experienced negligible change, while the upper beach (∼2–3m NAVD88) experienced typical winter erosion (Figure 2.6a). Elevation change analysis was conducted on cross-shore profiles every 100 m along the beach, and three were selected to illustrate the range of changes. The northernmost profile, MOP 677, experienced the least erosion (Figure 2.6b), while MOP 675 experienced the most foreshore erosion, with the 2 m contour moving about 25 m landward (Figure 2.6c). Significant vegetation is observed in section 1, with profile MOP 677 experiencing about 11 cm of dense vegetation growth between December 2019 and April 2020 (Figure 2.6b). Monitoring of dune evolution is ongoing.

2.3 Vulnerability Assessment

2.3.1 Total Water Levels Estimation

The study site's vulnerability to 50 and 100-year water level events, both pre- and post-dune construction, was evaluated by estimating total water levels (TWL) from open coast water levels and wave runup estimated using the formulation from Stockdon et al. (2006). $R_{2\%}$ has been previously field validated (Stockdon et al., 2006; Fiedler et al., 2015; Melet et al., 2018), and widely employed in coastal hazard assessments (e.g. Federal Emergency Management Agency (FEMA) of the United States, 2005; Heberger et al., 2009; Gallien, 2016; Serafin et al., 2017; Vitousek et al., 2017; Melet et al., 2018).

Equation (4.1) shows the 2% exceedance of wave runup (Stockdon et al., 2006), where β is the slope, H_0 is the deep water significant wave height, and the deep water wave length, $L_0 = g/2\pi f_p^2$, is computed from the peak frequency, f_p.

$$R_{2\%} = 1.1 \left(0.35\beta(H_0 L_0)^{0.5} + \frac{[H_0 L_0 (0.563\beta^2 + 0.004)]^{0.5}}{2} \right) \tag{2.1}$$

Total water level is defined as the sum of the nearest the NOAA tide gauge (La Jolla, California, 9410230 (National Oceanic and Atmospheric Administration (NOAA), 2020)) observed water levels (OWL) and $R_{2\%}$ and is given by,

$$TWL = OWL + R_{2\%} \tag{2.2}$$

Hourly significant wave heights and peak frequencies at the 10 m depth were estimated from a 61-year wave hindcast obtained from the United States Geological Survey (Shope et al., 2020). Pre-construction beach foreshore slopes and crests were estimated from 10 years of monthly Cardiff State Beach topography data collected by Scripps Institution of Oceanography (Ludka et al., 2019). Both wave hindcast and beach elevation values were estimated along ten shore-normal transects at existing Monitoring and Prediction (MOP)

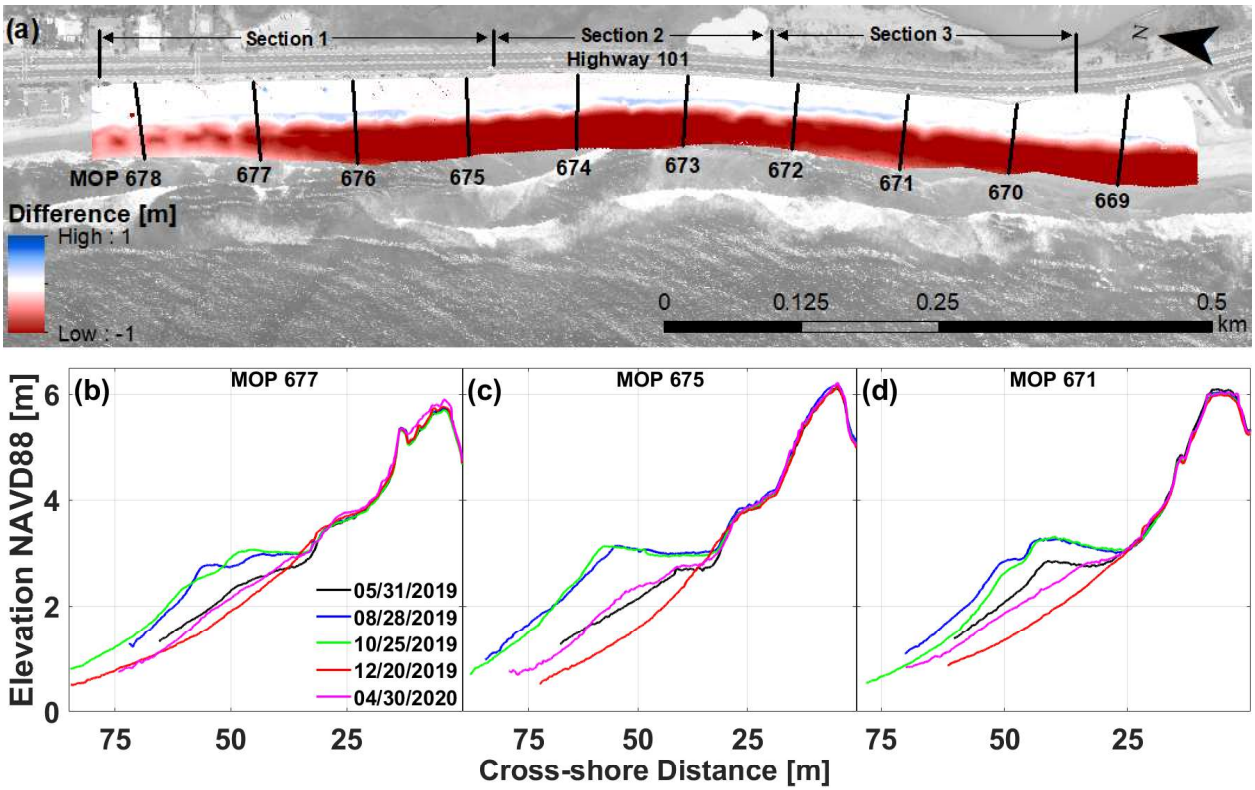

Figure 2.6: (a) DEM differences (color bar) from 8/28/2019 to 12/20/2019. Significant foreshore erosion is observed. MOP profiles 677 (b), 675 (c), and 671 (d) are shown with an additional spring survey (4/30/2020) highlighting significant vegetation growth along MOP677 (magenta).

profiles established by Scripps Institution of Oceanography Coastal Data Information Program (CDIP) program (O'Reilly et al., 2016). The MOP profiles, here MOP D0669 through MOP D0678 (referred as MOP 669 to MOP 678 in this study), are spaced every 100 m alongshore, from the southern to northern end of the project site, as shown in Figure 2.1b. Annual and seasonal mean foreshore slopes of each of the ten MOP lines were calculated from 0 m NAVD88 (∼MLLW) to the beach crest. Slopes of profile data that did not reach 0 m NAVD88 were calculated from the closest available point. Seasonal foreshore slopes were used to calculate total water levels in each corresponding season.

Hourly total water levels were estimated for MOP profiles 669 to 678 from 1948 to

2008, and annual maxima extracted. These annual maxima were fit to the Generalized Extreme Value (GEV) distribution to minimize the negative log-likelihood (e.g. Federal Emergency Management Agency (FEMA) of the United States, 2005; Huang et al., 2008; Xu and Huang, 2011). The GEV distribution can be utilized to statistically model and estimate the probability of extreme events (Coles et al., 2001) and has been widely used to quantify the frequency of extreme wave and total water level events (Muir and El-Shaarawi, 1986; Tawn, 1992; Ruggiero et al., 2001; Huang et al., 2008; Serafin and Ruggiero, 2014; Vitousek et al., 2017). Specifically, the GEV distribution should be used to estimate extreme water levels along open-coastlines such as the Pacific (Federal Emergency Management Agency (FEMA) of the United States, 2005; Huang et al., 2008). The annual maxima (n = 61) were fit to the GEV distribution minimizing the negative log-likelihood to estimate the 50- and 100-year TWL values.

The number of storm events, defined as consecutive hourly TWL events that occurred less than 72 h apart, that exceeded the pre-construction annual mean beach crest and post-construction dune crest were calculated, as well as the number of TWL events that reached and therefore would interact with the post-construction dune toe. These hourly total water levels were then estimated with the addition of sea-level rise. Sea-level rise projections from the Intergovernmental Panel on Climate Change (IPCC) for representative concentration pathway (RCP) 4.5, a moderate projection, and RCP 8.5, an extreme projection with little reductions in carbon emissions, were utilized (Church et al., 2013). The 61-year TWL time series, assuming wave stationarity, was superposed on the RCP 4.5 and 8.5 sea-level rise curves from 2020 to 2080 to obtain a projected TWL time series. Annual maxima and hourly TWL values were compared with dune toe and crest elevations to assess backshore vulnerability.

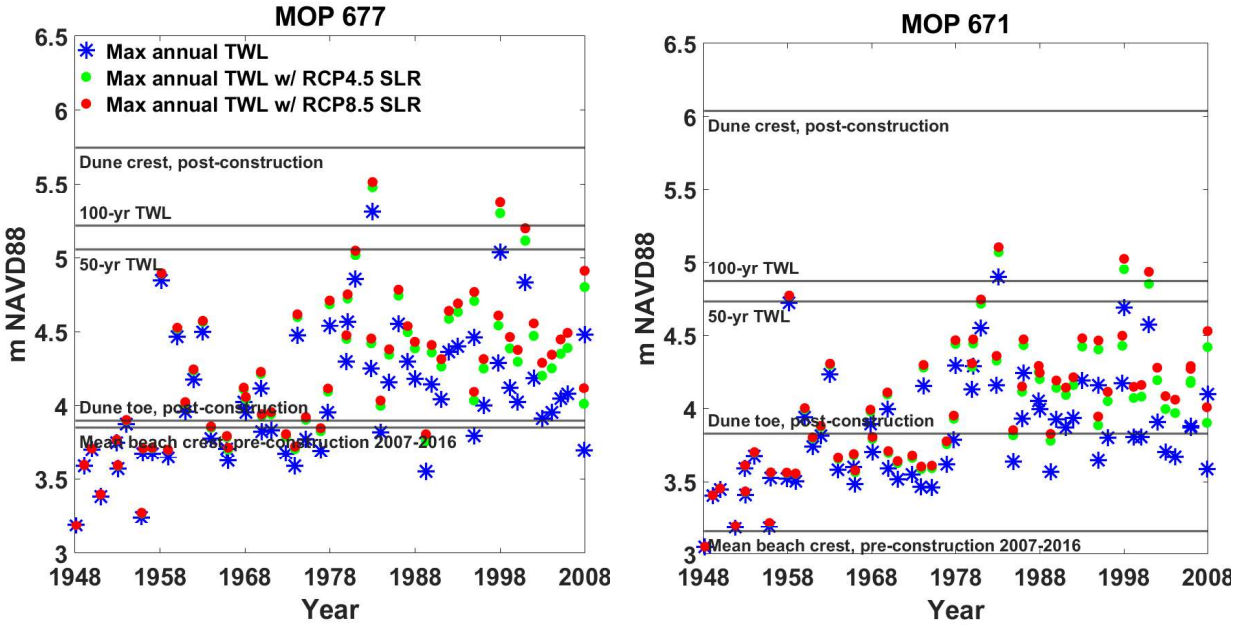

Figure 2.7: Annual maximum total water level (TWL) values from 1948 to 2008 for each MOP line without sea-level rise (blue markers). TWL time series superposed to 2020 to 2080 with projected sea-level rise for RCP 4.5 and 8.5 added (green and red markers, respectively). Black horizontal lines indicate values of mean beach crest pre-construction, dune crest and toe post-construction, and the 50 and 100-yr TWL values.

2.3.2 Vulnerability to Extreme Total Water Levels and Sea-level Rise

MOP transects 671 and 677 were previously identified (i.e., historical reports of wave overtopping and erosion) as profiles of interest to explore potential sea level rise vulnerability. MOP 671 is located in a wave focusing area and has the lowest annual mean beach crest height pre-construction of all ten profiles, and MOP 677 is a region of the beach historically known to overtop and flood Highway 101. The time-averaged beach crests pre-construction of MOP 671 and 677 are 3.16 and 3.85 m NAVD88, respectively. Sixty annual maximum TWL values exceeded the MOP 671 mean beach crest and 38 exceeded the MOP 677 mean beach crest value (Figure 2.7). Post-construction, the dune crest at MOP 671 and MOP 677 was 6.04 and 5.75 m, respectively, and no annual maximum TWL values exceed these dune crest values (Figure 2.7).

The TWL value associated with the 50-year and 100-year return periods derived from the generalized extreme value (GEV) distribution for MOP 671 are 4.73 and 4.87 m NAVD88, respectively (Figure 2.7). These values for MOP 677 are 5.06 and 5.21 m NAVD88, respectively (Figure 2.7). The new dune's crest heights are substantially higher than the 100-year event (Figure 2.7). TWLs are expected to interact with the dune toe (i.e., 'collision regime' (Sallenger, 2000)). Schubert et al. (2015) and Gallien et al. (2015) suggested that dune failure may occur through sustained dune toe interaction without ever overtopping the dune. The dune toe values for MOP 671 and 677 are 3.83 and 3.90 m NAVD88, respectively (Figures 2.5 and 2.7.) Results suggest that with the superposition of sea level rise from 2020–2080, the dune toe would interact with water levels for a total of 268 h at MOP 671 and 508 h at MOP 677, or 4.4 and 8.3 h per year on average, respectively.

The first winter season was relatively quiescent from a wave energy perspective. Although the living shoreline crest height is substantially above the expected stationary 100-year total water level event, this does not imply the dune may not experience substantial erosion. Critically, a dune may fail from sustained collision through mass wasting (i.e.,

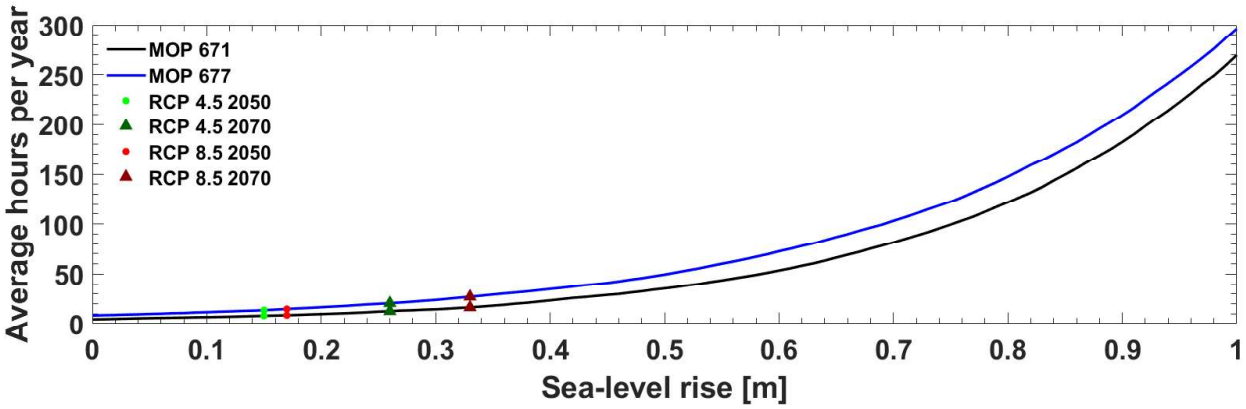

Figure 2.8: Average hours per year of dune toe interaction (collision hours) for MOP lines 671 (black curve) and 677 (blue curve) with added sea-level rise projected under RCP 4.5 and 8.5 at 2050 (circles) and 2070 (triangles).

notching, undercutting, avalanching) (e.g. Sallenger, 2000; Erikson et al., 2007; Palmsten and Holman, 2011; Schubert et al., 2015; Gallien et al., 2015)). If the 61-year TWL time series were repeated and projected from 2020 to 2080 (refer to Section 2.3), the dune toe would interact with the TWL on average about 4.4 h/year at MOP 671 and 8.3 h/year at MOP 677 at current sea levels (Figure 2.8). This would represent approximately 2–4 erosive storm events per year. From a management perspective, this level of exposure would likely be tractable. Periodic San Elijo lagoon mouth beneficial dredging reuse as dune renourishment would be able to augment the beach–dune system subsequent to energetic winters. However, as sea levels increase, dune toe-swash interaction increases exponentially (Figure 2.8), which has significant dune management implications. Even at RCP 4.5, by 2050 and 2070, the collision regime is 10–20 h/year for both MOP profiles (Figure 2.8). If this set of ∼5–10 storms arrived in succession during an active winter season, dune maintenance may be impossible and lead to substantial erosion or breaching. At 2070, fifty years from project construction, the more extreme sea-level rise scenario RCP 8.5 increases the average interaction hours to about 30 h/year (Figure 2.8). Notably, this analysis considered only sand elevation. Substantial vegetation is present on section 1 of the dune that may promote

resilience beyond the sand structure alone.

CHAPTER 3

Cardiff Dune Modeling

Throughout the five years of quarterly and storm event monitoring at Cardiff State Beach, mild erosion events were captured almost annually. During the first three years post-project construction, no extreme storms or flood events occurred. In January 2023, a historic energetic wave and storm event hit Southern California, resulting in widespread flooding, erosion, and damage. The January 6 storm event tested the Cardiff Living Shoreline for the first time against extreme events. Observations, of both long-term and short-duration extreme storm events, of hybrid coastal protection structures are exceedingly rare and are critically needed to inform coastal adaptation efforts (Almarshed et al., 2020). Work has been conducted to test morphological model initial skill at predicting event erosion for a hybrid structure.

3.1 Multi-substrate Observations and Modeling

Multi-substrate dunes have been investigated within a laboratory context. Figlus et al. (2015) conducted small scale physical model laboratory experiments to compare erosion of core-enhanced dunes with three different core types: a rock revetment, a clay core, and a reinforced concrete T-wall core. The study found the buried rock revetment slowed the rate of dune scarp retreat and resulted in less dune crest erosion compared to the sand dune only case. Kobayashi and Kim (2017) also performed small scale physical experiments to test four different protection structures, including a sand-buried rock seawall, against overtopping and overwash. The study revealed that the buried seawall initially behaved as a sand dune, with the sand decreasing roughness and increasing overtopping slightly. However, as the seawall

began to emerge, the structure behaved like a seawall only and did not retain any dune like properties. Additionally, the sand covering reduced settlement of the rock seawall. van Thiel de Vries (2012) investigated the morphodynamics of an engineered revetment-fronted dune. Notably, flume experiments present extensive scaling challenges (Van Rijn et al., 2011). Currently, coastal morphological models cannot resolve the simultaneous morphodynamics of multiple substrate sizes (Almarshed et al., 2020).

Multi-substrate modeling has been approached from both an empirical and numerical perspective. Various empirical runup and overtopping formulations exist for hard seawalls and rubble-mound dike structures (Almarshed et al., 2020). Such formulations include Owen (1980), Van der Meer and Stam (1992), De Waal and Van der Meer (1993), Ahrens et al. (1993), Van der Meer (2002), and van der Meer et al. (2016). Recently, a runup formulation using high resolution lab and field observations was developed by Blenkinsopp et al. (2022) to predict wave runup on composite beaches and dynamic cobble berm revetments. Notably, there are major limitations in representing all the relevant physical processes to wave overtopping, for example, porous flow in permeable sections of a structure, or the dynamic response of a structure such as the deformation of a rubble-mound during wave attack (Almarshed et al., 2020).

From a numerical perspective the cross-shore, 1D coastal numerical model CSHORE has previously been utilized to investigate the morphodynamics of a buried seawall structure in the laboratory (Kim et al., 2017; Kobayashi and Kim, 2017). The morphodynamics of four different structures were investigated: a berm-fronted beach with no dune, a sand dune, a rock seawall, and a dune buried seawall. In the study, CSHORE was extended to resolve sand transport on and inside the porous seawall structure on a fixed filter layer. Of note, in the seawall case only, CSHORE over-predicted erosion immediately fronting the seawall (at the toe) and under-predicted dune face erosion and sand deposition inside the porous seawall. Sand inside the porous structure was more mobile than expected (Kobayashi and Kim, 2017). Additionally, the assumption of no seawall settlement may have impacted these predictions

(Kobayashi and Kim, 2017). There was overall higher model agreement for the seawall with sand cover than the seawall alone possibly due to lower amount of settlement in this case due to the sand cover fill. However, CSHORE still predicted more erosion than observed in the foreshore. Additional experiments and field observations are needed to confirm CSHORE predictive skill in these hybrid structure cases (Kobayashi and Kim, 2017).

XBeach has also been utilized to simulate morphodynamics of sand and dune covered hard structures. van Thiel de Vries (2012) utilized physical model data from Steetzel (1987) large flume experiments to extend the capabilities of XBeach and include non-erodible dune revetments and seawalls. In van Thiel de Vries (2012), XBeach was found to predict the evolution of the erosion and runup of seawall-fronted dune reasonably well; however, the scour that formed in front of the structure was underestimated possibly due to missing wave physical processes in the model. Overall, it was found that the dune erosion above the revetment was reasonably predicted if the short wave runup distribution is included in the model formulation. Nederhoff et al. (2015) tested XBeach for skill at reproducing the erosion of the Bay Head, New Jersey buried relic seawall. The model, with calibration, was able to reproduce the cross-shore and alongshore effects of the hard seawall that were observed in the field. (Nederhoff et al., 2015). Smallegan et al. (2016) additionally utilized XBeach to investigate the morphodynamics of the Bay Head buried seawall during Hurricane Sandy, and found that the structure was advantageous over the dune-only case. Muller (2017) and Muller et al. (2018) evaluated potential hybrid protection structures to prevent further raising of a seawall in Galveston, Texas and found that a hybrid measure could mitigate wave impacts.

Jamal et al. (2014) utilized and modified XBeach to better model course-grained beaches during accretive (low to moderate energy) conditions; however, McCall et al. (2014) noted that this modification may not be representative of gravel beaches during high energy storm events. The numerical model XBeach was extended in McCall et al. (2014) and McCall et al. (2015) to include XBeach-G, a model to simulate hydrodynamics and morphodynamics of

gravel beaches. It includes a non-hydrostatic pressure correction to resolve individual waves, a groundwater model with infiltration and exfiltration processes, and groundwater effects on bed load transport (McCall et al., 2014, 2015). Bergillos et al. (2016) tested XBeach-G on a mixed sand-gravel (MSG) beach in southern Spain for ability to reproduce post-storm beach topography, and presented Brier Skill Scores higher than 0.89 (a value of 1 being perfect model performance). Three different grain sizes predominately characterized the study site: sand, a fine gravel, and course gravel. All three grain sizes were tested in the model, and different values of the sediment friction factor and Nielsen's boundary layer phase lag parameters. The best model performance predicting the post-storm beach profiles was found assuming the D_{50} of the entire beach as the largest gravel grain size, which was consistent with prior studies that found morphodynamic response of the site is dominated by coarse gravel fraction (Bergillos et al., 2016). XBeach-G also showed high skill at simulating hydrodynamics (wave transformation, runup, and overtopping) at a gravel beach in Cornwall, England (Almeida et al., 2017). Few numerical model studies and field observations have been conducted on gravel and mixed sand-gravel beaches, and more are needed as hybrid coastal protection structures begin gaining attention.

3.2 Cardiff Observations

Uncrewed aerial vehicle (UAV) quarterly and storm erosion surveys have continued from 2020-2023, to monitor the project performance and beach/dune evolution. Despite moderately energetic winter events the first two winter seasons of 2018 and 2019, the next two (2020, 2021) winter seasons experienced higher wave energy (Figure 3.1), exposing the cobble berm toe one year, and even eroding most of it another (2020-2021) (Figure 3.2). In January 2023, Southern California experienced a historic energetic wave event, resulting in large-scale flooding, erosion, and damage across the coastline (Figure 3.3).

In January 2023, Southern California experienced a historic energetic storm (H_s ~4 m,

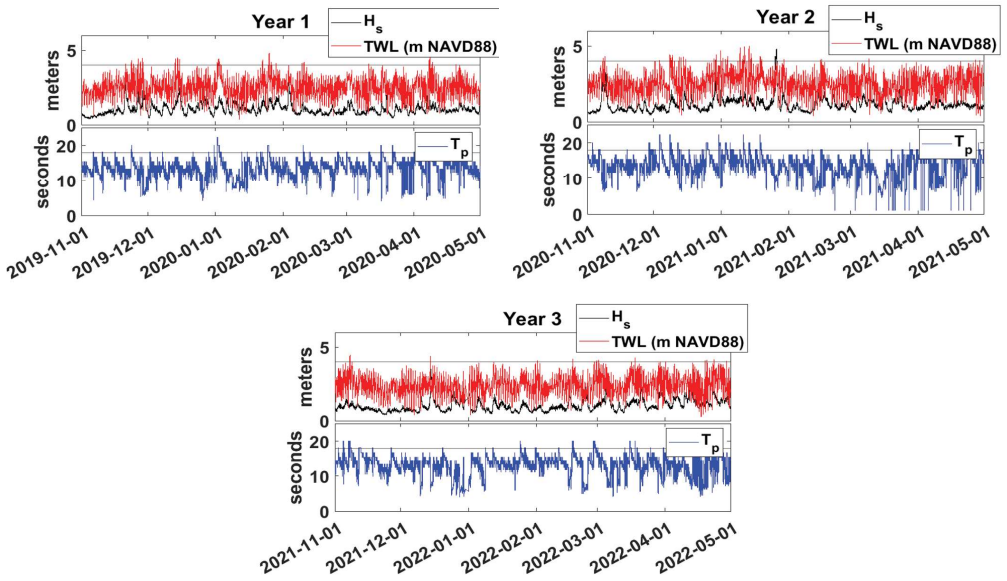

Figure 3.1: Winter 2020-2022 Cardiff beach offshore significant wave heights and total water levels. Black line indicates approximate dune toe elevation.

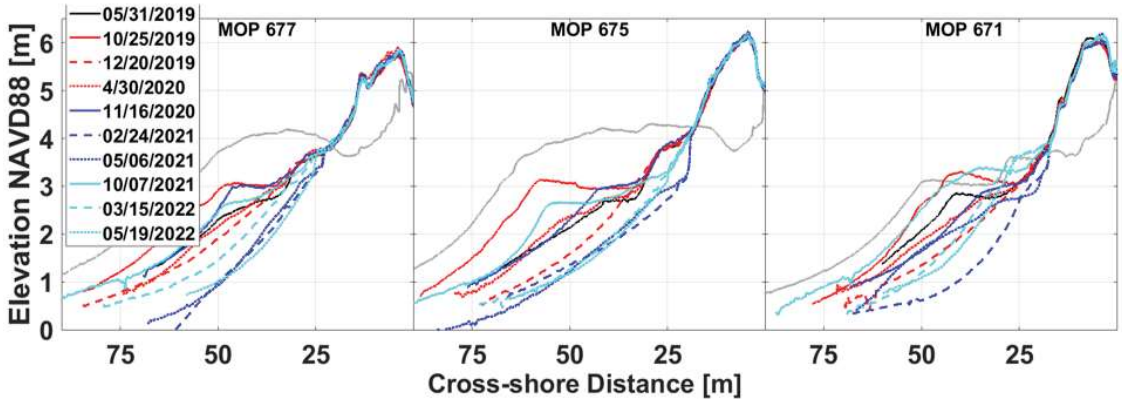

Figure 3.2: Winter 2020-2022 Cardiff beach and dune evolution

T_p ~20 s) which peaked on January 6. Cardiff State Beach experienced significant erosion of the hybrid dune structure and the buried cobble berm (Figure 3.4). Additionally, the dune structure experienced significant overwash onto the highway along the length of the dune.

A field campaign was undertaken from January 4 - 7, 2023, where topographical RTK and UAV surveys were conducted to measure pre-storm, during-storm, and post-storm topography and overwash extent. The survey conducted on January 6 took place after the peak of the storm had passed. An additional survey was conducted on January 18, 2023 to analyze additional erosion or short-term recovery of the beach. Nearshore bathymetry from ~0 m to -8 m NAVD88 depth was collected along shore-normal transects with a real-time-kinetic (RTK) dolly and jet ski survey on November 10, 2023. The transects were spaced at 100 m intervals along existing CDIP MOP profiles (O'Reilly et al., 2016). DEMs were generated in photogrammetric software Pix4D as described in Chapter 2.2.1. A bare earth digital terrain model (DTM) was created from the DEM by filtering cars, buildings, and other non-topographic objects that could create artificial flow obstructions and promote numerical instabilities.

The beach volume differences between January 4 and January 6 were estimated above four reference elevations. Volume losses above MSL, MHHW, and 2 m NAVD88 were 29%, 31%, 32%, respectively. The hybrid dune experienced a volume loss of about 6% above the dune toe (4 m NAVD88) post-storm. Observed foreshore erosion in the vertical ranged from ~1 to 1.5 m and ~18 to 25 m in the horizontal, with the largest differences seen at transect MOP 675 (dark pink to red, Figure 3.5). The dune toe experienced a loss of at least 1 m in the vertical at all three cross-shore locations, and by January 18th, after multiple energetic wave events, the toe experienced over 1.5 m of erosion at MOP 677 (Figure 3.5) and erosion continued until the April 20, 2023 survey. These were the largest beach changes and volume losses to date since the project construction. Notably, beach volume above 2 m NAVD88 increased after a nourishment along the length of the project dune toe in late May 2023, shown in Figure 3.7.

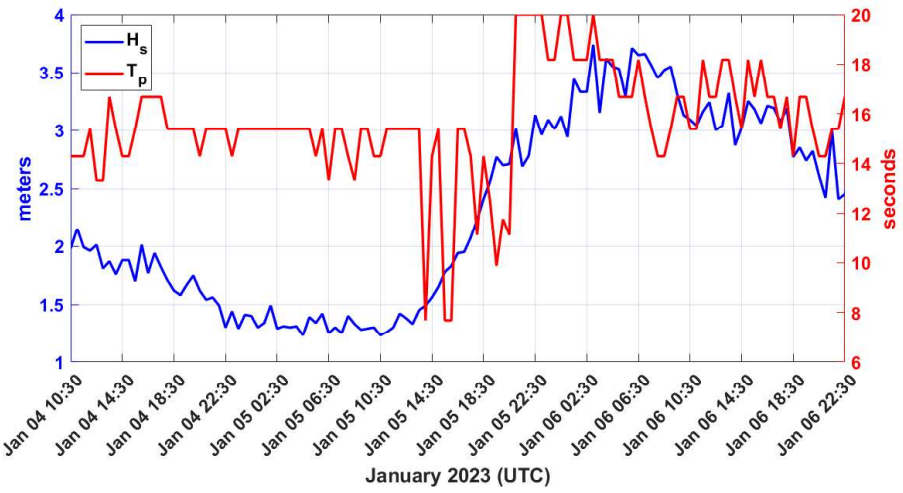

Figure 3.3: Deep water wave conditions from the nearest CDIP buoy (101 Torrey Pines Outer) during the January 2023 storm event.

Figure 3.4: Selected photos of the overwash and erosion event on January 6, 2023. Photo credit: Maria Winters and Margit Maple.

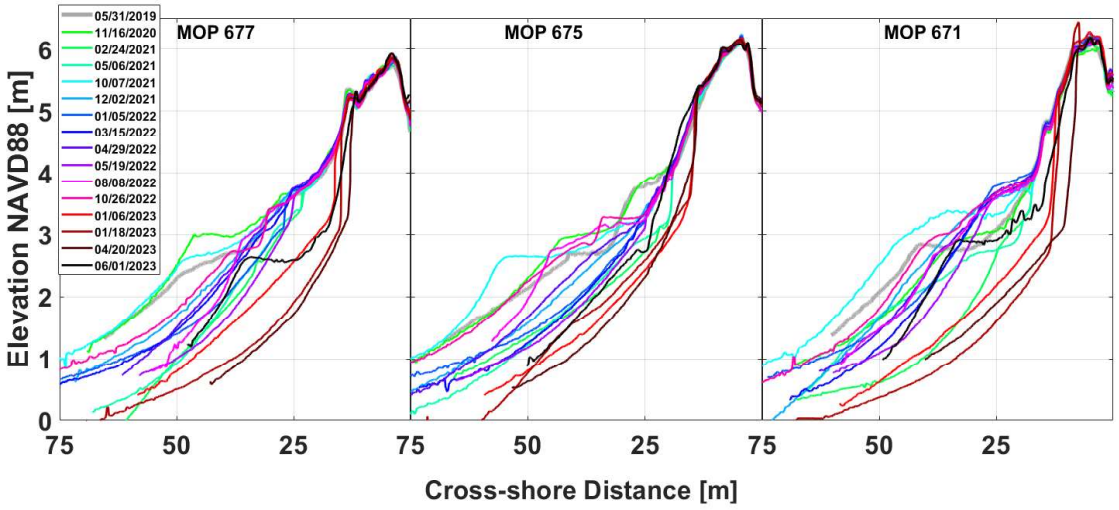

Figure 3.5: Cross-shore transects from selected surveys at MOP cross-shore locations.

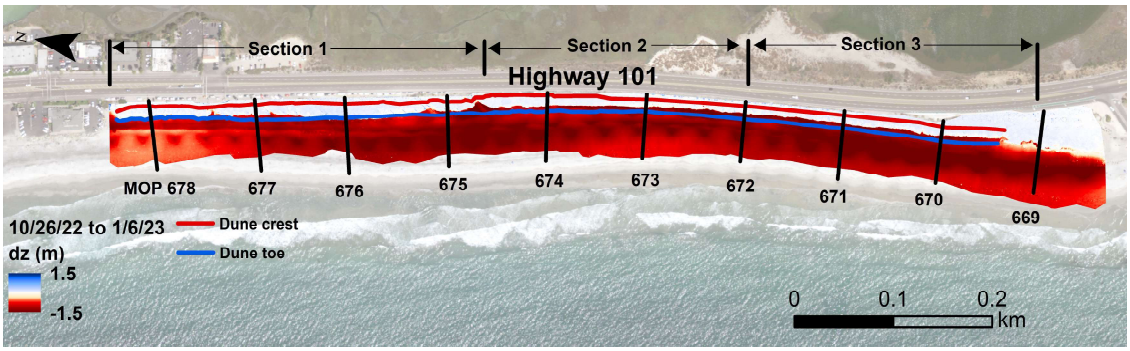

Figure 3.6: Fall and winter Cardiff beach and dune erosion from October 2022 to January 2023.

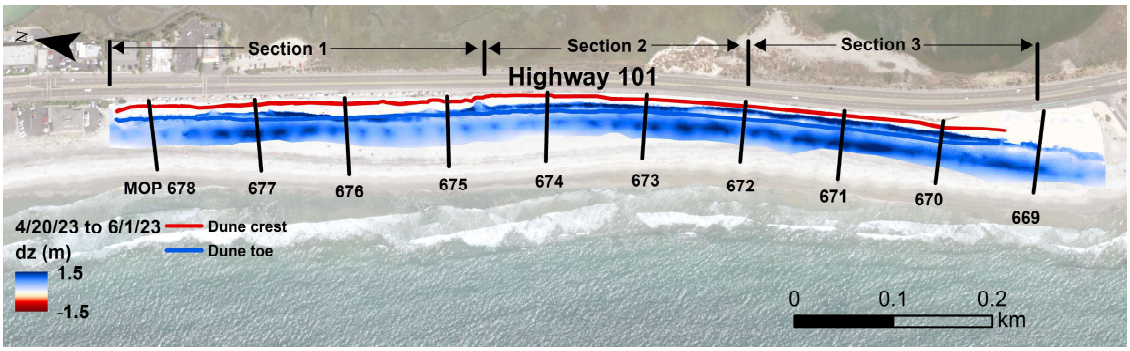

Figure 3.7: Cardiff beach from April to June 2023. Increase in sand elevation along the project includes sand placement along toe of dune in May 2023.

3.3 Model Grid Generation

The pre-storm (January 04, 2023) and post-storm (January 06, 2023) digital terrain model DTMs were merged with bathymetric data from October 9, 2018, representing a typical fall bathmetry. XBeach requires an offshore boundary depth to satisfy the wave group speed to wave celerity (C_g/C) ratio is ~ 0.8, in this case -42 m depth. The bathymetry collected extends to only -10 m offshore, so the DTMs were merged with additional offshore bathymetry from the San Diego 1/3 arc-second horizontal resolution Tsunami Inundation digital DEM, obtained from the open-access National Oceanic and Atmospheric Administration (NOAA) Digital Coast Data Access Viewer (NOAA Office for Coastal Management, 2021). Model grids were extracted and generated ESRI ArcMap from the pre-storm DTM and validation grids from the post-storm DTM. The model grid required for the LE04 model is a grid of the dune toe and above; in this case 4 m NAVD88 and above. XBeach grids were created with the XBeach gridding functions in the Deltares Open Earth Toolbox (Deltares, 2013) for MATLAB. For more information see Section 4.5.3.

In this study, dune erosion and hybrid structure models are tested for skill on this extreme, long period-dominated event. Morphology was modeled at the CDIP cross-shore location MOP675, a location investigated in Winters et al. (2020) from the time of the pre-storm survey, January 4, 2023 10:30 UTC to the immediate post-storm survey on January 6, 2023 23:30 UTC.

3.4 Cardiff Modeling

3.4.1 Analytical Dune Erosion Modeling: Larson et al. (2004)

The analytic wave impact model by Larson et al. (2004) (LE04) has been used to model sand dune toe retreat and volume loss (e.g., Splinter and Palmsten (2012)). Wave runup, R is parameterized in the LE04 model as:

$$R = 0.158\sqrt{H_{o,rms}L_o}, \tag{3.1}$$

where $H_{rms,o}$ is the root-mean-square deepwater wave height (approximated as $\sim 0.707 H_s$) and L_o is the deepwater wavelength, both in meters (m). The dune volume change above the toe per unit width alongshore, ΔV (m^3/m), is modeled as:

$$\Delta V = 4C_s(R - z_b)^2 \frac{t}{T}, \tag{3.2}$$

where R is the runup defined in Equation 3.1, z_b is the elevation of the dune toe (m), t (s) is the duration of exposure, and T (s) the wave period. C_s is the non-dimensional transport coefficient, defined in Larson et al. (2004) as

$$C_s = Ae^{-b\frac{H_{rms,o}}{D_{50}}}, \tag{3.3}$$

where the coefficient values of $A = 1.34{\times}10^{-3}$ and $b = 3.19{\times}10^{-4}$ and D_{50} the median grain size in millimeters (mm). The native D_{50} for this site, 0.16 mm, listed in Ludka et al. (2016) was utilized. This equation was found to be valid over the range of $H_{rms,o}/D_{50}$ in the study. The dune toe elevation each time step is modeled assumed to follow along a constant slope $tan\beta_t$

$$z_b(t) = tan\beta_t(t)x(t) + z_b(0), \tag{3.4}$$

where $tan\beta_t = tan\beta(0)$, the initial pre-storm beach slope. In this study $tan\beta(0)$ is defined from MSL to the elevation of the dune toe and is equal to 0.071 radians.

Models such as XBeach-G McCall et al. (2014) and CSHORE Kobayashi and Kim (2017) have been previously utilized to specifically model cobble beach and dune-buried sea wall erosion, respectively. However, as these do not yet resolve the simultaneous morphodynamics of multiple substrate types and size, dune volume change and toe retreat during the storm duration (from the pre-storm UAV survey date to post-storm survey date) were estimated

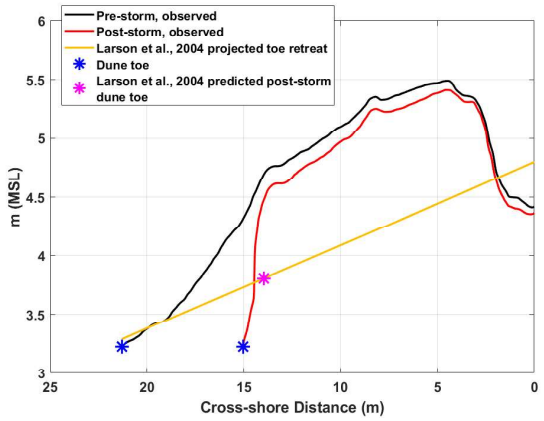

Figure 3.8: Selected cross-shore profile from the study site depicting pre- and post-storm dune topography measured by UAV surveys, as well as predicted dune toe retreat, $z_b(t)$, predicted by the Larson et al. (2004) model.

first using the LE04 model for initial skill on this mixed sand substrate structure at a single cross-shore location.

The observed dune volume loss was $\sim$ 5.07 m^3/m, while the LE04 model predicted a volume loss, ΔV, of 3.77 m^3/m. The modeled post-storm dune retreat at every time step in the storm, $z_b(t)$, is shown in Figure 3.8. LE04 assumes a constant toe retreat slope and constant water level, possibly accounting for the underestimation of the dune volume loss.

3.4.2 XBeach Dune Modeling

XBeach requires a tide time series and wave spectra as input (See Section 4.5.2). Tide boundary conditions were prescribed to the offshore boundary only with an offshore water-level time series, obtained from the nearest open-water tide gauge, NOAA La Jolla gauge 9410230 (National Oceanic and Atmospheric Administration (NOAA), 2020). The time series is composed of water-level values collected every 6-minutes. The landward boundary was prescribed water level values of -6 m every 6 minutes to allow water to pour into the backshore and eliminate non-physical flow reversal artifacts caused by a nearby boundary.

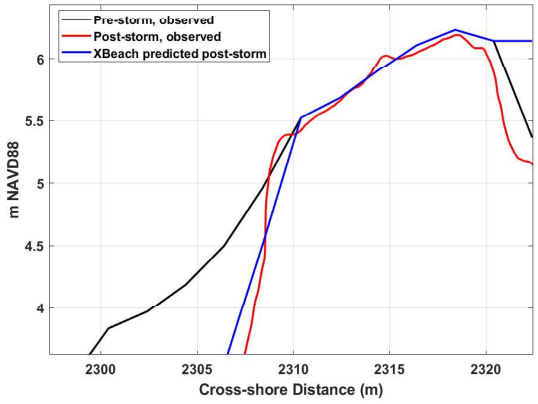

Figure 3.9: Selected cross-shore profile from the study site depicting pre- and post-storm dune topography measured by UAV surveys, as well as dune erosion predicted by XBeach.

Wave boundary conditions were prescribed to the offshore boundary as an hourly time series of wave spectra, which XBeach utilizes to generate a random wave time series (Deltares, 2018). The spectra were prescribed as hourly variance density spectra, where the wave energy is binned by frequency and direction. These spectra were obtained at approximately 10 meters depth and every 100 meters alongshore from the Scripps Institution of Oceanography Coastal Data Information Program (CDIP) Monitoring and Prediction (MOP) System (O'Reilly et al., 2016). Significant wave height was reverse-shoaled from -10 meters to the -42 meter offshore boundary depth. All model parameters, except median grain size (D_{50}) were left as their default values. A D_{50} value of 0.57 mm was reported at Cardiff State Beach in Ludka et al. (2016) and was utilized for this initial modeling study. For more information regarding the setup and parameterizations of XBeach, see Section 4.5.3. One model realization was tested, and the default hydrostatic XBeach overall predicted the retreat of the dune toe and face (Figure 3.9).

CHAPTER 4

Naval Amphibious Base Coronado

4.1 Site Description

Southern California beaches characterized by both temporary or permanent sand dune structures typically have foreshore slopes of ∼0.1 to 0.03 radians (Gallien et al., 2015). Coronado Beach is located approximately 14 km south of San Diego, California on a wide barrier spit in between the Pacific Ocean and San Diego Bay (Figure 4.1a). A large (i.e., FEMA 540) sand dune protecting Naval Amphibious Base Coronado was constructed using 28,000,000 m^3 of sand from the San Diego Bay dredging project (Flick, 1994). The median grain size (D50) reported most recently is ∼0.25 mm (Moffatt & Nichol, 2009). The dune structure is 1.3 km long, 6.77 m tall, and 48 m^3/m in volume above mean sea level (MSL) (Gallien et al., 2015). The dune toe is located approximately at 3.5 m with respect to the North American Vertical Datum 1988 (NAVD88), crest elevation ranges from approximately 6.5 to 7.5 m NAVD88, with multiple discontinuities such as pedestrian and vehicle access ways (Gallien et al., 2015). The dune is exposed to energetic swells, overtopping, and backshore flooding events in winter seasons (Gallien et al., 2015) and has failed during energetic wave events (Figure 4.2). In southern California, winter wave energy is primarily from storms originating in the Pacific Northwest ($240° < D_p < 320°$) with significant wave heights (H_s) over 2 m and swell frequencies of 12-18 s (Adams et al., 2008).

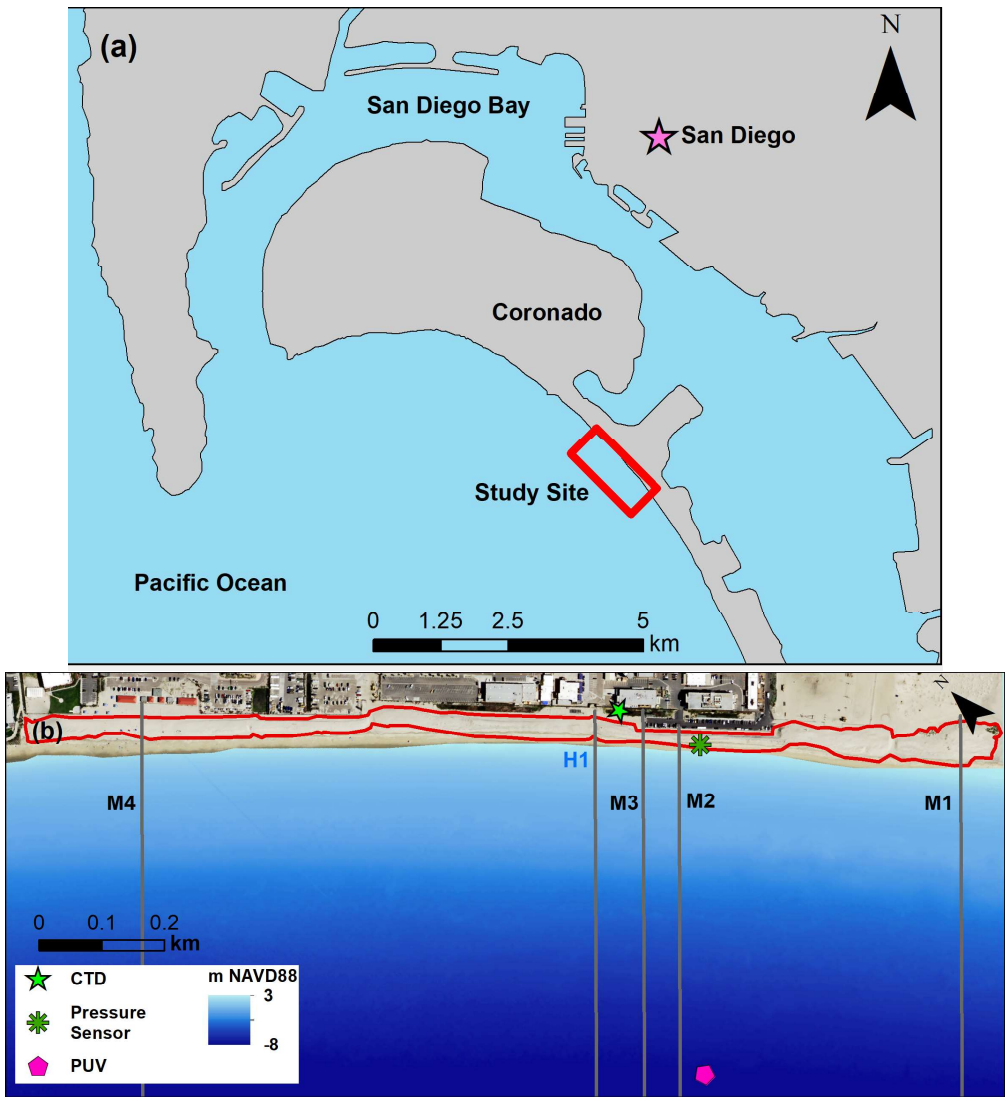

Figure 4.1: (a) Study site of the Naval Amphibious Base Coronado persistent dune in San Diego County, California, United States. Sand dune structure of interest outlined in red. (b) Image of dune and beach overlapped on nearshore bathymetry. Location of CTD, PUV (wave gauge), and pressure sensors indicated by green star, green asterisk, and magenta polygon, respectively. Modeled cross-shore transects indicated and labeled.

Figure 4.2: Photos of Coronado berm failure during March 5-7th, 2016 resulting in backshore parking lot flooding and undermining.

4.2 Event Description

In January 2017 a winter storm caused a dune breaching and overwash event. Energetic conditions were observed from January 21, 2017 to January 24, 2017. Tidal water levels during this event were modest, less than mean higher-high water (MHHW) (Figure 4.3a). Deep-water wave conditions reached a peak H_s of over 4.94 meters and peak period (T_p) of 20 s (Figure 4.3b). Beach states ranged from intermediate to reflective when the swash was interacting with the dune face (Figure 4.4a-c). Hourly total water levels (TWLs) were estimated during the storm event to estimate the time of peak overtopping and subsequent erosion (Figure 4.3a). TWL is defined as the observed open coast water level plus wave runup. Here, $R_{2\%}$ Stockdon et al. (2006) is used to characterize wave runup. $R_{2\%}$ is a field validated (Stockdon et al., 2006; Fiedler et al., 2015; Melet et al., 2018), widely used coastal hazard assessment metric (e.g. Federal Emergency Management Agency (FEMA) of the United States, 2005; Heberger et al., 2009; Gallien, 2016; Serafin et al., 2017; Vitousek et al., 2017; Melet et al., 2018).

Equation (4.1) shows the 2% exceedance of wave runup (Stockdon et al., 2006), where β is the active foreshore slope, H_0 is the deep water significant wave height, and the deep water wave length, $L_0 = g/2\pi f_p^2$, is computed from the peak frequency, f_p.

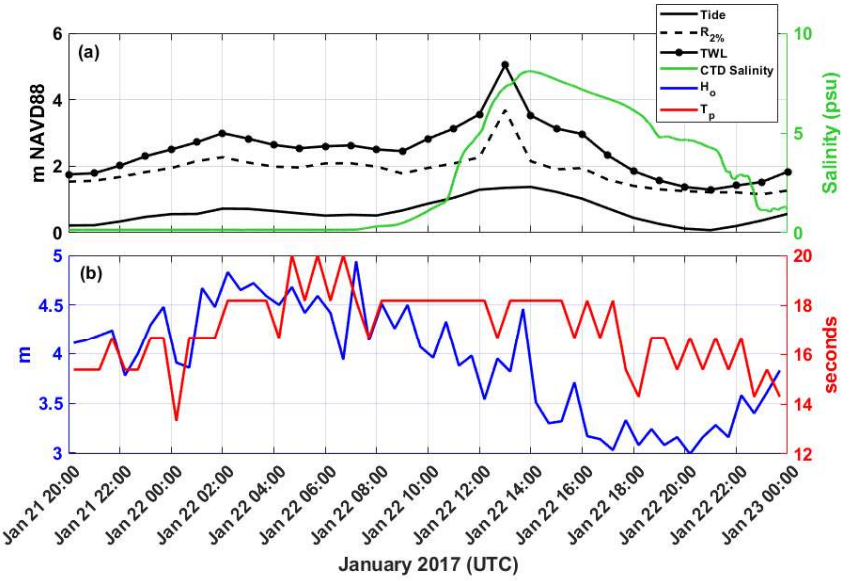

Figure 4.3: (a) Tide, Stockdon et al. (2006) $R_2\%$, total water level (TWL), and salinity signal from backshore CTD. Reader is referred to Section 4.2 for Stockdon et al. (2006) definitions. (b) offshore wave conditions from nearest deep water CDIP buoy (191 Point Loma) for duration of simulated storm from January 21-22, 2017.

$$R_{2\%} = 1.1\left(0.35\beta(H_0L_0)^{0.5} + \frac{[H_0L_0(0.563\beta^2+0.004)]^{0.5}}{2}\right) \tag{4.1}$$

Total water level is defined as the sum of the nearest the NOAA tide gauge (La Jolla, California, 9410230 (National Oceanic and Atmospheric Administration (NOAA), 2020)) observed water levels (OWL) and $R_{2\%}$ and is given by,

$$TWL = OWL + R_{2\%} \tag{4.2}$$

Six minute water levels were obtained from the nearest open coast tide gauge, La Jolla 9410230, approximately 30 km north (National Oceanic and Atmospheric Administration (NOAA), 2020). Hourly spectral wave parameters and variance density spectra were estimated from the CDIP Monitoring and Prediction (MOP) System, a non-stationary, linear, spectral refraction wave model (O'Reilly et al., 2016) along the 10 m depth contour with 100 m alongshore spacing. Total water levels were estimated along each of the modeled transects

(Figure 4.4). Beach slope (β) values were estimated every hour along the active foreshore between mean sea level (MSL) and the dune crest elevation (Table 4.1, Figure 4.4). Peak water levels and energetic waves occurred on January 22, 2017.

4.3 Observations

4.3.1 Topobathy

An extensive observational program in Winter 2016-2017 collected topography, bathymetry, and hydrodynamic data. Subaerial beach and dune topography were derived from unmanned aerial vehicle (UAV) photogrammetry. The UAV surveys were conducted on January 10, 21, and 24, 2017 with a SenseFly eBee fixed-wing mapping drone equipped with a Sony WX camera to capture aerial images. Topographical data products such as digital elevation models (DEMs) from the UAV surveys were generated with Pix4Dmapper, a structure-from-motion (SfM) software.

Nearshore bathymetry from 0 to -8 m NAVD88 depth was collected along shore-normal transects with a real-time-kinetic (RTK) dolly and jet ski survey on January 10, 2017. The transects were spaced at 100 m intervals along existing CDIP MOP profiles (O'Reilly et al., 2016). Bathymetric data profiles were interpolated in R (R Core Team, 2021) to create a DEM. In addition, subaerial beach topography was collected on January 10, 2017 via alongshore all-terrain vehicle (ATV) RTK surveys. Backshore topography and offshore bathymetry ($<$ - 8 m) in areas not captured by the field campaign were obtained on NOAA Digital Coast (NOAA Office for Coastal Management, 2021) from the 2016 United States Geological Survey (USGS) West Coast El Niño lidar survey and the San Diego 1/3 arc-second horizontal resolution Tsunami Inundation digital DEM, respectively. These DEM products were merged to create a seamless digital elevation model of the entire region. The priority given to each data source in the merged DEM is shown in Table 4.2. A bare earth digital terrain model (DTM) was created from the merged DEM by filtering cars, buildings,

Table 4.1: Ranges of beach conditions during duration of storm at each cross-shore location. Deepwater wave height obtained by reverse shoaling wave parameters obtained from CDIP MOP program at 10 meter depth to deep water.

Transect	$\mathbf{H}_o$ **(m)**	$\mathbf{T}_p$ **(s)**	$\mathbf{H}_o/\mathbf{L}_o$	β	ξ_o	$\boldsymbol{R^{IG}/R}$
M1	1.49 - 2.98	12.30 - 14.29	0.0034 - 0.0094	0.052 - 0.088	0.61 - 1.23	0.64 - 0.93
M2	1.58 - 2.91	14.29 - 16.67	0.0041 - 0.0085	0.047 - 0.083	0.63 - 1.10	0.69 - 0.92
M3	1.61 - 3.16	14.29 - 15.38	0.0044 - 0.0099	0.044 - 0.097	0.59 - 1.18	0.66 - 0.94
M4	1.34 - 2.52	15.38 - 20.00	0.0031 - 0.0058	0.040 - 0.067	0.60 - 1.11	0.69 - 0.93
P1	1.28 - 2.34	14.29 - 16.67	0.0033 - 0.0070	0.046 - 0.110	0.74 - 1.45	0.57 - 0.96

and other non-topographic objects that could create artificial flow obstructions and promote numerical instabilities.

Sensors were deployed onsite to monitor onshore hydrodynamics (Figure 4.1b). A buried Paroscientific pressure sensor sampling at 2 Hz was deployed at ∼2 m NAVD88, approximately 0.50 m below the sand surface near the dune toe to monitor waves. A conductivity-temperature-depth (CTD) sensor was deployed in a drainage ditch behind the dune to measure salinity and depth of marine overtopping events (Figure 4.1b). A Nortek Vector pressure and velocity sensor (PUV) was placed offshore at approximately 8 m depth to observe nearshore wave conditions. Wave power spectra, and therefore H_s, were estimated from PUV measured sea surface elevations offshore derived using linear wave theory and poroelastic theory to account for the instrument burial (Raubenheimer et al., 1998; Fiedler et al., 2015). PUV measured wave parameters were utilized to verify XBeach predicted wave heights and power spectra at the nearshore 8 meters depth. Onshore water level values were derived from the buried pressure sensor sand sub-surface pressure measurements using the hydrostatic pressure relation. Overtopped volume time series into the drainage ditch during the peak of the storm were estimated with a hypsometric analysis by estimating the drainage ditch area from UAV topographic data and multiplying by time-varying measured overtopped depths.

Table 4.2: Priority of geospatial data for creation of digital terrain model (DTM) used for Coronado breach and dune erosion modeling.

Priority	Location	Description	Source	Date	Resolution (m)	VRMSE (m)
1	Beach crest	UAV survey	Scripps	01-21-2017	0.02	0.05-0.10
2	Upper beach	UAV survey	Scripps	01-24-2017	0.02	0.05-0.10
3	Beach to -8 m	ATV, dolly, jet ski	Scripps	01-10-2017	0.8 along transect	0.05
4	Beach Edges	LiDAR DEM	USGS	2016	0.5	0.06
5	Offshore	1/3 arc second DEM	NOAA NGDC	various	10	0.1-5% of depth

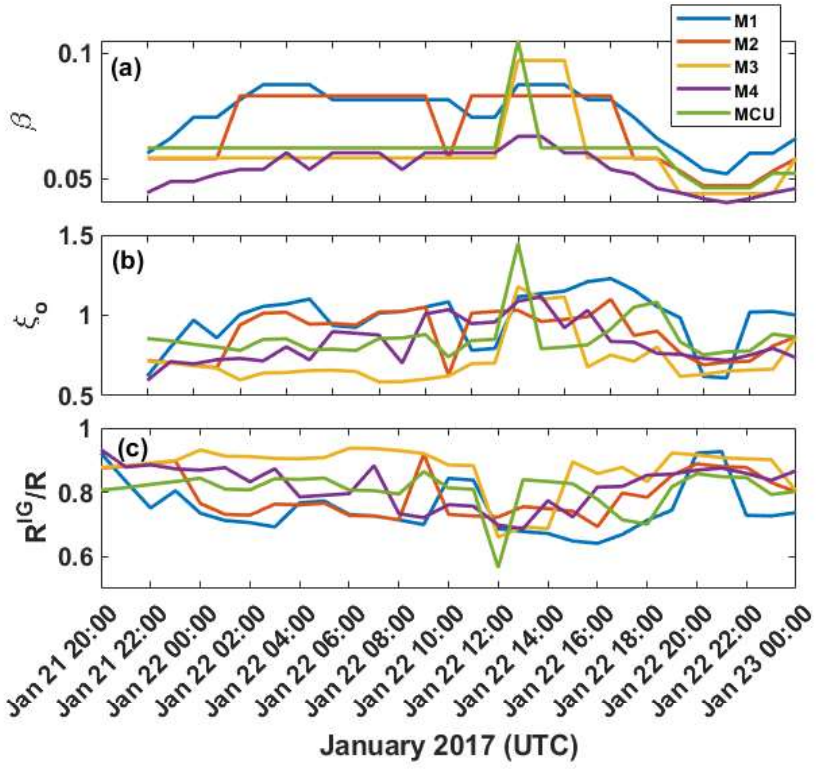

Figure 4.4: Observed (a) hourly swash face slope, (b) Iribarren number, and (c) R^{IG}/R ratios at each modeled transect (1D) for duration of storm event.

4.3.2 Beach and Dune Observed Morphology Changes

The dune toe and heel were identified where the beach slope was between 7°and 45°($\sim$ 0.12 to 0.79 radians), as in Gallien et al. (2015), where 45°is the angle of repose of wet sand (dune delineation shown in Figure 4.1b). The dune crest was identified as the point of maximum cross-shore elevation within this dune footprint. The pre-storm dune crest elevation values ranged from 4.5 m to 8.6 m NAVD88 and pre-storm dune toe elevation was $\sim$2.75 m NAVD88 (Figure 4.5d). The highest crest values were located around y = 1400 m along the dune while the lowest crest values were located near y = 800 m, y = 1200 m, and y = 1500 m, the access ways, and around $\sim$y = 1100 m, the main breach location (Figure 4.5d).

Dune volumes were estimated above the average toe elevation value of 2.75 m NAVD88. The pre-storm dune volume ranged from around $\sim$ 8.5 m^3 to 175 m^3 with an average volume of 63 m^3 (Figure 4.6a). The location along the dune with the lowest pre-storm volume was also the location of the lowest pre-storm crest, around y = 1100 m (Figure 4.5d, 4.6a). Beach slopes, from 0 m to 2 m NAVD88, ranged from 0.01 to 0.04 radians and the dune face slopes varied from 0.1 to 0.6 radians (Figure 4.7a). The area with the highest pre-storm beach and dune face slopes was between y = 1000 m and y = 1200 m (Figure 4.7a). Toe and crest distances to mean sea level (MSL), indicative of beach width, are shown in Figure 4.6c. Crest distances to MSL varied from about 23 m to 85 m, with the smallest crest distances (narrowest beach width) located between y = 900 m and 1100 m (Figure 4.6c).

Beach and dune elevation changes derived from UAV observations show erosion occurred primarily along the foreshore, particularly at y = 2000 m and between y = 1000 and 1200 m (Figure 4.5c). Other locations that experienced significant erosion occurred near the edges of the dune at the access way entrances (y = 800 m, 1200 m, 1500 m), with a loss of between 1 and 1.5 m in the vertical. Erosion tends to occur at dune section ends and edges, as observed and described in Gallien et al. (2015). Lowering of the dune crest occurred at several locations along with the dune, with the majority of crest erosion occurring between y

= 1000 m and 1200 m (Figure 4.5e). This area, also the location of transect M3, saw the most crest erosion, with a lowering of about 1.3 m (Figure 4.5e). The crest elevation increased at some locations, for example around ∼ y = 600 m to 700 m, likely due to overwash that occurred during the storm (Figure 4.5e). This location also saw an increase in post-storm dune volume (Figure 4.6b). Lowering of the dune toe occurred along the majority of the dune with the largest elevation decreases of 0.5 to 1 m (Figure 4.5e). Dune volume changes ranged from +11 m^3 to -38 m^3, with the highest volume increase at location ∼ y = 700 m and largest volume decreases between y = 1000 m and 1200 m and around the edges of the access ways (y = 800 m, y = 1200 m, and y = 1500 m) (Figure 4.6b). Overall dune slopes generally increased post-storm; however, between y = 1000 m to 1200 m, dune slope decreased post-storm (Figure 4.7b,c).

4.3.3 Swash and Overtopping Observations

Observations collected by the buried pressure sensor at the dune toe and CTD in the ditch behind the dune indicate when the breaching location (y = 1000 m to 1200 m) was in the collision and overwash regimes. Individual swash excursions recorded at the dune toe (Figure 4.8a) indicate indicate when the dune is interacting with the swash. The dune was in the collision regime from approximately January 22, 2017 00:00 to 07:00 UTC (Figure 4.8a) and then transitioned and remained in the overwash regime until approximately January 22, 2017 14:00 UTC, as indicated by the spike in salinity and water depth recorded by the CTD in the backshore drainage ditch (Figure 4.8b). Local weather observations confirmed there was no precipitation that could have contributed to water depth increases in the drainage ditch. Total overtopped volume was estimated using a hypsometric analysis, scaling the observed overtopped depth by the surface area of the drainage ditch derived from the UAV topographic elevation maps.

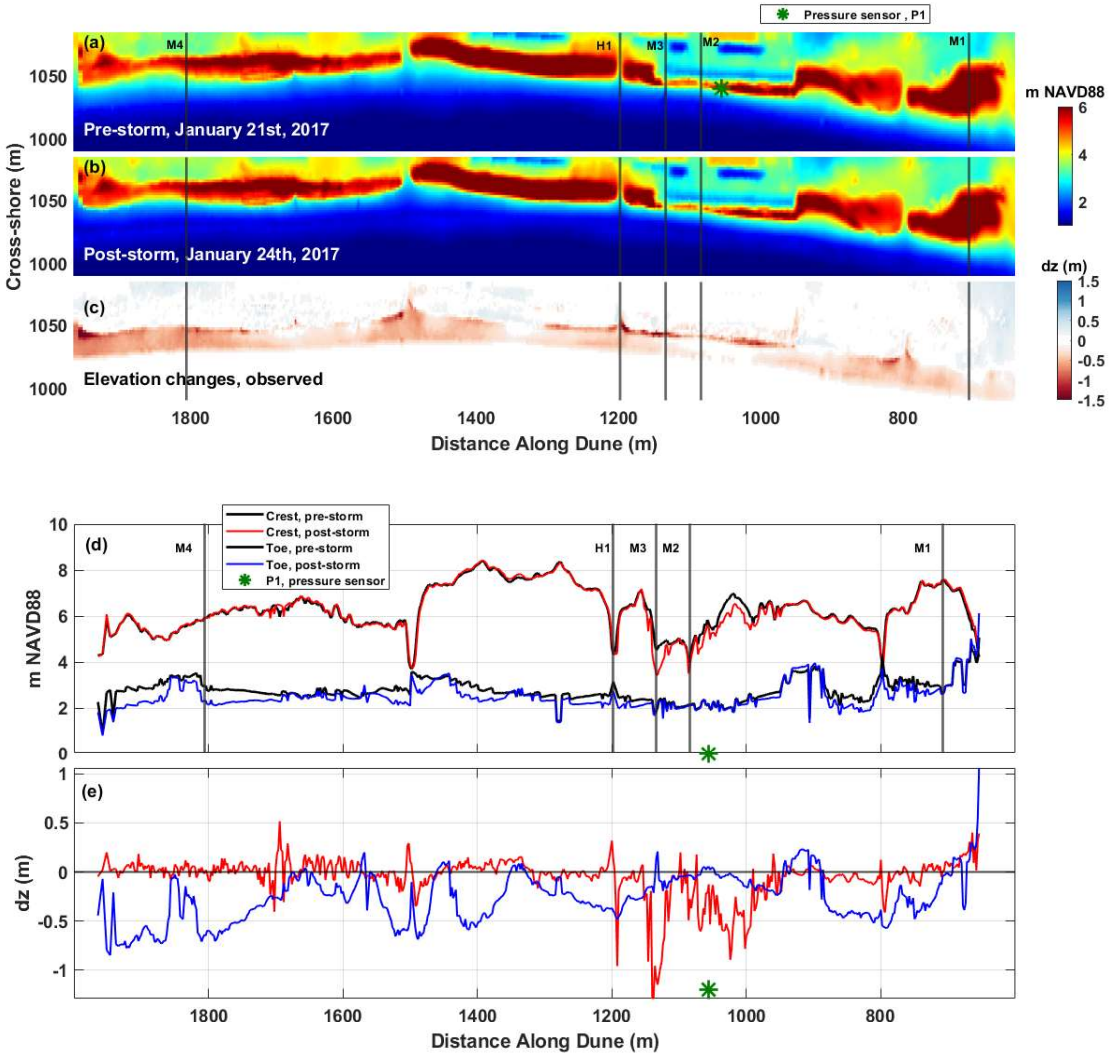

Figure 4.5: (a) Observed dune pre-storm on 1/21/2017 (b) observed post-storm on 1/24/2017 and (c) elevation difference map between the two dates. Modeled cross-shore transects of interest are indicated with black lines and corresponding labels. (d) Observed elevations of the dune toe and crest pre- and post-storm. (e) Observed changes in dune toe and crest elevations. Green asterisk indicates alongshore location of the buried dune face pressure sensor, P1.

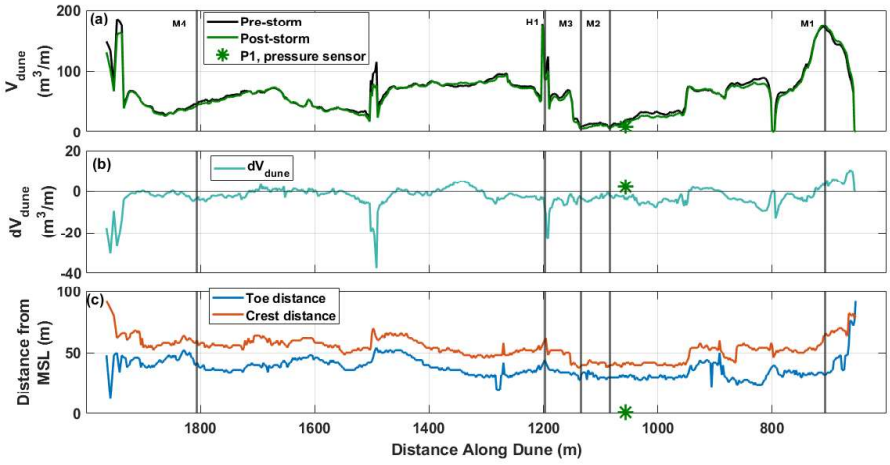

Figure 4.6: (a) Dune volume pre-storm and post storm from UAV observations. (b) Dune volume change along length of dune between pre and post storm. (c) Distance from dune toe and crest to mean sea level elevation pre-storm. Green asterisk indicates alongshore location of the buried dune face pressure sensor, P1.

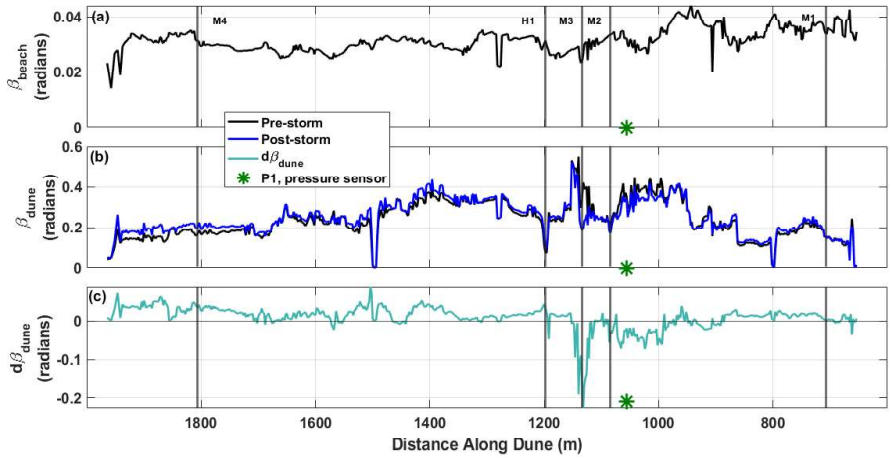

Figure 4.7: (a) Pre-storm beach beach slope, β_{beach}, estimated from MLLW to the dune toe (b) Pre and post-storm dune slope, β_{dune}, estimated from the dune toe to dune crest and (c) the change in dune slope after the storm event, dβ_{dune}.

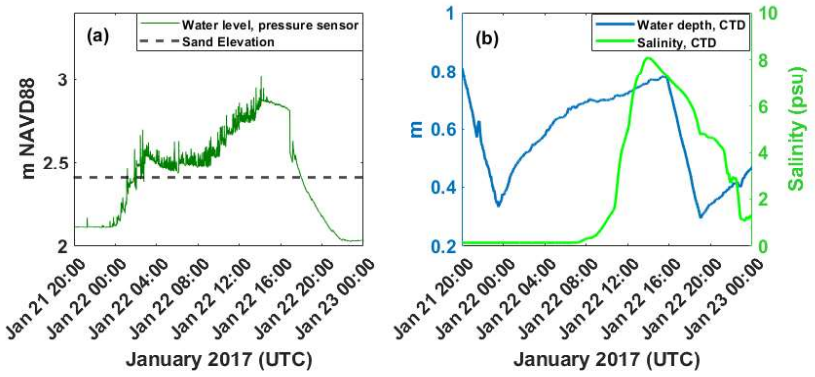

Figure 4.8: (a) Buried pressure sensor, P1, water level elevation measurements and (b) CTD water depth and salinity measurements in backshore ditch during peak of storm.

4.4 Grid Generation

A grid of the study area was generated by merging topographic and bathymetric observations with additional beach topography and offshore bathymetry provided by the 2016 United States Geological Survey (USGS) West Coast El Niño Lidar survey and the San Diego 1/3 arc-second horizontal resolution Tsunami Inundation digital DEMs, respectively, to obtain the appropriate model domain size. Both can be obtained from the open-access National Oceanic and Atmospheric Administration (NOAA) Digital Coast Data Access Viewer (NOAA Office for Coastal Management, 2021). The priority given to each data source in the merged DEM is shown in Table 4.2. A pre-storm (January 21, 2017) and post-storm (January 24, 2017) digital terrain model (DTM) were created in ESRI ArcMap from the merged DEM by filtering cars, buildings, and other sharply vertical objects that can create numerical instabilities. DTMs were interpolated to a coarser, uniform 50 cm or 2 m resolution grid prior to model grid creation. Model grids for SBeach, CSHORE, and XBeach were extracted and generated from the pre-storm DTM and validation grids from the post-storm DTM. Morphology was modeled at four cross-shore locations, transects M1-M4, with SBeach, CSHORE, and surfbeat 1D XBeach.

4.5 Numerical Model Descriptions and Setup

4.5.1 SBeach

SBeach is a one-dimensional, semi-empirical model used to estimate beach and dune change due along cross-shore profiles to storm waves and water levels (Larson and Kraus, 1989). The model is based upon the 'equilibrium profile' concept of Bruun (1954b) where beach profiles evolve to an equilibrium state. Sediment transport is proportional to the difference between present and calculated equilibrium wave energy dissipation (Larson and Kraus, 1989). SBeach has been applied to large wave tank experiments and field data from U.S. East Coast events (e.g., Larson and Kraus, 1989; Larson et al., 1990; Glover and Hales, 1991; Rosati et al., 1993) and has been tested on barrier island and dune overwash and breaching events along the coasts of Maryland and South Carolina, United States and showed success at reproducing post-hurricane overwash sediment transport landward and dune evolution (Donnelly et al.; Donnelly, 2008).

The SBeach 1D, non-uniform grids were generated using the uniformly spaced 2 m DTMs and the built-in SBeach variable grid generation tool. SBeach defines the seaward boundary as the location where incident waves begin to shoal, and the depth where there is no significant sediment motion (Larson and Kraus, 1989). The program automatically calculates this point using the input transect, storm conditions, and the exponential decay equation to determine the onset of significant sand movement (Larson and Kraus, 1989). Cell grids were split into three regions where highly erosive areas have greater resolution (Rosati et al., 1993). From the seaward boundary to 0 m NAVD88, the grid resolution was 10 m. From 0 m to 1.5 m NAVD88, the resolution was 5 m. The remainder of the transect, including the dune and the subaerial beach, had a 2 m grid cell size.

Storm input data for SBeach includes wave angle, water elevation, wave height, period, and wind. A 28-hour irregular wave simulation was ran using a 1 hour time-step for wave height, period, and water elevation. The effects of wind speed and direction were ignored

and wave angle was assumed to be directed onshore ($\theta = 0$). For each transect, the input wave water depth was set as the offshore water depth.

The primary test variable was *BMAX* (maximum slope prior to avalanching). Leadon (2015) tested the model's sensitivity to changes in sediment grain size and (referred to as the *MSPA* parameter in their study) on beaches along the Florida and Louisiana coast. They found that flatter, less-steep beaches showed better calibration efforts with higher values of K and *BMAX*, while conversely, for steep beaches, the opposite was true, such that lower values of K and *BMAX* were better for parameterization. For these simulations, the default *BMAX* was 45 degrees. A lower *BMAX* value of 28.5 was chosen to better calibrate the model for transects M1, M3, and M4, and a *BMAX* value of 30 was chosen for transect M2 to reduce over-erosion (Table 4.3).

The input effective grain size was the *D50* of the site, 0.25 mm, and the landward surf zone depth was set to the first tide time-step. Sand was set to remain on the grid to match CSHORE simulations. Sediment transport parameters, such as the transport rate coefficient (K) and the overwash transport parameter (*Eps*), were found to have minimal effects on the output profile. For all simulations, these variables were left at their default entries (Table 4.3).

4.5.2 CSHORE

CSHORE is a one-dimensional numerical coastal response model that is applied to cross-shore transects (Kobayashi, 2016). Its main components are a combined wave and current model based on a time- and depth-averaged continuity and momentum equations, wave-action (energy) and roller energy equations, a probabilistic model for the intermittently wet and dry zone, empirical formulas for wave runup, and a time-averaged sediment transport model for both suspended and bed load (Kobayashi, 2016). Summarized below (Equations 4.3 - 4.9) are the hydrodynamic and morphodynamic model equations.

The CSHORE time-averaged cross-shore continuity and momentum equations derived from the non-linear shallow water wave equations are expressed as:

$$\overline{hU} = q_o \tag{4.3}$$

$$\frac{d}{dx}\left(\overline{hU^2} + \frac{g}{2}\overline{h^2}\right) = -gS_{bx}\overline{h} - \frac{1}{2}f_b\overline{|U|U} \tag{4.4}$$

where:

h : instantaneous water depth,

U : instantaneous cross-shore velocity,

q_o : combined overtopping and overflow rate,

g : gravitational acceleration,

S_{bx} : cross-shore bottom slope and is $= \dfrac{dz_b}{dx}$,

z_b : bed elevation,

f_b : bottom friction factor

The standard deviation of the free surface elevation, η, is given by:

$$\frac{\sigma_n}{\overline{h}} = \left(\frac{2}{P_w} - 2 + P_w\right) \tag{4.5}$$

$$U = \alpha\sqrt{gh} + U_s \tag{4.6}$$

where:

P_w : the probability of h > 0 at any cross-shore location,

$\overline{h}$: mean water depth for the wet duration,

U : instantaneous cross-shore velocity,

α : a positive constant, set to 2,

U_s : a steady velocity added which allows for inclusion of undertow and overtopping,

g : gravitational acceleration

The hydrodynamics force the sediment transport model in CSHORE to estimate the depth-averaged suspended load, q_s, and bed load, q_b. The net cross-shore sediment transport rate is the sum of the net bed load and suspended load transport rates. The cross-shore suspended transport rate is given by:

$$q_s = \left(a\overline{U} + a_o U_o\right) V_s \tag{4.7}$$

$$U_o = \frac{q_o}{\overline{h}} \tag{4.8}$$

The cross-shore bed-load transport is expressed as:

$$q_b = \frac{bP_b\sigma_U^3}{g\left(s-1\right)} G_s \tag{4.9}$$

where:

a : suspended load parameter,

a_o : empirical overtopping parameter,

U_o : onshore current caused by the wave overtopping rate,

V_s : suspended sediment volume per unit horizontal bottom area,

b : bedload parameter,

P_b : the probability of sediment movement,

σ_U : standard deviation of the horizontal velocity,

s : specific gravity of the sediment,

G_s : bottom slope function which is a function of the cross-shore profile slope,

α : a positive constant, set to 2,

U_s : a steady velocity added which allows for inclusion of undertow and overtopping,

g : gravitational acceleration

CSHORE has been successfully utilized in wave flume experiments and on beaches on the East Coast and Europe (e.g., Kobayashi and Jung, 2012; Do et al., 2016; Quan and Kobayashi, 2015; Harter and Figlus, 2017; Kobayashi et al., 2018; Payo et al., 2020). More recently, CSHORE was applied to beaches along the United States Pacific coast with limited success (Kalligeris et al., 2020).

Cross-shore 1D uniform grids for CSHORE were created along the transects of interest (Figure 4.5a) from the pre-storm DTM. CSHORE defines the seaward boundary as the location outside of the surf zone where the wave setup and setdown is zero (Kobayashi, 2013). Input and post-storm validated transects were then smoothed, cleaned and cropped to their required offshore boundary depths (Johnson et al., 2012).

The CSHORE input features are wave conditions, beach bathymetry, and many param-

eterization variables. Wave conditions include the root-mean-squared wave height (H_{rms}), spectral peak period (T_P), the incident wave angle (θ), wind speed (W_{10}), and direction (Kobayashi, 2009). Parameters such as the bedload (b), the suspended load (a), and the suspended efficiency (e_f, e_b) adjust the sensitivity of sediment transport and profile evolution. In combination, the value of these four sediment-transport parameters were tested by (Johnson et al., 2012) to determine settings for the Atlantic and Pacific coast. The bedload parameter, b, determines the amount of bedload sediment transport, often resulting in an increase of foreshore sediment build up in the form of a bar. The suspended load parameter, a, is responsible for the on-shore wave-related sediment transport and is highly sensitive to the calibration of this parameter. The suspension efficiency parameters e_f and e_b are responsible for sediment suspension due to energy dissipation related to breaking waves and bottom friction. e_b is the main parameter that determines the magnitude of transport due to a breaking wave and e_f measures the magnitude of transport due to bottom friction. Increasing e_b and e_f results in increased suspended sediment concentration and foreshore erosion.

The Atlantic and Pacific parameter sets refer to the different combinations of b, a, e_f and e_b (Johnson et al., 2012). After consulting with one of the CSHORE developers, an additional parameter set (from now referred to as the "Suggested") was tested. Default values for sediment transport related parameters were also tested. All parameters, unless stated otherwise, were left as the default values. After a series of tests, the parameters *iroll* and *iwcint* which are responsible for wave roller conditions and wave/current interactions were turned on to increase model stability and output quality. The parameter *ilab* was turned on to mimic natural wave conditions. Wind effects were neglected and all wave energy was directed onshore ($\theta = 0$). Each transect was ran using the same set of base parameters, with each run changing the sediment specific parameter sets (Table 4.3).

4.5.3 XBeach

XBeach (Roelvink et al., 2009) is an open-source process-based flow and sediment transport model that solves a depth-averaged time dependent wave action balance that forces a depth-averaged Generalized Lagrangian Mean (GLM) formulation of the nonlinear shallow water (NLSW) equations (Equations 4.10-4.12). XBeach was created to efficiently simulate hydro-morphodynamics under the assumption of a saturated surf zone (Roelvink et al., 2018), and explicitly accounts for infra-gravity (IG) timescale physics critical to beach erosion processes. Sediment concentrations in the water column are simulated by solving the depth-averaged advection-diffusion equation of Galappatti and Vreugdenhil (1985) with a source-sink term based on equilibrium sediment concentrations (Equation 4.13). The concentration, C is used to solve for the sediment transport rates in the cross-shore and alongshore directions, q_{s_x} and q_{s_y}, respectively, from which the bed is updated based on continuity with the Exner equation.

$$\frac{\partial u^L}{\partial t} + u^L\frac{\partial u^L}{\partial x} + v^L\frac{\partial u^L}{\partial y} + fv^L - \nu_h\left(\frac{\partial^2 u^L}{\partial x^2} + \frac{\partial^2 u^L}{\partial y^2}\right) = \frac{\tau_{sx}}{\rho h} - \frac{\tau^E_{bx}}{\rho h} - g\frac{\partial \eta}{\partial x} + \frac{F_x}{\rho h} + \frac{F_{v,x}}{\rho h} \tag{4.10}$$

$$\frac{\partial v^L}{\partial t} + u^L\frac{\partial v^L}{\partial x} + v^L\frac{\partial v^L}{\partial y} + fu^L - \nu_h\left(\frac{\partial^2 v^L}{\partial x^2} + \frac{\partial^2 v^L}{\partial y^2}\right) = \frac{\tau_{sy}}{\rho h} - \frac{\tau^E_{by}}{\rho h} - g\frac{\partial \eta}{\partial y} + \frac{F_y}{\rho h} + \frac{F_{v,y}}{\rho h} \tag{4.11}$$

$$\frac{\partial \eta}{\partial t} + \frac{\partial hu^L}{\partial x} + \frac{\partial hv^L}{\partial y} = 0, \tag{4.12}$$

where:

u^L, v^L : Lagrangian velocities in the x- and y-direction respectively,

f : Coriolis coefficient,

ν_h : horizontal viscosity,

τ_{sx}, τ_{sy} : wind shear stresses,

h : water depth,

τ_{bx}, τ_{by} : bed shear stresses,

g : acceleration due to gravity,

η : water level,

F_x, F_y : wave-induced stresses,

$F_{v,x}, F_{v,y}$: vegetation-induced stresses.

For detailed model formulations information, the reader is referenced to Roelvink et al. (2018). XBeach has been used to model overwash and dune erosion during storm events and also in laboratory experiments (e.g. Roelvink et al., 2009; McCall et al., 2010; Splinter and Palmsten, 2012; McCall et al., 2014; Palmsten and Splinter, 2016; Berard et al., 2017). Here, XBeachX version 1.23.5527 is used to estimate wave driven erosion, breaching, and overtopping of the Coronado dune during the January 2017 long-period swell event.

$$\frac{\partial hC}{\partial t} + \frac{\partial hCu^E}{\partial x} + \frac{\partial hCv^E}{\partial y} + \frac{\partial}{\partial x}\left[D_h h \frac{\partial C}{\partial x}\right] + \frac{\partial}{\partial y}\left[D_h h \frac{\partial C}{\partial y}\right] = \frac{hC_{eq} - hC}{T_s} \tag{4.13}$$

where:

h : water depth,

C : depth-averaged sediment concentration which varies on the wave-group time scale,

u^E, v^E : Eulerian velocities(short-wave-averaged velocity observed at a fixed point)
in the x- and y-direction respectively,

D_h : sediment diffusion coefficient,

C_{eq} : depth-averaged equilibrium sediment concentration which varies on the wave-group time scale,

T_s : adaptation time representing entrainment of sediment.

The XBeach simulations were conducted using the most recent stable version of XBeachX in both 1D (i.e., cross-shore transects) and 2D. XBeach can run in two modes: hydrostatic or non-hydrostatic. Hydrostatic mode resolves wave groups, where as non-hydrostatic can resolve individual waves. Hydrostatic mode has two options: stationary and instationary (surfbeat) mode. Stationary mode solves wave-averaged equations and neglects infragravity waves, which is useful for conditions where incident waves are relatively small or high frequency (Deltares, 2018). Surfbeat mode resolves variations of the short waves on the wave group scale (the short wave envelope) as well as the long waves associated with them (Deltares, 2018). Therefore wave-driven currents, wind-driven currents, long (infragravity) waves, and runup and rundown of long wave are resolved. Erosion simulations in this work were run in hydrostatic surfbeat mode, as the breaching event being simulated is an extreme event with large waves and swash motions dominating, and surfbeat mode is recommended for such events (Deltares, 2018). To simulate swash zone hydrodynamics such as runup and overtopping non-hydrostatic XBeach is suggested (Deltares, 2018) and has previously been used to simulate breaching and overtopping (e.g., Roelvink et al., 2009; McCall et al., 2010; Gallien, 2016; Elsayed and Oumeraci, 2017). Non-hydrostatic mode was utilized to simulate swash, runup, and overtopping during the storm event along 1D transects that were updated hourly from XBeach hydrostatic transects.

Cross-shore transects were extracted from the merged DTM to create beach profile model grids to utilize in 1D surfbeat XBeach. One-dimensional grids were generated utilizing the XBeach gridding functions in the Deltares Open Earth Toolbox (Deltares, 2013) for MATLAB. The toolbox receives the x- and z-elevation profiles from the DTM as input and creates an optimized XBeach grid. Optimization includes assigning sufficient grid resolution to describe long waves and multiple grid point per features; in this case the recommended onshore resolution for modeling dune erosion is 1 to 2 meters (Deltares, 2018). Grids were created 0.5 m at the shore and dune. Final simulated beds from the 1D surfbeat simulations were utilized as the input grids for the non-hydrostatic XBeach simulations. Non-hydrostatic grid resolution ranged from a maximum of 8 m to a minimum of 0.5 m. The 2D model grid was created from the DTM with the Deltares Open Earth Toolbox (Deltares, 2013) for MATLAB. Additional optimization of the 2D XBeach grid included extending and flattening the offshore boundary to the appropriate depth (in this case from 10 meters to 37 meters depth). The 2D grid covers a domain of 3020 m in the alongshore by 1275 m in the cross-shore, resulting in 709 alongshore by 262 cross-shore grid cells, with a maximum offshore cross-shore resolution of 23 m and onshore resolution of 2 meters. The extent of the grid in the alongshore direction was set to include only the dune area of interest, and the cross-shore extent was determined by the offshore depth requirement. The validation grid was created identically, with the UAV dataset from January 24th, 2017 as first priority.

XBeach requires flow, tide, or surge boundary conditions specified at each side of the model domain or grid. Additionally, wave boundary conditions must be imposed at the offshore boundary. Each boundary of the domain was assigned the default XBeach boundary type. The offshore boundary and the landward boundary were both set as a weakly-reflective (absorbing-generating) boundary, which allows for obliquely-incident and obliquely-reflected waves to pass through the boundary with minimal reflection (Deltares, 2018). The offshore boundary depth was implemented in 37 m of water consistent with the recommendation for intermediate depth where the wave group speed to wave celerity (C_g/C) is ~ 0.8. Lateral

boundaries were set as no-gradient (i.e., free slip), or Neumann boundaries, which prescribe a zero-gradient, or no change, in water surface elevation and velocity at those boundaries (Deltares, 2018). A zero-gradient condition is required because these boundaries are artificial, as the model domain is limited and the real coastline would continue; therefore, the information prescribed at these boundaries must not negatively influence the simulation results (Deltares, 2018). Waves can enter the domain obliquely, and because the model domain is cut short in the alongshore direction, portions of the beach grid can experience wave shadowing. Wave shadowing occurs where alongshore zones of the coast do not receive obliquely propagated wave energy. To address this, cyclic boundary conditions were applied to allow the oblique incident waves to exit the bottom lateral boundary and re-enter through the top (Roelvink et al., 2018).

Tide boundary conditions were prescribed to the offshore boundary only with an offshore water-level time series, obtained from the nearest open-water tide gauge, NOAA La Jolla gauge 9410230 (National Oceanic and Atmospheric Administration (NOAA), 2020). The time series is composed of water-level values collected every 6-minutes. The landward boundary was prescribed water level values of -6 m every 6 minutes to allow water to pour into the backshore and eliminate non-physical flow reversal artifacts caused by a nearby boundary. Wave boundary conditions were prescribed to the offshore boundary as an hourly time series of wave spectra, which XBeach utilizes to generate a random wave time series (Deltares, 2018). The spectra were prescribed as hourly variance density spectra, where the wave energy is binned by frequency and direction. These spectra were obtained at approximately 10 meters depth and every 100 meters alongshore from the Scripps Institution of Oceanography Coastal Data Information Program (CDIP) Monitoring and Prediction (MOP) System (O'Reilly et al., 2016). Significant wave height was reverse-shoaled from 10 meters to the 37 meter offshore boundary depth.

XBeach has previously been applied to energetic storm events characterized by long period swell, as well to more reflective coastlines, with mixed success. Vousdoukas et al.

(2012) applied calibrated XBeach to an energetic storm event (H_s = 4 m, T_p = 15 s) intermediate to reflective coastline at Faro Beach, Portugal. Improved model performance was found by increasing *facua* and *wetslp* to reduce offshore transport and limit upper beach face avalanching. XBeach model performance and parameter sensitivity depending on the Sallenger (2000) dune erosion regime has previously been reported. For example Simmons et al. (2017) found *facua* more sensitive in simulations dominated by the collision regime, while the parameter *smax* is more sensitive during the overwash regime. The parameter *facua* has shown to be one of the most sensitive parameters controlling offshore erosion of beaches and events primarily in the swash and collision regimes (e.g., Vousdoukas et al., 2012; Splinter and Palmsten, 2012; De Vet, 2014; Simmons et al., 2015). Elsayed and Oumeraci (2017) concluded there is a linear relationship between beach foreshore slope and the optimal value of *facua* by summarizing beach slopes and *facua* values in published XBeach modeling studies. Avalanching, sediment transport, and morphology settings were turned on in the simulation to simulate beach and dune erosion. The avalanching term is critical in allowing sandy material from the face of the dune to slump, or avalanche, to the foreshore during storm-induced erosion in the collision regime (Deltares, 2018).

XBeach has been known to overestimate erosion during high-velocity, overwash conditions characterized by sheet flow (e.g., McCall et al., 2010; De Vet, 2014), and previously, artificial transport limiters were utilized in the model to limit erosion during these conditions such as the parameter *smax*, the maximum Shields parameter before initiation of sheet flow. De Vet (2014) suggested use of a physics-based transport limiter, the inclusion of the effects of soil dilatancy at high velocity flows. It is suggested to turn on the *dilatancy* for overwash and breach conditions in the most recent stable release XBeach manual (Deltares, 2018) and its use has improved XBeach model performance (e.g., De Vet, 2014; Elsayed and Oumeraci, 2017).

All model simulations were first run with their default settings as recommended for initial model testing by Deltares (2018) and corresponding D50 value, 0.25 mm, for the study

Table 4.3: Parameters, listed by model, considered in this study along with parameter descriptions. Boldface parameter values indicate model default values.

Model	Parameter	Parameter Description	Values
SBeach	*BMAX*	Maximum profile slope before avalanching occurs, in degrees	**28.5**, 30
	K	Transport rate coefficient which directly modifies the sediment transport rate	**1.75 x 10^{-6}**
	Eps	Overwash transport parameter	**0.002**
	D50	D50 grain size, in millimeters	0.25
CSHORE	*b*	Bedload parameter	**0.002**
	a	Suspended load parameter	**0.2**, 0.5
	e_b	Suspension efficiency parameter	**0.005**, 0.01
	e_f	Suspension efficiency parameter	**0.01**, 0.02
	D50	D50 grain size, in millimeters	0.25
XBeach*	*facua*	Calibration factor time averaged flows due to wave skewness and asymmetry	**0.1**, 0.12, 0.15
	dilatancy	Switch to reduce critical shields number due to dilatancy	**0**, 1
	D50	D50 grain diameters for all sediment classes, in meters	0.0025

*The calibrated XBeach parameter set from Kalligeris et al. (2020) was utilized in this study. See study for the full list of parameter values used.

site. XBeach parameters were then selected and adjusted based on previous work in the literature summarized above. From pressure sensor observations at the dune toe and salinity measurements behind the dune (Figure 4.8), the intermediate to reflective storm event is characterized by the collision and overwash regimes; therefore, after default parameter simulations, the parameters *facua* and *dilatancy* were adjusted for selected XBeach simulations. In the 1D XBeach simulations, a *facua* value of 0.12 was selected based off slope from $\sim$ 0 m NAVD88 to dune crest (Elsayed and Oumeraci, 2017). Additionally, Kalligeris et al. (2020) calibrated 1D XBeach parameters to Southern California beaches, and this optimal parameter set was tested in the 1D XBeach simulations. In 2D several values of *facua* ranging from 0.1 (default) to 0.15 were tested. A value of 0.15 resulted in the highest predictive skill at the breaching location. The reader is directed to Table 4.3 for all model parameter values used.

4.5.4 Model Scenarios and Evaluation

Morphology was investigated and modeled at four cross-shore locations, transects M1-M4 with SBeach, CSHORE, and surfbeat 1D XBeach. It should be noted that SBeach and CSHORE simulated hourly simulated beds. Additional hydrodynamic modeling was conducted at locations M2, M3, locations where breaching was observed, as well as H1, an access way that cuts through the dune, and pressure sensor location P1. Non-hydrostatic 1D XBeach was utilized simulate wave runup and overtopping/overwash. Hydrostatic surfbeat XBeach1D was utilized to predict post storm beds; these were utilized as input beds for the non-hydrostatic XBeach simulations. The simulations cover the period between January 21, 2017 20:00 UTC to January 22, 2017 24:00 UTC, a total of 28 hours. The simulation time covers the peak of the high water level and energetic wave event (Figure 4.3) with additional model spin up time. XBeachX MPI (Message Passing Interface) supports parallel processing to increase computational speed, which is particularly useful for 2D simulations with large domain sizes. The 2D simulation in this work was run with the MPI version of XBeachX utilizing 19 nodes on a Windows 64-bit desktop for around 14 hours.

Dune erosion and breaching during the storm event was simulated and compared with post-storm observed dune parameters including dune toe and crest elevations, dune slopes, and volume changes. Several fit measures were estimated to quantify model performance. The Brier Skill Score (BSS) is a commonly used metric to evaluate coastal morphological model performance (e.g., McCall et al., 2010; Simmons et al., 2017, 2019; Kalligeris et al., 2020). It compares the mean square difference between the observations and model predictions with the mean square difference between the observations and baseline prediction, usually taken to be no bed change (VanRijn et al., 2003). A BSS value of 1 indicates model predictions prefectly match observations, VanRijn et al. (2003). BSS values were calculated along the dune face of the modeled profiles to compare modeled and observed bed elevation change. The root-mean-square-error (RMSE), bias and R^2 values were calculated between the observations and model predictions as additional model performance indicators.

To quantify hydrodynamic model performance, simulated water levels, nearshore wave parameters and power spectra, and overtopped volumes were compared to observations. Nearshore wave parameters and power spectra were derived from the measured sea surface elevation at the nearshore PUV as in Fiedler et al. (2015). Cumulative dune toe wave collision/interaction hours observed at the buried pressure sensor were estimated for the duration of the storm by summing total hours in which individual, consecutive wave excursions (Figure 4.8a) were separated by 5 minutes or less, indicating infragravity waves in the recorded sea-surface elevation time series. This was then compared with modeled hourly cumulative wave collisions from non-hydrostatic 1D XBeach, and hydrostatic surfbeat 1D and 2D XBeach. Observed cumulative marine overtopping volumes in the drainage ditch backing the dune breach were compared to modeled cumulative overtopped volumes. Modeled cumulative overtopped volumes were estimated by scaling the total 1D overtopped volume (in m^3/m) by the representative beach reach lengths (in m) of each transect to m^3 as in (Gallien, 2016). Dune breach time and duration during the peak of the storm event were compared to modeled breach times and duration.

Table 4.4: Simulations, listed by cross-shore location and model, considered in this study. A dash indicates the model was not run at the selected locations.

Transect	SBeach	CSHORE	XBeach 1D Hydrostatic (SB)	XBeach 1D Non-hydrostatic	XBeach 2D Hydrostatic (SB)
M1	✓	✓	✓	-	✓
M2	✓	✓	✓	✓	✓
M3	✓	✓	✓	✓	✓
M4	✓	✓	✓	-	✓
P1	-	-	✓	✓	✓
H1	-	-	✓	✓	✓

4.6 Results

4.6.1 Hydrodynamic Modeling

Nearshore wave parameters and spectra predicted by non-hydrostatic XBeach were examined to quantify hydrodynamic performance. Hourly significant wave heights were measured at the deployed PUV nearshore and compared to modeled XBeach non-hydrostatic wave heights (Figure 4.9a.). Predicted H_s values match relatively well with those observed for the duration of the storm; however, the peak H_s was predicted four hours earlier than what was observed (Figure 4.9a). The wave power spectrum was produced from the sea surface elevation measured by the deployed PUV at 8 m depth offshore (Figure 4.9b) at the two peak hours of the storm, from January 22, 2017 1200 UTC to 1400 UTC, and compared to power spectra produced by non-hydrostatic XBeach. The model captured the peak observed frequency of 0.05 Hz (T_p of $\sim$20 s) relatively well (Figure 4.9b.), with less accuracy predicting observed infragravity waves in the lower frequencies. Hydrostatic default XBeach overpredicted wave interaction hours at both of the deployed buried pressure locations, while non-hydrostatic overpredicted interaction hours at location P1 by almost one and half hours (Table 4.5). Overall, non-hydrostatic XBeach predicted total interaction hours at both locations within 1.5 hours or less, while hydrostatic XBeach predicted within 3.25 hours or less.

4.6.2 Modeled Overtopping

Observed overtopping during the storm began on January 22, 2017 at approximately 0700 UTC and continued until approximately 1400 UTC, as indicated by the observed marine overtopping measured by the backshore salinity and depth sensor (Figure 4.10). The 1D default non-hydrostatic XBeach model most closely predicted the overtopping start and time, while 1D surfbeat XBeach predicted the start time about 6 hours earlier than observed (Figure 4.10). All models predicted overtopping end time within 2 hours. The observed cu-

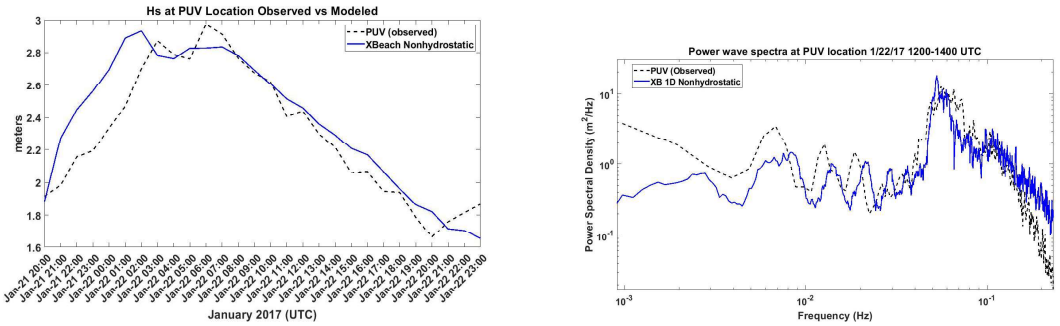

Figure 4.9: Observed and modeled significant wave height and power wave spectra at PUV location.

mulative marine overtopped volume after the peak of the storm (January 22, 2017 0700-1400) estimated with the hypsometric analysis was on the order of 34 m^3. Modeled overtopped volumes along model profiles (rows in XBeach 2D), in m^3, through breaching transects were estimated by multiplying overtopped volumes in m^3 by breach reach length of 5 meters. Overtopped volumes from all transects that overtopped in each set of one-dimensional XBeach simulations with the same parameters, both hydrostatic and non-hydrostatic, were summed to obtain a cumulative two-dimensional overtopped volume along all overtopping locations on the beach. Summed cumulative overtopped volume from all default 1D XBeach non-hydrostatic simulations estimated within 1 m^3 of observed (Figure 4.10). Overtopped volume estimated by default 1D surfbeat XBeach overestimated cumulative overtopping by $\sim$40 m^3 while 1D surfbeat XBeach parameterized with *facua* and *dilatancy* overestimated by $\sim$10 m^3 (Figure 4.10).

Table 4.5: Observed and modeled wave interaction/collision hours at the buried pressure sensor 1 (P1).

Location/Sensor	**Observed**	**Non-hydrostatic 1D XBeach (default)**	**Hydrostatic 1D XBeach (default)**
Pressure Sensor 1)	14.75	16.2	18

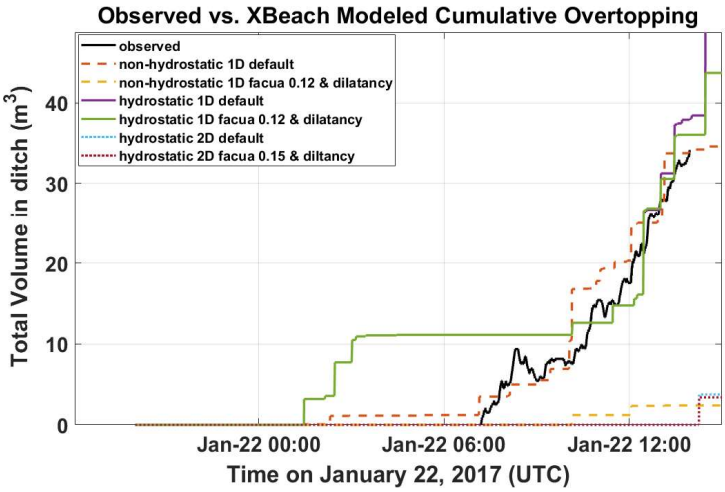

Figure 4.10: Cumulative overtopped volume in cubic meters predicted by different modes of XBeach (1D non-hydrostatic, 1D hydrostatic, and 2D hydrostatic) into backshore drainage ditch and observed cumulative overtopping.

4.6.3 Morphological Modeling

Examining the BSS evaluated from 2 m NAVD88 to the dune crest along each cross-shore transect M1-M4, all skill scores were less than 0.5. Reasonable skill may be assigned if the BSS $\in$ (0.3,0.6] (VanRijn et al., 2003), and anything less than 0.3 is considered poor skill. A negative skill score (i.e., BSS $<$ 0) indicates poor skill and indicates model performance worse than no change prediction. The majority of models exhibit negative skill, particularly at locations M1 and M2 where all BSS values are negative (Figure 4.14). Reasonable skill (BSS $\in$ (0.3,0.6]) is exhibited by CSHORE and 1D XBeach, where the highest skill at M3 is 0.362 by default CSHORE at breach location M3 (Figure 4.14).

Qualitatively both SBeach and CSHORE tend to predict the post-storm dune crest elevation and profile shape with some accuracy, with the CSHORE Pacific parameters producing over erosion of the crests at Transects M2 and M3 (Figure 4.11b,c). SBeach with the higher $BMAX$ value displays under erosion of the dune face at M1 and M2, while CSHORE default parameters resulted in both slight under and over erosion of the dune face (Figure 4.11a,b).

Over erosion of the dune face is also produced by the CSHORE Pacific parameters at M2 and M3 (Figure 4.11b,c). Briar Skill Scores were generally poor for SBeach. Similarly, CSHORE BSS were low. M1 and M2 were negative regardless of the parameter set. Only the breached transect M3 was positive for SBeach, BSS values of 0.18 and 0.15, and CSHORE, BSS values from 0.23 to 0.36 (Figure 4.14).

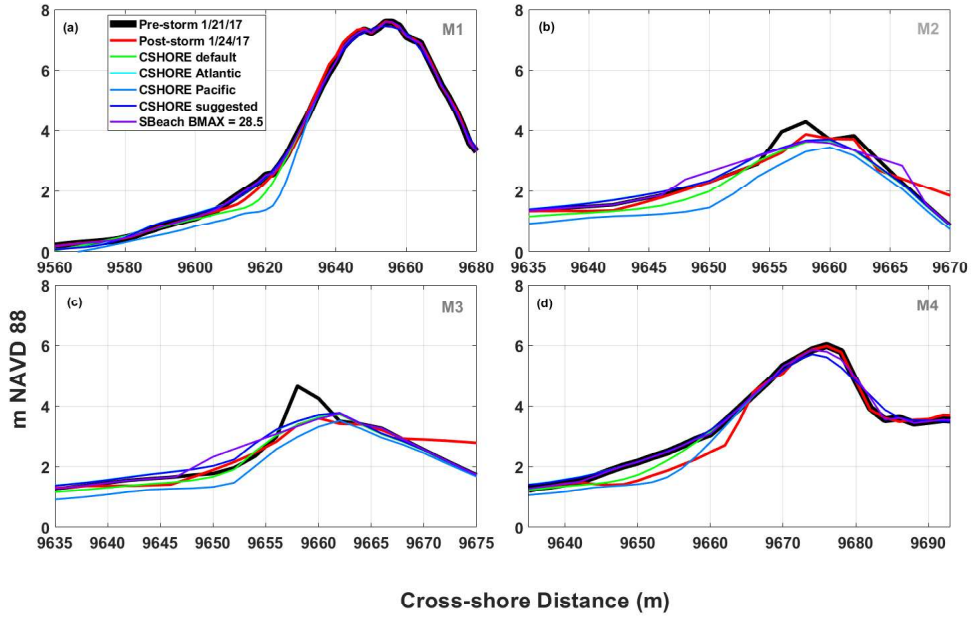

Figure 4.11: SBeach and CSHORE modeling results

Generally XBeach over erodes the dune face (Figure 4.12). Default 1D and 2D XBeach simulated dune crest elevations closer to the observed post-storm values; however default XBeach produced the most over erosion at M1 through M3, with 1D simulating more erosion than 2D (Figure 4.12a-c). XBeach 1D simulations utilizing the parameter set from Kalligeris et al. (2020) predicted very little erosion of the dune, except at transect M2 where some dune face erosion is evident (Figure 4.12b). Simulations utilizing the higher *facua* parameter value and enabled dilatancy produced less dune face erosion than the default set-up, and at M2 this also resulted in under erosion of the post-storm dune crest (Figure 4.12).

Overall the XBeach 2D simulations successfully predicted high erosion in the area of

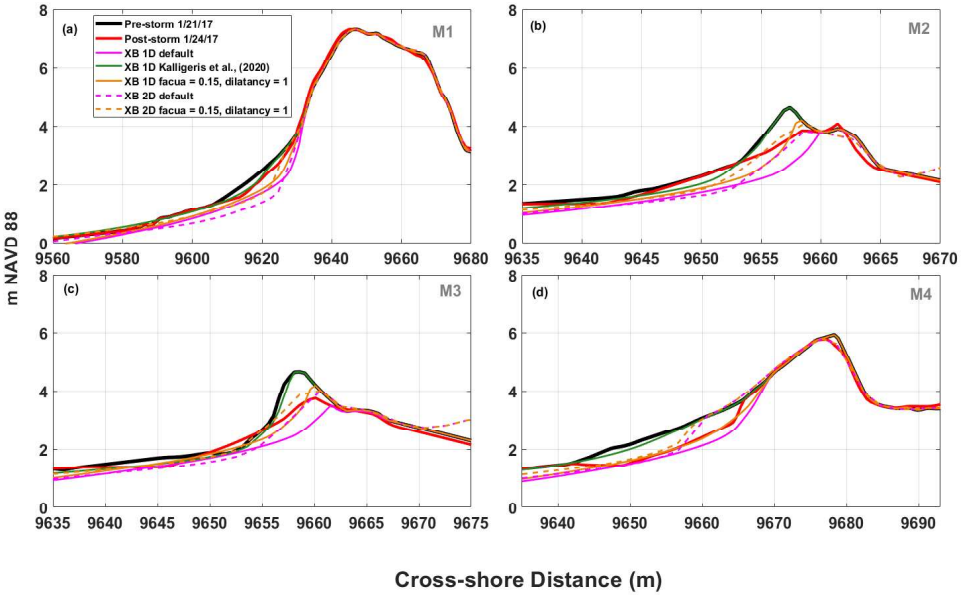

Figure 4.12: XBeach 1D and 2D modeling results

interest, the area around M2 and M3 between 1000 m and 1200 m in the alongshore, as evident in the difference maps in Figure 4.15(c-e). Default 2D XBeach produced over erosion in this area of interest (Figure 4.15d), while the tuned model produced erosion of a similar magnitude to the observations (Figure 4.15e). XBeach 2D estimated the post-storm dune crest elevation magnitude at the breaching location M3, which experienced the highest crest erosion, more accurately than at locations with less crest erosion such as the location between profile M2 and pressure sensor 1 (near y = 1050 m) (Figure 4.16b). Overall, XBeach 2D predicted the magnitude of dune toe elevation, dune volume, and dune slope decreases well in the areas with most extreme change (Figure 4.16c-e).

SBeach and CSHORE were more successful at predicting the post-storm dune crest, dune face slope, and dune volumes than XBeach (Figure 4.13). Overall, the dune crest, volume sand slopes were more closely predicted by all three models compared to the dune toe (Figure 4.13). Not one cross-shore location's post storm dune toe elevation was best estimated by the same model and parameter set (Figure 4.13). Notably, the 1D XBeach model paramaterized

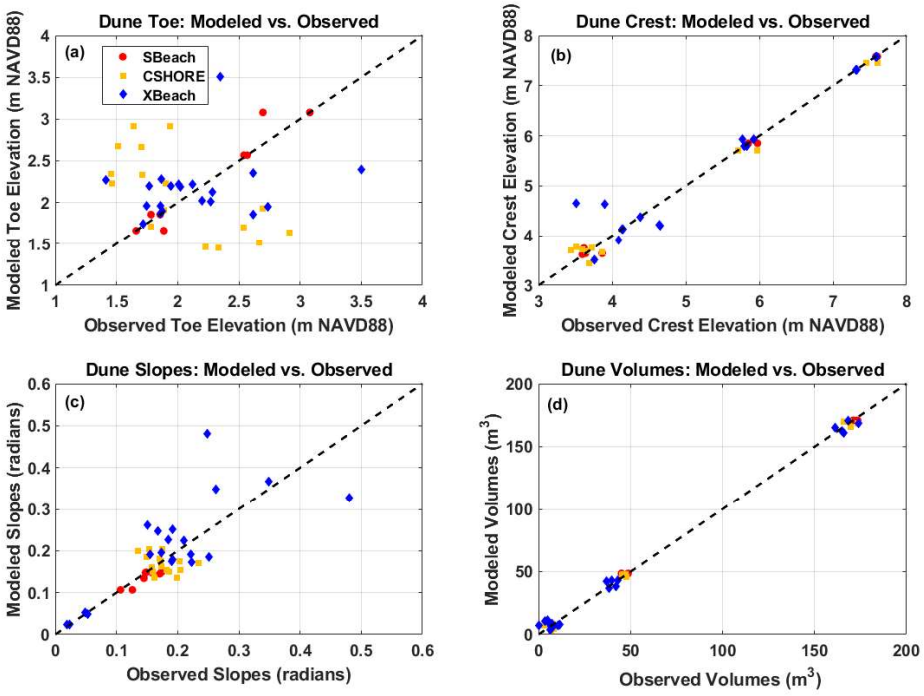

Figure 4.13: Regression plots of observed and modeled dune characteristics.

with *facua* and *dilatancy* predicted the dune toe elevation most closely at profile M2, while 1D XBeach Kalligeris et al. (2020) parameters and 2D XBeach paramaterized with *facua* and *dilatancy* predicted the toe most successfully at breach M3. The dune crest at breaching location M2 was most closely predicted by default 1D XBeach, while at breach M3 CSHORE default and suggested parameter sets most accurately estimated the post-storm crest (Figure 4.12). Location M1's post storm dune crest was closely predicted by all SBeach and 2D XBeach parameter sets, while the crest of M4 was best captured by all 1D XBeach parameter sets (Figure 4.12.

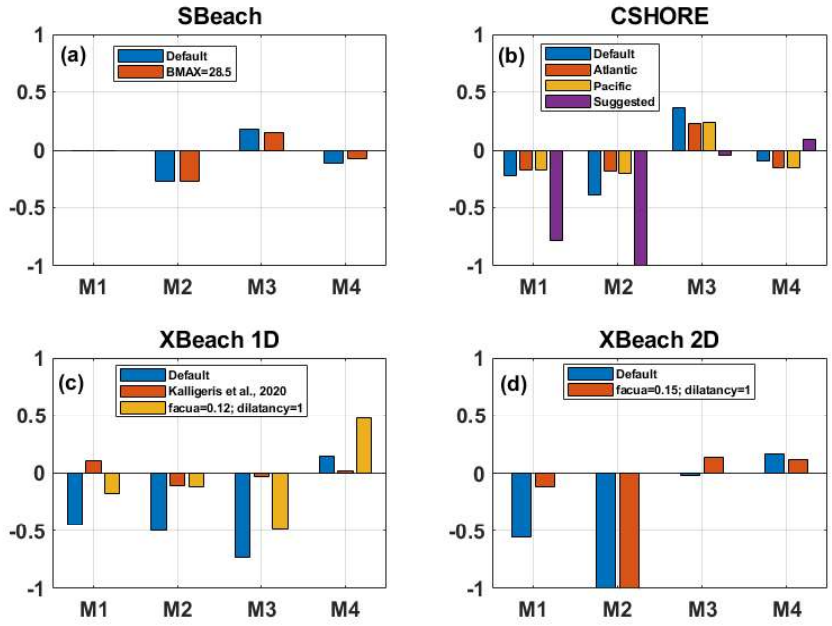

Figure 4.14: BSS values across all models and cross-shore locations. BSS only estimated from 2 m NAVD88 to the dune crest.

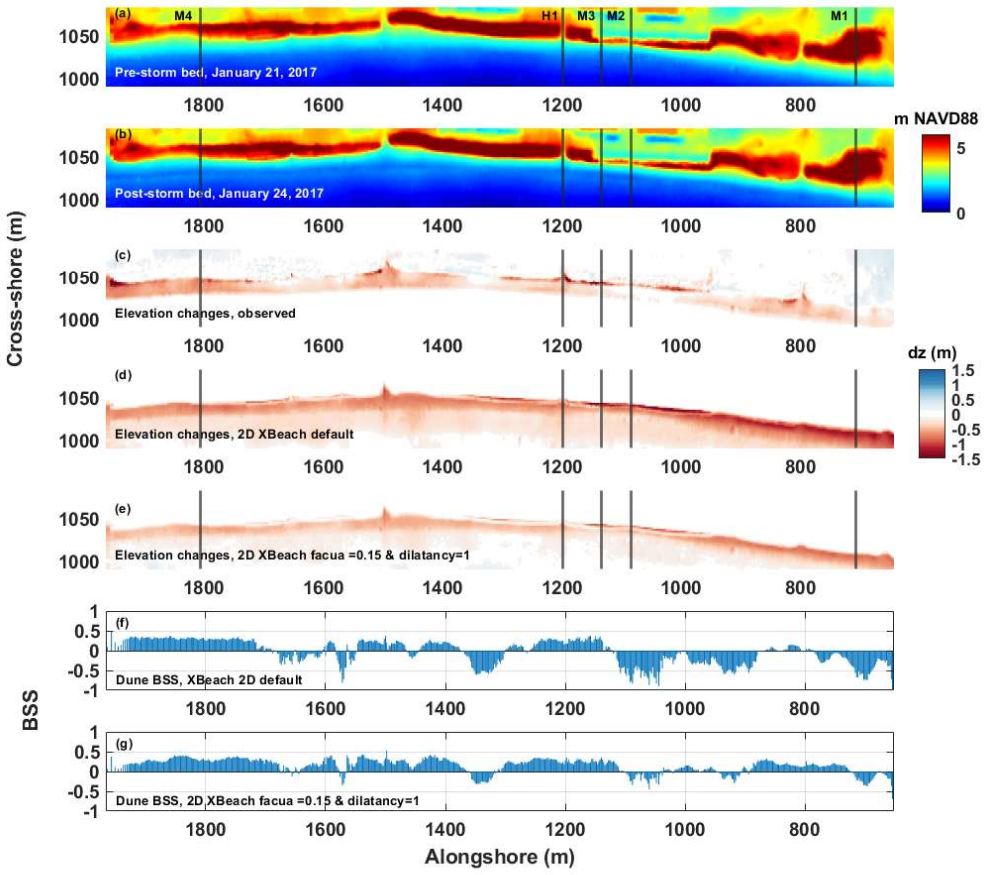

Figure 4.15: (a) Observed pre-storm elevation bed with modeled cross-shore transects of interest indicated by black lines. (b) Observed post-storm bed. (c) Observed beach elevation change from pre- to post-storm (d),(e) XBeach 2D modeled beach elevation change from pre- to post-storm. (f),(g) Brier Skill Score for every cross-shore location (each cross-shore grid row) for both 2D XBeach simulations. BSS only estimated from 2 m NAVD88 to the dune crest.

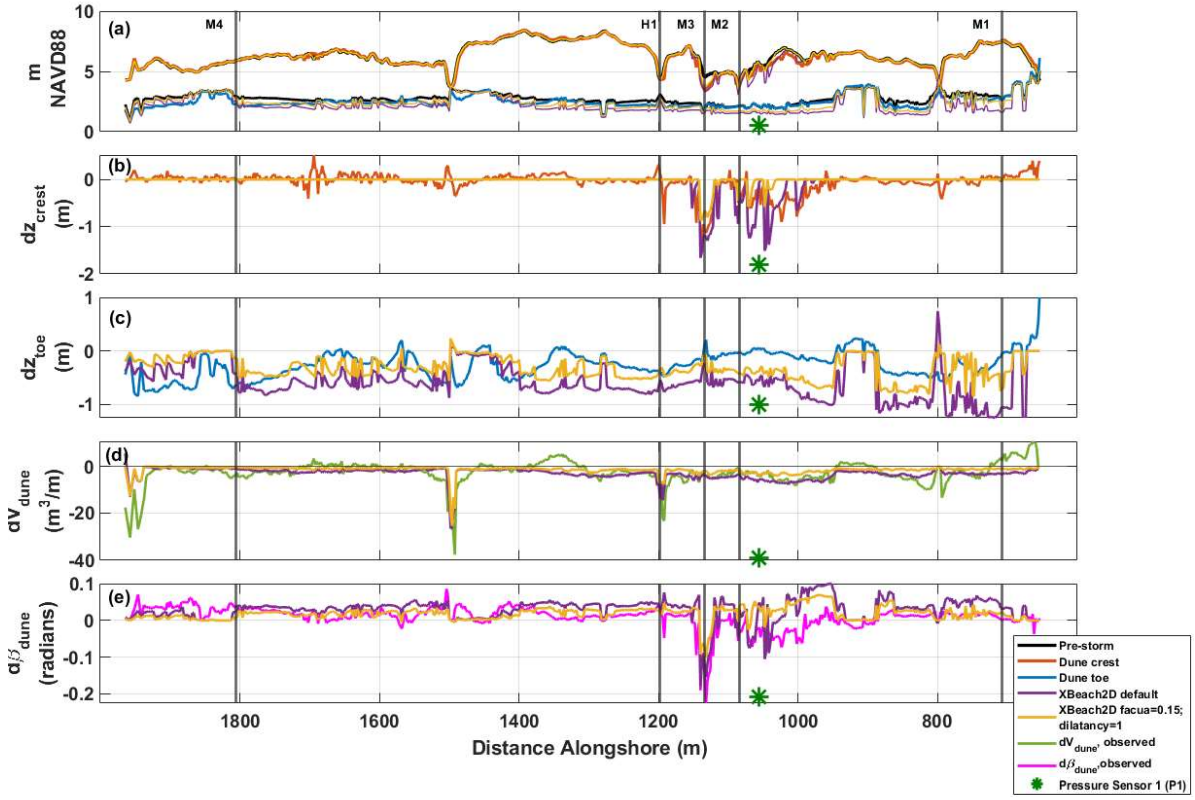

Figure 4.16: Observed and XBeach 2D modeled (a) dune crest and toe heights (b) crest and (c) toe changes from pre- to post-storm (d) dune volume change from pre- to post-storm (e) dune face slope change from pre- to post-storm. Green asterisk indicates alongshore location of the buried pressure sensor, P1.

4.7 Discussion

4.7.1 Morphological Modeling

The majority of skill scores exhibited by all three models are negative (Figure 4.14); however, despite this, each model reasonable reproduces different individual dune characteristics, at different beach locations and during different dune erosion regimes. SBeach and CSHORE exhibited the highest BSS values at breaching locations M2 and M3 and reproduced the post-storm dune slopes at these location with the most success (Figure 4.11), with SBeach and CSHORE predicting the dune slope more accurately than XBeach as a whole (Figure 4.13c). The majority of all three model simulations reproduced the post-storm dune volume with high success and the post-storm dune toe elevation with low success, except for SBeach exhibiting success predicting the dune toe (Figure 4.13).

XBeach showed positive morphological skill at locations M1 and M4 in 1D, with reasonable skill shown at M4 (Figure 4.14). In 2D, additional positive skill at locations M3 and M4 in 2D (Figure 4.14). Notably, bed predictions at location M2 made by XBeach 2D resulted in even more negative BSS values; in fact no positive BSS value was obtained at M2 by any of the models (Figure 4.14). XBeach 2D most successfully predicted post-storm change along portions along the dune that experienced the largest decreases in toe and crest elevations, dune volume and dune slope (Figures 4.16). Notably, the breach area of the beach with the highest pre-storm dune slope of 0.55 near transect M3 (Figure 4.16) experienced the largest magnitude of dune crest lowering (Figure 4.16c). Additionally, the highest volume losses along the dune occurred at the dune ends and access ways (y = 1500 m, y = 1200 m, y = 800 m) (Figure 4.16d). Because the post-storm survey did not capture the beach foreshore, the skill scores were estimated along the subaerial beach and dune only; post-storm beach foreshore information would have provided valuable insight on model performance in this area during this opportunistic field campaign.

Two factors may in part explain some of XBeach's limited success in predicting the

post-storm dune morphology. First, XBeach was primarily developed for extreme storm events along dissipative coastlines, such as the Dutch, European and United States East coasts, dominated by infragravity swash (Roelvink et al., 2009, 2018) and having typically moderately to gently sloped foreshores (e.g., McCall et al., 2010; de Winter et al., 2015; Schweiger et al., 2020). XBeach, when applied with its default parameters, has shown mixed results on more intermediate to reflective coastlines characterized by more incident swash and steeper slopes, displaying a tendency to overestimate beach and dune erosion (e.g., Splinter and Palmsten, 2012; Simmons et al., 2019; Kalligeris et al., 2020; Cohn et al., 2021). All cross-shore locations in this study were in an intermediate-to-reflective beach state (defined as $0.3 < R^{IG}/R < 4.0$ in Wright and Short (1983)) for the entire duration of the storm, except location M1 for one hour post-storm peak, and the surfzone was saturated ($R^{IG}/R > 0.85$) the full duration except for locations M1, M4 and P1 (Table 4.1, Figure 4.4). Secondly, in contrast to Kalligeris et al. (2020) which evaluated XBeach performance with limited success on moderately energetic Southern California beaches, the storm simulated here was highly energetic ($H_s > 4$ m; $T_p \sim 20$ s) and of shorter duration, an event of magnitude XBeach favors.

SBeach and CSHORE obtained higher Brier Skill Scores and were more successful than XBeach at predicting selected post-storm dune morphology (Figure 4.13a, b; Figure 4.14b, c). Similarly, in prior studies default SBeach has previously shown higher success than default XBeach at predicting storm-induced dune change of intermediate-to-reflective beaches (e.g., Callaghan et al., 2013; Simmons et al., 2019; Kalligeris et al., 2020; Cohn et al., 2021; Simmons and Splinter, 2022). This may also be in part due to the model formulations of SBeach and CSHORE. SBeach was originally developed with data from lab experiments and initially tested and developed for beaches along the United States East Coast (Schoonees and Theron, 1995), but it also has previously been validated with beach erosion data from Torrey Pines, also located in Southern California (Kalligeris et al., 2020). In this study, SBeach shows success similar to previous studies on predicting post-storm beach morphology

such as Callaghan et al. (2013), Simmons et al. (2019), Simmons and Splinter (2022), where SBeach displayed overall higher skill than XBeach at an intermediate beach in Eastern Australia. It is suggested that SBeach produces less erosion on less dissipative beaches due to its lack of infragravity energy in the model formulation (e.g., Larson and Kraus, 1989; Callaghan et al., 2013; Simmons et al., 2019; Simmons and Splinter, 2022).

CSHORE also displayed higher skill than XBeach in this study similar to prior applications of the model to steeper, more intermediate coastlines (e.g., Simmons et al., 2019; Kalligeris et al., 2020; Cohn et al., 2021). Interestingly, the CSHORE default and 'Atlantic' parameter sets showed higher skill than the 'Pacific' parameter set, similarly to Kalligeris et al. (2020). CSHORE also predicted the post-storm dune face slope with high success such as in Cohn et al. (2021) at the FRF in Duck, North Carolina, an intermediate beach. While CSHORE has been applied at other intermediate beaches (U.S. Army Corps of Engineers, 1994), CSHORE does not explicitly resolve infragravity swash effects. Additionally, the CSHORE 'Atlantic' parameter set were developed for steeper sloped beaches (Johnson et al., 2012) which may contribute to its success at predicting morphology at this site partially characterized by an intermediate beach phase at the peak of the winter storm.

4.7.1.1 Models in the Collision vs. Overwash Regime

The dune structure at this site underwent the collision and overwash regimes along different cross-shore locations during this energetic winter storm. Locations M1 and M4 were in the collision regime and experienced dune toe and face erosion while locations M2 and M3 were both in the collision and then overwash regime at the high tide and peak of the storm, resulting in lowering of their crests (Figure 4.12b,c). Increasing the value of *facua* and enabling the *dilatancy* parameter increased the BSS values in both XBeach 1D and 2D; however, values remained negative in 1D at breaches M2 and M3 even with this modification. Both XBeach 1D and XBeach 2D displayed higher skill scores at M4, which experienced considerable erosion at the dune face, than at either M2 or M3 (Figure 4.14); in fact, all XBeach

simulations produced negative skill scores at M2. However, BSS values were mostly negative at location M1, which only experienced minor erosion in the collision regime, including the BSS values produced by SBeach and CSHORE (Figure 4.14). Over-prediction of post-storm dune erosion at beaches experiencing overwash and breaching has been noted in the literature (e.g., McCall et al., 2010; De Vet, 2014; Simmons et al., 2017), which the findings here show agreement with. However, other studies have found that the XBeach model better predicts post-storm dune morphology in the overwash regime than in the collision regime (e.g., Berard et al., 2017; Schweiger et al., 2020).

SBeach and CSHORE have shown to be generally successful predicting beach and/or dune change, including in the collision regime (e.g., Callaghan et al., 2013; Simmons et al., 2019) and in the overwash regime (e.g., Schoonees and Theron, 1995; Wise and Kraus; Donnelly, 2008; Harter and Figlus, 2017). SBeach was found to perform with greater success than XBeach at Narrabeen-Collaroy Beach, an intermediate beach along the Australian coastline, at predicting post-storm morphology (Callaghan et al., 2013; Simmons et al., 2019), including against calibrated XBeach across a 39-year range of storm magnitudes (Simmons and Splinter, 2022). However, when calibrated with field data, calibrated XBeach produced improved skill over calibrated SBeach along this beach (Simmons et al., 2019). Harter and Figlus (2017) successfully simulated overwash of a barrier island in Gulf of Mexico using CSHORE with a skill at one transect of 0.61 and better captured the post-storm beach slope and shoreline than XBeach but did not capture the foredune morphology. This is likely because CSHORE does not explicitly resolve sheet flow associated with inundation during overwash (Harter and Figlus, 2017). Additionally, CSHORE does not include infragravity swash, only incident swash, perhaps contributing to its success predicting dune erosion of the breaching locations that experienced runup and overwash on the steeper dune face.

van Wiechen et al. (2023) tested a suite of models, including Larson et al. (2004) and XBeach, against data from the 1993 LIP11D experiments carried out at the Delta Flume in the Netherlands that investigated dune erosion in the collision regime (Arcilla, 1994). In

agreement with this study's findings, there was not a single model that produced accurate predictions for all scenarios; simpler models, in some cases, may prove to be better tools than more complex models (van Wiechen et al., 2023).

4.7.2 Overtopping Modeling

Despite poor or negative skill scores, both hydrostatic and non-hydrostatic XBeach reasonably estimated cumulative marine overtopped volume into the backshore (Figure 4.10). Care should be taken in selecting a beach reach length when scaling 1D simulated overtopping volumes (m^3/m) to (m^3); beach reach length must only include alongshore lengths with unchanging foreshore slopes and major characteristics overall. Selection of a different reach length would yield different predicted overflow volumes. Hydrostatic mode predicted about 22% more wave interaction hours at the dune toe in comparison to non-hydrostatic mode (Table 4.5). Non-hydrostatic XBeach includes incident band swash, required for relatively steep beaches Roelvink et al. (2018), and the swash was interacting with the dune face for more than a quarter of the storm duration. Additionally, the event was characterized by a partially saturated surf zone across different cross-shore locations, a combined 36% of the time, characterizing the event as partially dissipative but still mostly intermediate to reflective compared to European coastlines (Wright and Short, 1983) that XBeach was developed and parameterized with (Roelvink et al., 2009, 2018). Although the event was primarily characterized as intermediate to reflective, it was sufficiently energetic, perhaps explaining both model's success in predicting overtopping in this case. Previous work has found that XBeach, in hydrostatic surfbeat mode, underestimates runup on more intermediate beaches, likely due to surfbeat mode lacking resolved incident swash (e.g., Stockdon et al., 2014; Cohn et al., 2021). Notably, these studies tested the model on storm events in the collision regime.

XBeach non-hydrostatic swash prediction skill has not yet been tested comprehensively on a wide range of dissipative to reflective wave conditions (de Beer et al., 2021). Additionally, few studies have directly, and quantitatively, compared the capability of both

XBeach hydrostatic and non-hydrostatic mode (de Beer et al., 2021). Gallien (2016) validated backshore overtopping magnitudes and extent observations against both hydrostatic and non-hydrostatic overtopping predictions at another southern California beach and found that XBeach non-hydrostatic mode predicted an order of magnitude higher overtopping volumes compared to hydrostatic mode. Notably, the study site in Gallien (2016) was steeper (slopes $\sim$ 0.09 to 0.13) than the present study site (slopes $\sim$ 0.03); therefore XBeach hydrostatic likely underestimated incident swash process. de Beer et al. (2021) showed that the XBeach surfbeat model predicts setup at the waterline similarly to the non-hydrostatic model for all conditions on an intermediate-reflective beach in Duck, North Carolina. Lashley et al. (2018) demonstrated that both XBeach modes were able to accurately predict both maximum and two percent exceedance swash runup on a fringing reef.

The study presented here demonstrates very similar overtopping predictions by both XBeach modes; however, detailed measurements and description of runup and individual overtopping excursion over the dune crest were not observed during the field campaign. Detailed information regarding the range of application of XBeach hydrostatic is needed, given the wide application of this mode in engineering practice (de Beer et al., 2021); therefore, additional analysis quantitatively comparing runup, including the difference in incident and infragravity swash is needed.

4.7.3 Limitations

Notably, this study only considers a single deterministic run for each model, and only one storm event is considered here; more data from this site and model testing would be required to more thoroughly compare morphological models and both hydrostatic and non-hydrostatic XBeach hydrodynamic modeling capabilities. Additionally, this study utilizes XBeach*X*. Recently, a newer, improved version of the model XBeach *Halloween* was released. XBeach results were not compared to prior studies cited here which tested XBeach *Groundhog* and *Kingsday*. Vousdoukas et al. (2012) noted that including backshore infrastructure would be

an improvement, as it is expected to interact with overwash flow. Elsayed and Oumeraci (2017) found improved XBeach performance at a beach with asphalt roads and parking lots with a much higher Shields parameter and concluded this was likely due to hindered erosion by higher soil and sand compaction beneath the asphalt. Also of note, care must be taken during model grid creating; the suggested grid cell size to model dune erosion with XBeach hydrostatic, as stated in the manual (Deltares, 2013) is 2 meters; however, on smaller scale berm-dune structures, 2-meter resolution perhaps insufficiently fine to resolve smaller berm features such as walk ways and access ways.

4.8 Conclusions

Three coastal and dune erosion models were tested and compared with a high-resolution overwash and breacing event data set at a beach dominated by long period swell: SBeach, CSHORE, and XBeach. Morphology prediction skill were tested with all three models. XBeach 1D and 2D was also used to evaluate runup and overtopping volumes. Hydrostatic and non-hydrostatic XBeach predicted same order of magnitude marine overtopping volume backshore of the dune and compared to the observed salinity and depth observations. SBeach and CSHORE displayed higher morphological model skill at predicting the post-storm dune morphology, particularly at the location of overwash and breaching, where XBeach has been shown to overestimate erosion. Both SBeach and CSHORE resolve incident swash processes and lack explicit inclusion of infragravity waves, perhaps partially explaining their higher skill at locations that experience swash and overwash interaction along the steeper dune face. Interestingly, XBeach 1D produced higher skill scores compared to XBeach 2D.

This study serves as a test of dune hydromorphodynamics in a high-energy, long-period swell application. Additional high resolution event based observations are urgently needed to test and further develop process based models. Additional investigation is required to characterize missing or poorly resolved physics for sites dominated by long-period swell.

CHAPTER 5

Conclusions and Future Work

5.1 Conclusions

Extensive field observation and modeling were conducted to test and validate a suite of analytical and numerical morphological models. Current coastal morphological models do not display high predictive skill at these and other high energy intermediate to reflective sites. Current process based models can provide qualitative information about dune erosion and overtopping; however, specific morphodynamic predictions are limited in their success.

5.2 Future Work

Future work involves continued observations and morphological modeling to develop improved characterization of erosion processes in wave dominated, dune protected environments. The living shoreline project at Cardiff State Beach should continue to be monitored using UAV and/or LiDAR. Quarterly (seasonal) surveys and pre/post event surveys will provide key validation datasets for advancing the numerical modeling of hybrid dunes. Additionally, longer-term dune and beach behavior should be analyzed to consider the impacts of the hybrid dune structure on the surrounding areas.

Current dune morphological models have been developed for surge dominated coasts. Sediment transport parameterizations are highly empirical and developed primarily with data from dissipative coastlines in Europe and along the U.S. Gulf and Atlantic coasts. XBeach

has been shown to over erode the beach face and dunes in long period swell, tidally dominated (e.g., California) applications (Kalligeris et al., 2020). Additionally, multi-substrate dunes and living shorelines have not been well modeled in the literature. Developing and validating both empirical and numerical multi-substrate models in long period swell dominated environments is fundamental to engineering design and advancing coastal resilience. In XBeach, suspended and bed loads are parameterized with wave skewness and asymmetry from Ruessink et al. (2012), both of which were parameterized with data from the Dutch and French coasts and not recommended for beaches with steeper slopes than 1:30. Additional field and laboratory experiments are needed for steeper, energetic beaches dominated by long period swell to more accurately characterize wave skewness and asymmetry. Additionally, the effects of vegetation, beach groundwater and porosity, and wave obliquity on dune erosion are not fully understood (van Wiechen et al., 2023). Continued observation and modeling efforts are critical to identify and parameterize fundamental physics dominating in long period swell environments.

Bibliography

Adams, P.N., Inman, D.L., Graham, N.E., 2008. Southern california deep-water wave climate: characterization and application to coastal processes. Journal of Coastal Research 24, 1022–1035.

Ahrens, J.P., Seelig, W.N., Ward, D.L., Allsop, N., 1993. Wave runup on and wave reflection from coastal structures, in: Ocean Wave Measurement and Analysis, ASCE. pp. 489–502.

Allan, J., Komar, P., 2004. Environmentally compatible cobble berm and artificial dune for shore protection. Shore & Beach 72(1), 9–18.

Almarshed, B., Figlus, J., Miller, J., Verhagen, H.J., 2020. Innovative Coastal Risk Reduction through Hybrid Design: Combining Sand Cover and Structural Defenses. Journal of Coastal Research 36, 174.

Almeida, L.P., Masselink, G., McCall, R., Russell, P., 2017. Storm overwash of a gravel barrier: Field measurements and xbeach-g modelling. Coastal Engineering 120, 22–35.

Andrews, B., Gares, P.A., Colby, J.D., 2002. Techniques for gis modeling of coastal dunes. Geomorphology 48, 289–308.

Arcilla, A., 1994. The delta flume'93 experiment. Coastal Dynamics 1994, ASCE .

Armaroli, C., Ciavola, P., Perini, L., Calabrese, L., Lorito, S., Valentini, A., Masina, M., 2012. Critical storm thresholds for significant morphological changes and damage along the Emilia-Romagna coastline, Italy. Geomorphology 143-144, 34–51.

Athanasiou, P., van Dongeren, A., Giardino, A., Vousdoukas, M., Antolinez, J.A.A., Ranasinghe, R., 2022. Estimating dune erosion at the regional scale using a meta-model based on neural networks. Natural Hazards and Earth System Sciences 22, 3897–3915.

Basco, D.R., 1999. The economic analysis of "soft" versus "hard" solutions for shore protection: An example, in: Coastal Engineering 1998, pp. 1449–1460.

Bayle, P.M., Blenkinsopp, C.E., Martins, K., Kaminsky, G.M., Weiner, H.M., Cottrell, D., 2023. Swash-by-swash morphology change on a dynamic cobble berm revetment: High-resolution cross-shore measurements. Coastal Engineering , 104341.

Bayle, P.M., Kaminsky, G.M., Blenkinsopp, C.E., Weiner, H.M., Cottrell, D., 2021. Behaviour and performance of a dynamic cobble berm revetment during a spring tidal cycle in north cove, washington state, usa. Coastal Engineering 167, 103898.

de Beer, A.F., McCall, R.T., Long, J.W., Tissier, M.F., Reniers, A.J., 2021. Simulating wave runup on an intermediate–reflective beach using a wave-resolving and a wave-averaged version of xbeach. Coastal Engineering 163.

Berard, N.A., Mulligan, R.P., da Silva, A.M.F., Dibajnia, M., 2017. Evaluation of XBeach performance for the erosion of a laboratory sand dune. Coastal Engineering 125, 70–80.

Bergillos, R.J., Masselink, G., McCall, R.T., Ortega-Sánchez, M., 2016. Modelling overwash vulnerability along mixed sand-gravel coasts with xbeach-g: case study of playa granada, southern spain. Coastal engineering proceedings 1, 13.

Beuzen, T., Harley, M.D., Splinter, K.D., Turner, I.L., 2019. Controls of Variability in Berm and Dune Storm Erosion. Journal of Geophysical Research: Earth Surface 124, 2647–2665.

Blenkinsopp, C.E., Bayle, P.M., Conley, D.C., Masselink, G., Gulson, E., Kelly, I., Almar, R., Turner, I.L., Baldock, T.E., Beuzen, T., McCall, R.T., Rijper, H., Reniers, A., Troch, P., Gallach-Sanchez, D., Hunter, A.J., Bryan, O., Hennessey, G., Ganderton, P., Tissier, M., Kudella, M., Schimmels, S., 2021. High-resolution, large-scale laboratory measurements of a sandy beach and dynamic cobble berm revetment. Scientific Data 2021 8:1 8, 1–11.

Blenkinsopp, C.E., Bayle, P.M., Martins, K., Foss, O.W., Almeida, L.P., Kaminsky, G.M., Schimmels, S., Matsumoto, H., 2022. Wave runup on composite beaches and dynamic cobble berm revetments. Coastal Engineering 176.

Boers, M., 2012. Technisch rapport duinwaterkeringen en hybride keringen 2011. 1206018-001-HYE-0009 .

Boudreau, R., Sloop, R., Holloway, A., Rivera, J., 2018. Maui's resilient living shoreline project provides adaptation strategy for critical infrastructure. Shore & Beach 86, 26–35.

Bruun, P., 1954a. Coast erosion and the development of beach profiles. volume 44. US Beach Erosion Board.

Bruun, P., 1954b. Coast erosion and the development of beach profiles. volume 44. US Beach Erosion Board.

Bruun, P., 1983. Beach scraping - Is it damaging to beach stability? Coastal Engineering 7, 167–173.

Callaghan, D.P., Ranasinghe, R., Roelvink, D., 2013. Probabilistic estimation of storm erosion using analytical, semi-empirical, and process based storm erosion models. Coastal Engineering 82, 64–75.

Carson, M., Köhl, A., Stammer, D., A. Slangen, A., Katsman, C., W. van de Wal, R., Church, J., White, N., 2016. Coastal sea level changes, observed and projected during the 20th and 21st century. Climatic Change 134, 269–281.

Ceia, F.R., Patrício, J., Marques, J.C., Dias, J.A., 2010. Coastal vulnerability in barrier islands: The high risk areas of the Ria Formosa (Portugal) system. Ocean and Coastal Management 53, 478–486.

Church, J.A., Clark, P.U., Cazenave, A., Gregory, J.M., Jevrejeva, S., Levermann, A., Merrifield, M.A., Milne, G.A., Nerem, R.S., Nunn, P.D., et al., 2013. Sea level change. in:

Climate Change 2013: The Physical Science Basis. Contribution of Working I to the Fifth Assessment Report of the Intergovernmental Panel on Climate Change. .

Cohn, N., Brodie, K.L., Johnson, B., Palmsten, M.L., 2021. Hotspot dune erosion on an intermediate beach. Coastal Engineering 170, 103998.

Coles, S., Bawa, J., Trenner, L., Dorazio, P., 2001. An introduction to statistical modeling of extreme values. volume 208. Springer.

Cooper, J.A.G., Pilkey, O.H., 2004. Sea-level rise and shoreline retreat: Time to abandon the Bruun Rule. Global and Planetary Change 43, 157–171.

Coveney, S., Roberts, K., 2017. Lightweight UAV digital elevation models and orthoimagery for environmental applications: data accuracy evaluation and potential for river flood risk modelling. International Journal of Remote Sensing 38, 3159–3180.

Crossett, K., Ache, B., Pacheco, P., Haber, K., 2013. National Coastal Population Report: Population Trends from 1970 to 2010. NOAA State of the Coast Report Series , 22.

De Vet, P., 2014. Modelling sediment transport and morphology during overwash and breaching events. URL: `https://repository.tudelft.nl/islandora/object/uuid%3Ad4e21d44-fcef-498b-b2e5-83df3b0e0c47`.

De Waal, J., Van der Meer, J., 1993. Wave runup and overtopping on coastal structures. pp. 1758–1771.

Deltares, 2013. XBeach Documentation: Release XBeach v1.23.5527 XBeachX FINAL.

Deltares, 2018. XBeach Documentation: Release XBeach v1.23.5527 XBeachX FINAL. URL: `https://oss.deltares.nl/web/xbeach/home`.

Dette, H.H., Uliczka, K., 1987. Prototype investigation on time-dependent dune recession and beach erosion, in: Coastal Sediments, ASCE. pp. 1430–1444.

Dias, J.A., Ferreira, Ó., Matias, A., Vila-Concejo, A., Sá-Pires, C., 2003. Evaluation of soft protection techniques in barrier islands by monitoring programs: case studies from ria formosa (algarve-portugal). Journal of Coastal Research , 117–131.

Dickson, M.E., Kench, P.S., Kantor, M.S., 2011. Longshore transport of cobbles on a mixed sand and gravel beach, southern hawke bay, new zealand. Marine Geology 287, 31–42.

Didier, D., Baudry, J., Bernatchez, P., Dumont, D., Sadegh, M., Bismuth, E., Bandet, M., Dugas, S., Sévigny, C., 2019. Multihazard simulation for coastal flood mapping: Bathtub versus numerical modelling in an open estuary, eastern canada. Journal of Flood Risk Management 12, e12505.

Dissanayake, P., Brown, J., Karunarathna, H., 2014. Modelling storm-induced beach/dune evolution: Sefton coast, Liverpool Bay, UK. Marine Geology 357, 225–242.

Do, K., Kobayashi, N., Suh, K.D., Jin, J.Y., 2016. Wave Transformation and Sand Transport on a Macrotidal Pocket Beach. Journal of Waterway, Port, Coastal, and Ocean Engineering 142, 04015009.

Do, K., Shin, S., Cox, D., Yoo, J., 2018. Numerical simulation and large-scale physical modelling of coastal sand dune erosion. Journal of Coastal Research , 196–200.

Donnelly, C., 2008. Coastal overwash: processes and modelling. Ph.D. thesis.

Donnelly, C., Ranasinghe, R., Larson, M., . Numerical modeling of beach profile change caused by overwash, in: Coastal Dynamics 2005, pp. 1–14.

D'Alessandro, F., Tomasicchio, G.R., Francone, A., Leone, E., Frega, F., Chiaia, G., Saponieri, A., Damiani, L., 2020. Coastal sand dune restoration with an eco-friendly technique. Aquatic Ecosystem Health & Management , 1–8.

Edelman, T., 1972. Dune erosion during storm conditions. Coastal Engineering Proceedings 1, 66.

Edelman, T.I., 1968. Dune erosion during storm conditions. Coastal Engineering Proceedings 1, 46.

Edge, B.L., Ewing, L., Erickson, K.M., Magoon, O.T., 2003. Application of coastal engineering in coastal zone management. Advances in Coastal Structures Design. ASCE , 200–215.

Elsayed, S.M., Oumeraci, H., 2016. Combined modelling of coastal barrier breaching and induced flood propagation using xbeach. Hydrology 2016, Vol. 3, Page 32 3, 32.

Elsayed, S.M., Oumeraci, H., 2017. Effect of beach slope and grain-stabilization on coastal sediment transport: An attempt to overcome the erosion overestimation by XBeach. Coastal Engineering 121, 179–196.

Erikson, L.H., Larson, M., Hanson, H., 2007. Laboratory investigation of beach scarp and dune recession due to notching and subsequent failure. Marine Geology 245, 1–19.

Everts, C., Eldon, C., Moore, J., 2002. Performance of cobble berms in southern california. Shore and Beach 70, 5–14.

Federal Emergency Management Agency (FEMA) of the United States, 2005. Final Draft Guidelines for Coastal Flood Hazard Analysis and Mapping for the Pacific Coast of the United States. Technical Report.

Fiedler, J.W., Brodie, K.L., McNinch, J.E., Guza, R.T., 2015. Observations of runup and energy flux on a low-slope beach with high-energy, long-period ocean swell. Geophysical Research Letters 42, 9933–9941.

Figlus, J., West, N.A., Almarshed, B., Jonkman, S.N., 2015. Conceptual design and physical model study of core-enhanced dunes as hybrid coastal defence structures, in: Coastal Structures and Solutions to Coastal Disasters Joint Conference 2015, American Society of Civil Engineers Reston, VA. pp. 65–73.

Fisher, J.S., Overton, M.F., 1985. Numerical model for dune erosion due to wave uprush., ASCE. pp. 1553–1558.

Fisher, J.S., Overton, M.F., Chisholm, T., 1987. Field measurements of dune erosion, in: Proceedings of the Coastal Engineering Conference, ASCE. pp. 1107–1115.

Flick, R.E., 1994. Shoreline Erosion Assessment and Atlas of the San Diego Region. California Department of Boating and Waterways; San Diego Association of Governments.

Foss, O., Blenkinsopp, C.E., Bayle, P.M., Martins, K., Schimmels, S., Almeida, L.P., 2023. Comparison of dynamic cobble berm revetments with differing gravel characteristics. Coastal Engineering 183, 104312.

Fox-Kemper, B., 2021. Ocean, cryosphere and sea level change. Climate Change 2021 – The Physical Science Basis. Contribution of Working Group I to the Sixth Assessment Report of the Intergovernmental Panel on Climate Change , 1211–1362.

Galappatti, G., Vreugdenhil, C., 1985. A depth-integrated model for suspended sediment transport. Journal of Hydraulic Research 23, 359–377.

Gallien, T., Kalligeris, N., Delisle, M.P., Tang, B.X., Lucey, J., Winters, M., 2018. Coastal flood modeling challenges in defended urban backshores. Geosciences (Switzerland) 8.

Gallien, T.W., 2016. Validated coastal flood modeling at Imperial Beach, California: Comparing total water level, empirical and numerical overtopping methodologies. Coastal Engineering 111, 95–104.

Gallien, T.W., O'Reilly, W.C., Flick, R.E., Guza, R.T., 2015. Geometric properties of anthropogenic flood control berms on southern California beaches. Ocean and Coastal Management 105, 35–47.

Gallien, T.W., Sanders, B.F., Flick, R.E., 2014. Urban coastal flood prediction: Integrating wave overtopping, flood defenses and drainage. Coastal Engineering 91, 18–28.

Garcia, T., Ferreira, Ó., Matias, A., Dias, J.A., 2010. Overwash vulnerability assessment based on long-term washover evolution. Natural Hazards 54, 225–244.

Gharagozlou, A., Dietrich, J.C., Karanci, A., Luettich, R.A., Overton, M.F., 2020. Storm-driven erosion and inundation of barrier islands from dune-to region-scales. Coastal Engineering 158, 103674.

Glick, P., Kostyack, J., Pittman, J., Briceno, T., Wahlund, N., 2014. Natural Defenses from Hurricanes and Floods: Protecting America's Communities and Ecosystems in an Era of Extreme Weather. National Wildlife Federation.

Glover, L.B., Hales, L.Z., 1991. Numerical simulation of beach profile response to hurricane hugo, in: Coastal Sediments, ASCE. pp. 1712–1726.

van de Graaff, J., 1977. Dune erosion during a storm surge. Coastal Engineering 1, 99–134.

Griggs, G.B., 2005. The impacts of coastal armoring. Shore and beach 73, 13–22.

Hanley, M., Hoggart, S., Simmonds, D., Bichot, A., Colangelo, M., Bozzeda, F., Heurtefeux, H., Ondiviela, B., Ostrowski, R., Recio, M., et al., 2014. Shifting sands? coastal protection by sand banks, beaches and dunes. Coastal Engineering 87, 136–146.

Harley, M.D., Ciavola, P., 2013. Managing local coastal inundation risk using real-time forecasts and artificial dune placements. Coastal Engineering 77, 77–90.

Harris, M.E., Ellis, J.T., Barrineau, P., 2020. Evaluating the geomorphic response from sand fences on dunes impacted by hurricanes. Ocean and Coastal Management 193.

Harter, C., Figlus, J., 2017. Numerical modeling of the morphodynamic response of a low-lying barrier island beach and foredune system inundated during Hurricane Ike using XBeach and CSHORE. Coastal Engineering 120, 64–74.

Harvey, M.E., Giddings, S.N., Stein, E.D., Crooks, J.A., Whitcraft, C., Gallien, T., Largier, J.L., Tiefenthaler, L., Meltzer, H., Pawlak, G., Thorne, K., Johnston, K., Ambrose, R., Schroeter, S.C., Page, H.M., Elwany, H., 2020. Effects of elevated sea levels and waves on southern California estuaries during the 2015–2016 El Niño. Estuaries and Coasts 43, 256–271.

Heberger, M., Cooley, H., Herrera, P., Gleick, P.H., Moore, E., 2009. The impacts of sea-level rise on the california coast.

Hinkel, J., Aerts, J.C., Brown, S., Jiménez, J.A., Lincke, D., Nicholls, R.J., Scussolini, P., Sanchez-Arcilla, A., Vafeidis, A., Addo, K.A., 2018. The ability of societies to adapt to twenty-first-century sea-level rise. Nature Climate Change 8, 570–578.

Hovenga, P.A., Ruggiero, P., Itzkin, M., Jay, K.R., Moore, L., Hacker, S.D., 2023. Quantifying the relative influence of coastal foredune growth factors on the u.s. mid-atlantic coast using field observations and the process-based numerical model windsurf. Coastal Engineering 181, 104272.

Huang, W., Xu, S., Nnaji, S., 2008. Evaluation of GEV model for frequency analysis of annual maximum water levels in the coast of United States. Ocean Engineering 35, 1132–1147.

Hughes, S., Chiu, T., 1981. Beach and dune rosion during severe storms. Coastal and Oceanographic Engineering Department, University of Florida, Gainsville, Florida. Technical Report. UFL/COEL-TR.

Hunter, J., 2012. A simple technique for estimating an allowance for uncertain sea-level rise. Climatic Change 113, 239–252.

Irish, J.L., Lynett, P.J., Weiss, R., Smallegan, S.M., Cheng, W., 2013. Buried relic seawall mitigates Hurricane Sandy's impacts. Coastal Engineering 80, 79–82.

Jamal, M., Simmonds, D., Magar, V., 2014. Modelling gravel beach dynamics with xbeach. Coastal Engineering 89, 20–29.

Johnson, B.D., Kobayashi, N., Gravens, M.B., 2012. Cross-Shore Numerical Model CSHORE for Waves, Currents, Sediment Transport and Beach Profile Evolution Coastal and Hydraulics Laboratory. Technical Report.

Judge, E.K., Overton, M.F., Fisher, J.S., 2003. Vulnerability indicators for coastal dunes. Journal of Waterway, Port, Coastal and Ocean Engineering 129, 270–278.

Kalligeris, N., Smit, P.B., Ludka, B.C., Guza, R.T., Gallien, T.W., 2020. Calibration and assessment of process-based numerical models for beach profile evolution in southern California. Coastal Engineering 158, 103650.

Karunarathna, H., Brown, J., Chatzirodou, A., Dissanayake, P., Wisse, P., 2018. Multi-timescale morphological modelling of a dune-fronted sandy beach. Coastal Engineering 136, 161–171.

Kim, H.D., Kobayashi, N., Cárdenas, X.C., 2017. Experimental and numerical study on rock seawall in swash zone to reduce wave overtopping and overwash of sand beach .

Kobayashi, N., 1987. Analytical Solution for Dune Erosion by Storms. Journal of Waterway, Port, Coastal, and Ocean Engineering 113, 401–418.

Kobayashi, N., 2009. Efficient wave and current models for coastal structures and sediments, in: Selected Papers of the Symposium Held in Honor of Philip L-F Liu's 60th Birthday - Nonlinear Wave Dynamics, World Scientific Publishing Co. Pte Ltd. pp. 67–87.

Kobayashi, N., 2013. Cross-shore numerical model cshore 2013 for sand beaches and coastal structures .

Kobayashi, N., 2016. Coastal Sediment Transport Modeling for Engineering Applications. Journal of Waterway, Port, Coastal, and Ocean Engineering 142, 03116001.

Kobayashi, N., Jung, H., 2012. Beach Erosion and Recovery. Journal of Waterway, Port, Coastal, and Ocean Engineering 138, 473–483.

Kobayashi, N., Kim, H.D., 2017. Rock Seawall in the Swash Zone to Reduce Wave Overtopping and Overwash of a Sand Beach. Journal of Waterway, Port, Coastal, and Ocean Engineering 143, 04017033.

Kobayashi, N., Zhu, T., Mallavarapu, S., 2018. Equilibrium Beach Profile with Net Cross-Shore Sand Transport. Journal of Waterway, Port, Coastal, and Ocean Engineering 144, 04018016.

Kochnower, D., Reddy, S.M., Flick, R.E., 2015. Factors influencing local decisions to use habitats to protect coastal communities from hazards. Ocean and Coastal Management 116, 277–290.

Komar, P.D., Allan, J.C., 2010. "design with nature" strategies for shore protection: The construction of a cobble berm and artificial dune in an oregon state, in: Puget Sound Shorelines and the Impacts of Armoring—Proceedings of a State of the Science Workshop, May 2009: U.S. Geological Survey Scientific Investigations Report 2010-5254, pp. 117–126.

Kratzmann, M.G., Hapke, C.J., 2012. Quantifying Anthropogenically Driven Morphologic Changes on a Barrier Island: Fire Island National Seashore, New York. Journal of Coastal Research 28, 76 – 88.

Kraus, N.C., Smith, J.M., 1994. SUPERTANK Laboratory Data Collection Project. Volume 1. Main Text. Technical Report. USACE Coastal Engineering Reasearch Center Vicksburg, MS.

Kriebel, D.L., 1991. Advances in numerical modeling of dune erosion, Publ by ASCE. pp. 2304–2317.

Kriebel, D.L., Dean, R.G., 1985. Numerical simulation of time-dependent beach and dune erosion. Coastal Engineering 9, 221–245.

Küng, O., Strecha, C., Beyeler, A., Zufferey, J.C., Floreano, D., Fua, P., Gervaix, F., 2011. The accuracy of automatic photogrammetric techniques on ultra-light UAV imagery. Technical Report.

Larson, M., Erikson, L., Hanson, H., 2004. An analytical model to predict dune erosion due to wave impact. Coastal Engineering 51, 675–696.

Larson, M., Kraus, N.C., 1989. Sbeach: Numerical model for simulating storm-induced beach change. report 1, empirical foundation and model development .

Larson, M., Kraus, N.C., Byrnes, M.R., 1990. Sbeach: numerical model for simulating storm-induced beach change. report 2, numerical formulation and model tests .

Lashley, C.H., Roelvink, D., van Dongeren, A., Buckley, M.L., Lowe, R.J., 2018. Nonhydrostatic and surfbeat model predictions of extreme wave run-up in fringing reef environments. Coastal Engineering 137, 11–27.

Leadon, M., 2015. Beach slope and sediment-grain-size trends as a basis for input parameters for the sbeach erosion model. Journal of Coastal Research 31, 1375–1388.

Ludka, B.C., Gallien, T.W., Crosby, S.C., Guza, R.T., 2016. Mid-el niño erosion at nourished and unnourished southern california beaches. Geophysical Research Letters 43, 4510–4516.

Ludka, B.C., Guza, R.T., O'Reilly, W.C., Merrifield, M.A., Flick, R.E., Bak, A.S., Hesser, T., Bucciarelli, R., Olfe, C., Woodward, B., Boyd, W., Smith, K., Okihiro, M., Grenzeback, R., Parry, L., Boyd, G., 2019. Sixteen years of bathymetry and waves at San Diego beaches. Scientific data 6, 161.

Masselink, G., Tuck, M., McCall, R., van Dongeren, A., Ford, M., Kench, P., 2019. Physical and Numerical Modeling of Infragravity Wave Generation and Transformation on Coral Reef Platforms. Journal of Geophysical Research: Oceans 124, 1410–1433.

Matias, A., Ferreira, Ó., Mendes, I., Dias, J.A., Vila-Concejo, A., 2005. Artificial Construction of Dunes in the South of Portugal. Journal of Coastal Research 213, 472–481.

Matsumoto, H., Young, A.P., Guza, R.T., 2020. Observations of surface cobbles at two southern California beaches. Marine Geology 419, 106049.

McCall, R.T., Masselink, G., Poate, T.G., Roelvink, J.A., Almeida, L.P., 2015. Modelling the morphodynamics of gravel beaches during storms with XBeach-G. Coastal Engineering 103, 52–66.

McCall, R.T., Masselink, G., Poate, T.G., Roelvink, J.A., Almeida, L.P., Davidson, M., Russell, P.E., 2014. Modelling storm hydrodynamics on gravel beaches with XBeach-G. Coastal Engineering 91, 231–250.

McCall, R.T., Van Thiel de Vries, J.S., Plant, N.G., Van Dongeren, A.R., Roelvink, J.A., Thompson, D.M., Reniers, A.J., 2010. Two-dimensional time dependent hurricane overwash and erosion modeling at Santa Rosa Island. Coastal Engineering 57, 668–683.

Van der Meer, J., 2002. Technical report wave run-up and wave overtopping at dikes. TAW report (incorporated in the EurOtop manual) .

van der Meer, J., Allsop, N., Bruce, T., De Rouck, T., Kortenhous, A., Pullen, T., Schüttrumpf, H., Troch, P., Zanuttigh, B., 2016. EurOtop: Manual on wave overtopping of sea defences and related structures: an overtopping manual largely based on European research, but for worldwide application. URL: `www.overtopping-manual.com`.

Van der Meer, J.W., Stam, C.J.M., 1992. Wave runup on smooth and rock slopes of coastal structures. Journal of waterway, Port, coastal, and Ocean Engineering 118, 534–550.

Melet, A., Meyssignac, B., Almar, R., Le Cozannet, G., 2018. Under-estimated wave contribution to coastal sea-level rise. Nature Climate Change 8, 234–239.

Mendelssohn, I.A., Hester, M.W., Monteferrante, F.J., Talbot, F., 1991. Experimental dune building and vegetative stabilization in a sand- deficient barrier island setting on the Louisiana coast, USA. Journal of Coastal Research 7, 137–149.

Miller, D.L., Thetford, M., Yager, L., 2001. Evaluation of sand fence and vegetation for dune building following overwash by Hurricane Opal on Santa Rosa Island, Florida. Journal of Coastal Research 17, 936–948.

Mitasova, H., Overton, M., Harmon, R.S., 2005. Geospatial analysis of a coastal sand dune field evolution: Jockey's Ridge, North Carolina. Geomorphology 72, 204–221.

Moffatt & Nichol, 2009. Final coastal regional sediment management plan for the san diego region executive summary.

Moffatt & Nichol, 2015. Cardiff Beach Living Shoreline Project Final Feasibility Study. Technical Report. Moffatt & Nichol.

Morris, R.L., Konlechner, T.M., Ghisalberti, M., Swearer, S.E., 2018. From grey to green: Efficacy of eco-engineering solutions for nature-based coastal defence. Global change biology 24, 1827–1842.

Muir, L.R., El-Shaarawi, A., 1986. On the calculation of extreme wave heights: a review. Ocean Engineering 13, 93–118.

Muller, H., van Rooijen, A., Idier, D., Pedreros, R., Rohmer, J., 2017. Assessing Storm Impact on a French Coastal Dune System Using Morphodynamic Modeling. Journal of Coastal Research 332, 254–272.

Muller, J., 2017. A hybrid solution for the galveston seawall. Additional thesis, TU Delft .

Muller, J., Figlus, J., De Vries, S., 2018. Xbeach simulation of hybrid coastal protection: a galveston seawall test case. Coastal Engineering Proceedings , 100–100.

National Oceanic and Atmospheric Administration (NOAA), 2020. NOAA Tides and Currents. URL: https://tidesandcurrents.noaa.gov/.

Nederhoff, C., Lodder, Q., Boers, M., den Bieman, J., Miller, J., 2015. MODELING THE EFFECTS OF HARD STRUCTURES ON DUNE EROSION AND OVERWASH, World Scientific Pub Co Pte Lt.

Nicholls, R., Wong, P., Burkett, V., Codignotto, J., Hay, J., McLean, R., Ragoonaden, S., Woodroffe, C., 2007. Coastal systems and low-lying areas. in: *Climate Change 2007: Impacts, Adaptation and Vulnerability. Contribution of Working Group II to the Fourth Assessment Report of the Intergovernmental Panel on Climate Change* , 315–356.

Nicholls, R.J., 2011. Planning for the impacts of sea level rise. Source: Oceanography 24, 144–157.

Nishi, R., Kraus, N.C., 1997. Mechanism and calculation of sand dune erosion by storms, in: Proceedings of the Coastal Engineering Conference, ASCE. pp. 3034–3047.

NOAA Office for Coastal Management, 2021. Noaa data access viewer. URL: https://coast.noaa.gov/dataviewer/#/.

Nordstrom, K.F., Gamper, U., Fontolan, G., Bezzi, A., Jackson, N.L., 2009. Characteristics of coastal dune topography and vegetation in environments recently modified using beach fill and vegetation plantings, veneto, italy. Environmental Management 44, 1121–1135.

Nordstrom, K.F., Hartman, J.M., Freestone, A.L., Wong, M., Jackson, N.L., 2007. Changes in topography and vegetation near gaps in a protective foredune. Ocean and Coastal Management 50, 945–959.

Nordstrom, K.F., Jackson, N.L., 2018. Constraints on restoring landforms and habitats on storm-damaged shorefront lots in New Jersey, USA. Ocean and Coastal Management 155, 15–23.

Odériz, I., Knöchelmann, N., Silva, R., Feagin, R.A., Martínez, M.L., Mendoza, E., 2020. Reinforcement of vegetated and unvegetated dunes by a rocky core: A viable alternative for dissipating waves and providing protection? Coastal Engineering , 103675.

O'Reilly, W.C., Olfe, C.B., Thomas, J., Seymour, R.J., Guza, R.T., 2016. The California coastal wave monitoring and prediction system. Coastal Engineering 116, 118–132.

van Ormondt, M., Nelson, T.R., Hapke, C.J., Roelvink, D., 2020. Morphodynamic modelling of the wilderness breach, Fire Island, New York. Part I: Model set-up and validation. Coastal Engineering 157, 103621.

Overton, M., Fisher, J., Stone, A., 1990. Large scale laboratory tests of dune erosion, in: Coastal Engineering 1990, pp. 2471–2480.

Overton, M.F., Fisher, J.S., Young, M.A., 1988. Laboratory Investigation of Dune Erosion. Journal of Waterway, Port, Coastal, and Ocean Engineering 114, 367–373.

Overton, M.F., Pratikto, W.A., Lu, J.C., Fisher, J.S., 1994. Laboratory investigation of dune erosion as a function of sand grain size and dune density. Coastal Engineering 23, 151–165.

Owen, M., 1980. Design of seawalls allowing for wave overtopping. Report Ex 924, 39.

Pagán, J.I., Bañón, L., López, I., Bañón, C., Aragonés, L., 2019. Monitoring the dune-beach system of Guardamar del Segura (Spain) using UAV, SfM and GIS techniques. Science of the Total Environment 687, 1034–1045.

Palmsten, M.L., Holman, R.A., 2011. Infiltration and instability in dune erosion. Journal of Geophysical Research: Oceans 116.

Palmsten, M.L., Splinter, K.D., 2016. Observations and simulations of wave runup during a laboratory dune erosion experiment. Coastal Engineering 115, 58–66.

Passeri, D.L., Long, J.W., Plant, N.G., Bilskie, M.V., Hagen, S.C., 2018. The influence of bed friction variability due to land cover on storm-driven barrier island morphodynamics. Coastal Engineering 132, 82–94.

Payo, A., Wallis, H., Ellis, M.A., Barkwith, A., Poate, T., 2020. Application of portable streamer traps for obtaining point measurements of total longshore sediment transport rates in mixed sand and gravel beaches. Coastal Engineering 156, 103580.

Pendleton, L., Mohn, C., Vaughn, R.K., King, P., Zoulas, J.G., 2012. Size matters: The economic value of beach Erosion and Nourishment in Southern California. Contemporary Economic Policy 30, 223–237.

Plant, N.G., Stockdon, H.F., 2012. Probabilistic prediction of barrier-island response to hurricanes. Journal of Geophysical Research: Earth Surface 117, 3015.

Pullen, T., Allsop, N., Bruce, T., Kortenhaus, A., Schüttrumpf, H., Van der Meer, J., 2007. EurOtop wave overtopping of sea defences and related structures: assessment manual.

Quan, R., Kobayashi, N., 2015. Pile fence to reduce wave overtopping and overwash of dune. Journal of Waterway, Port, Coastal, and Ocean Engineering 141, 04015005.

R Core Team, 2021. R: A Language and Environment for Statistical Computing. R Foundation for Statistical Computing. Vienna, Austria. URL: `https://www.R-project.org/`.

Raubenheimer, B., Elgar, S., Guza, R.T., 1998. Estimating wave heights from pressure measured in sand bed. Journal of Waterway, Port, Coastal, and Ocean Engineering 124, 151–154.

Rella, A., Miller, J., 2012. A Comparative Cost Analysis of Ten Shore Protection Approaches at Three Sites Under Two Sea Level Rise Scenarios. Staatsburg, New York: Hudson River Sustainable Shorelines Project.

van Rijn, L.C., 2009. Prediction of dune erosion due to storms. Coastal Engineering 56, 441–457.

Roelvink, D., McCall, R., Mehvar, S., Nederhoff, K., Dastgheib, A., 2018. Improving predictions of swash dynamics in xbeach: The role of groupiness and incident-band runup. Coastal Engineering 134, 103–123.

Roelvink, D., Reniers, A., van Dongeren, A., van Thiel de Vries, J., McCall, R., Lescinski, J., 2009. Modelling storm impacts on beaches, dunes and barrier islands. Coastal Engineering 56, 1133–1152.

Rosati, J.D., Wise, R.A., Kraus, N.C., Larson, M., 1993. Sbeach: Numerical model for simulating storm-induced beach change. Report 3 User's Manual .

Ruessink, B., Ramaekers, G., Van Rijn, L., 2012. On the parameterization of the free-stream non-linear wave orbital motion in nearshore morphodynamic models. Coastal engineering 65, 56–63.

Ruggiero, P., Komar, P.D., McDougal, W.G., Marra, J.J., Beach, R.A., 2001. Wave runup, extreme water levels and the erosion of properties backing beaches. Journal of coastal research , 407–419.

Saleh, F., Weinstein, M.P., 2016. The role of nature-based infrastructure (NBI) in coastal resiliency planning: A literature review. Journal of Environmental Management 183, 1088–1098.

Sallenger, J., 2000. Storm impact scale for barrier islands. Journal of Coastal Research 16, 890–895.

Schambach, L., Grilli, A.R., Grilli, S.T., Hashemi, M.R., King, J.W., 2018. Assessing the impact of extreme storms on barrier beaches along the Atlantic coastline: Application to the southern Rhode Island coast. Coastal Engineering 133, 26–42.

Schoonees, J.S., Theron, A.K., 1995. Evaluation of 10 cross-shore sediment transport/ morphological models. Coastal Engineering 25, 1–41.

Schubert, J.E., Gallien, T.W., Majd, M.S., Sanders, B.F., 2015. Terrestrial laser scanning of anthropogenic beach berm erosion and overtopping. Journal of Coastal Research 31, 47–60.

Schweiger, C., Kaehler, C., Koldrack, N., Schuettrumpf, H., 2020. Spatial and temporal evaluation of storm-induced erosion modelling based on a two-dimensional field case including an artificial unvegetated research dune. Coastal Engineering 161.

Schweiger, C., Schuettrumpf, H., 2021. Considering the effect of land-based biomass on dune erosion volumes in large-scale numerical modeling. Journal of Marine Science and Engineering 9.

Serafin, K.A., Ruggiero, P., 2014. Simulating extreme total water levels using a time-dependent, extreme value approach. Journal of Geophysical Research: Oceans 119, 6305–6329.

Serafin, K.A., Ruggiero, P., Stockdon, H.F., 2017. The relative contribution of waves, tides, and nontidal residuals to extreme total water levels on us west coast sandy beaches. Geophysical Research Letters 44, 1839–1847.

Shope, J.B., Erikson, L.H., Barnard, P.L., Storlazzi, C.D., Serafin, K.A., Doran, K.J., Stockdon, H.F., Reguero, B.G., Mendez, F.J., Castanedo, S., Cid, A., Cagigal, L., 2020. Characterizing Storm-Induced Coastal Change Hazards Along the U.S. West Coast: U.S. Geological Survey Summary of Methods to accompany Data Release .

Sigren, J.M., Figlus, J., Armitage, A.R., 2014. Coastal sand dunes and dune vegetation: Restoration, erosion, and storm protection Coastal Ridge-Runnel Migration View project Rapid storm response unit for the upper Texas Gulf coast View project. Shore & Beach 82, 5–12.

Silva, R., Martínez, M., Odériz, I., Mendoza, E., Feagin, R., 2016. Response of vegetated dune–beach systems to storm conditions. Coastal Engineering 109, 53–62.

Simmons, J.A., Harley, M.D., Marshall, L.A., Turner, I.L., Splinter, K.D., Cox, R.J., 2017. Calibrating and assessing uncertainty in coastal numerical models. Coastal Engineering 125, 28–41.

Simmons, J.A., Marshall, L.A., Turner, I.L., Splinter, K.D., Cox, R.J., Harley, M.D., Hanslow, D.J., Kinsela, M.A., 2015. A more rigorous approach to calibrating and assessing the uncertainty of coastal numerical models 2015, 22nd.

Simmons, J.A., Splinter, K.D., 2022. A multi-model ensemble approach to coastal storm erosion prediction. Environmental Modelling and Software 150.

Simmons, J.A., Splinter, K.D., Harley, M.D., Turner, I.L., 2019. Calibration data requirements for modelling subaerial beach storm erosion. Coastal Engineering 152, 103507.

Smallegan, S.M., Irish, J.L., Dongeren, A.R.V., Bieman, J.P.D., 2016. Morphological response of a sandy barrier island with a buried seawall during hurricane sandy.

Splinter, K.D., Kearney, E.T., Turner, I.L., 2018. Drivers of alongshore variable dune erosion during a storm event: Observations and modelling. Coastal Engineering 131, 31–41.

Splinter, K.D., Palmsten, M.L., 2012. Modeling dune response to an East Coast Low. Marine Geology 329-331, 46–57.

Steetzel, H., 1987. A model for beach and dune profile changes near dune revetments, in: Coastal Sediments, ASCE. pp. 87–97.

Stockdon, H.F., Doran, K.S., Sallenger, A.H., 2009. Extraction of Lidar-Based Dune-Crest Elevations for Use in Examining the Vulnerability of Beaches to Inundation During Hurricanes. Journal of Coastal Research 10053, 59–65.

Stockdon, H.F., Holman, R.A., Howd, P.A., Sallenger, A.H., 2006. Empirical parameterization of setup, swash, and runup. Coastal Engineering 53, 573–588.

Stockdon, H.F., Sallenger, A.H., Holman, R.A., Howd, P.A., 2007. A simple model for the spatially-variable coastal response to hurricanes. Marine Geology 238, 1–20.

Stockdon, H.F., Thompson, D.M., Plant, N.G., Long, J.W., 2014. Evaluation of wave runup predictions from numerical and parametric models. Coastal Engineering 92, 1–11.

Stokes, K., Poate, T., Masselink, G., King, E., Saulter, A., Ely, N., 2021. Forecasting coastal overtopping at engineered and naturally defended coastlines. Coastal Engineering 164.

Stronkhorst, J., Lagendijk, O., Stronkhorst, J., Lagendijk, O., 2012. Toekomstbestendige verharde zeeweringen: verkenning naar adaptieve oplossingen in een zandige kust: eindrapport ten behoeve van het Deltaprogramma Kust. Deltares.

Sutton-Grier, A.E., Wowk, K., Bamford, H., 2015. Future of our coasts: The potential for natural and hybrid infrastructure to enhance the resilience of our coastal communities, economies and ecosystems. Environmental Science and Policy 51, 137–148.

Sweet, W.V., Park, J., 2014. From the extreme to the mean: Acceleration and tipping points of coastal inundation from sea level rise. Earth's Future 2, 579–600.

Taherkhani, M., Vitousek, S., Barnard, P.L., Frazer, N., Anderson, T.R., Fletcher, C.H., 2020. Sea-level rise exponentially increases coastal flood frequency. Scientific reports 10, 1–17.

Tawn, J.A., 1992. Estimating probabilities of extreme sea-levels. Journal of the Royal Statistical Society: Series C (Applied Statistics) 41, 77–93.

Temmerman, S., De Vries, M.B., Bouma, T.J., 2012. Coastal marsh die-off and reduced attenuation of coastal floods: A model analysis. Global and Planetary Change 92, 267–274.

Temmerman, S., Meire, P., Bouma, T.J., Herman, P.M., Ysebaert, T., De Vriend, H.J., 2013. Ecosystem-based coastal defence in the face of global change. Nature 504, 79–83.

U.S. Army Corps of Engineers, 1994. Coastal Engineering Technical Note. Application of SBeach to Coastal Projects .

U.S. Army Corps of Engineers, 2008. Coastal Engineering Manual. U.S. Army Corps of Engineers, Washington D.C.

Van Rijn, L., Tonnon, P., Sánchez-Arcilla, A., Cáceres, I., Grüne, J., 2011. Scaling laws for beach and dune erosion processes. Coastal Engineering 58, 623–636.

Van Rijn, L.C., 2011. Coastal erosion and control. Ocean and Coastal Management 54, 867–887.

van Wiechen, P., de Vries, S., Reniers, A., Aarninkhof, S., 2023. Dune erosion during storm surges: A review of the observations, physics and modelling of the collision regime. Coastal Engineering 186, 104383.

VanRijn, L.C., Walstra, D.J.R., Grasmeijer, B., Sutherland, J., Pan, S., Sierra, J.P., 2003. The predictability of cross-shore bed evolution of sandy beaches at the time scale of storms and seasons using process-based profile models .

Vellinga, P., 1982. Beach and dune erosion during storm surges. Coastal Engineering 6, 361–387.

Vitousek, S., Barnard, P.L., Fletcher, C.H., Frazer, N., Erikson, L., Storlazzi, C.D., 2017. Doubling of coastal flooding frequency within decades due to sea-level rise. Scientific Reports 7, 1399.

Voorendt, M., Vrijling, J., Voortman, H., 2015. Structural evaluation of multifunctional flood defenses using generic element types, in: Coastal Structures and Solutions to Coastal Disasters Joint Conference 2015, American Society of Civil Engineers Reston, VA. pp. 365–374.

Vousdoukas, M.I., Ferreira, Ó., Almeida, L.P., Pacheco, A., 2012. Toward reliable storm-hazard forecasts: Xbeach calibration and its potential application in an operational early-warning system. Ocean Dynamics 62, 1001–1015.

van Thiel de Vries, J., 2012. Dune erosion above revetments. Coastal Engineering Proceedings , 95–95.

Walling, K., Herrington, T., Miller, J.K., 2016. Hurricane sandy damage comparison: Ocean-front houses protected by a beach and dune system with vs. without a rock seawall. Shore & Beach 84, 35–41.

Wernette, P., Houser, C., Lehner, J., Evans, A., Weymer, B., 2020. Investigating the Impact of Hurricane Harvey and Driving on Beach-Dune Morphology. Geomorphology 358.

Williams, J.J., de Alegría-Arzaburu, A.R., McCall, R.T., Dongeren, A.V., 2012. Modelling gravel barrier profile response to combined waves and tides using xbeach: Laboratory and field results. Coastal Engineering 63, 62–80.

de Winter, R.C., Gongriep, F., Ruessink, B.G., 2015. Observations and modeling of alongshore variability in dune erosion at Egmond aan Zee, the Netherlands. Coastal Engineering 99, 167–175.

Winters, M.A., Leslie, B., Sloane, E.B., Gallien, T.W., 2020. Observations and Preliminary Vulnerability Assessment of a Hybrid Dune-Based Living Shoreline. Journal of Marine Science and Engineering 8, 920.

Wise, R.A., Kraus, N.C., . Simulation of beach fill response to multiple storms, ocean city, maryland, in: Beach Nourishment Engineering and Management Considerations, ASCE. pp. 133–147.

Wong, P.P., Losada, I.J., Gattuso, J.P., Hinkel, J., Khattabi, A., McInnes, K.L., Saito, Y., Sallenger, A., et al., 2014. Coastal systems and low-lying areas. in: *Climate Change 2014: Impacts, Adaptation, and Vulnerability. Part A: Global and Sectoral Aspects. Contribution of Working Group II to the Fifth Assessment Report of the Intergovernmental Panel on Climate Change* 2104, 361–409.

Woolard, J.W., Colby, J.D., 2002. Spatial characterization, resolution, and volumetric change of coastal dunes using airborne lidar: Cape hatteras, north carolina. Geomorphology 48, 269–287.

Wright, L., Short, A., 1983. Morphodynamics of beaches and surf zones in australia. CRC Handbook of Coastal Processes and Erosion , 35–64.

Xu, S., Huang, W., 2011. Estimating extreme water levels with long-term data by gev distribution at wusong station near shanghai city in yangtze estuary. Ocean Engineering 38, 468–478.

Zhang, K., Liu, H., Li, Y., Xu, H., Shen, J., Rhome, J., Smith III, T.J., 2012. The role of mangroves in attenuating storm surges. Estuarine, Coastal and Shelf Science 102, 11–23.